POLITECNICO DI TORINO

Corso di Laurea in
Ingegneria Aerospaziale

Tesi di Laurea Magistrale

Free Vibration Analysis of Rotating Functionally Graded Material Beams

Supervisors:
Prof. Fiorenzo A. Fazzolari
Prof. Erasmo Carrera

Candidate:
Lorenzo Chianchiano

A.A 2017/2018

A voi che mi avete sempre sostenuto e guidato..

Alla mia famiglia dedico questo traguardo e nuovo punto di partenza.

Summary

Beam structures are extensively used in aerospace, civil, naval and mechanical application because of their high versatility. The beam structural element allows the modeling of structural element such as aircraft wing spars, helicopter rotor and turbomachinery blades, robot harms as well as concrete metal/composite construction in civil and naval engineering, respectively.

During last decades Functionally Graded Materials (FGMs) have raised a lot of interest. In several applications they are more attractive than classic fiber-reinforced composites because of their outstanding properties. In addition, FGMs have turned out to be more advantageous, since problems such as delamination, fiber failure, adverse hygroscopic effects etc, are effectively eliminated or non-existent. Functionally Graded structures are largely studied not only for the practical applications of concept in a wide variety of thermal shielding problems but also in other field, these materials have almost unlimited potential in many other technological applications such as, for example, the production of biocompatible prosthesis.

The aim of the present thesis is to investigate the free vibration behavior of three-dimensional rotating, metallic and functionally graded beams accounting the Coriolis effect. The geometry of the analyzed beams change according to the variation of some parameters of interest such as length-to-thickness ratio (slenderness ratio), tip chord-root chord ratio (taper ratio), the pre-twist angle.

The investigation is carried out by using the method of power series expansion of displacement components. This approach allows obtaining refined structural theories that account for variable kinematic description. Indeed, each displacement variable, in the displacement field, can be expanded at any desired order independently from the others and regarding to the result accuracy and computational cost. The weak-form of the governing equations is derived via the Principle of stationary action of Hamilton (or from the PVD), while the Ritz method is used as solution technique. Algebraic Ritz functions are employed in the analysis. Using the Gram-Schmidt process these functions have been orthogonalized in order to enhance significantly the computational stability of the code. The equations are written in terms of fundamental nuclei, which do not vary with the theory order.

Convergence and accuracy of the proposed formulation have been examined. The

effect of significant parameters such as slenderness ratio, taper ratio, pre-twist angle and the angular velocity, on the natural frequencies, is discussed and compared with both, results available in literature and those obtained by using an Finite Element Analysis commercial software.

Sommario

Le travi sono ampiamente utilizzate in applicazioni aerospaziali, civili, navali e meccaniche grazie alla loro versatilità. Gli elementi strutturali trave consentono di modellizzare strutture come i longheroni alari, le pale di rotori di elicotteri e turbomacchine, bracci robotici e strutture metalliche od in composito per applicazioni civili o navali. Negli ultimi decenni i Functionally Graded Materials (FGM) hanno richiamato l'attenzione poiché, grazie alle loro eccezionali proprietà, in diverse applicazioni, questi risultano preferibili ai classici compositi rinforzati con fibre. Gli FGMs presentano dei vantaggi rispetto ai compositi classici poiché per questi, problemi come la delaminazione, il cedimento di fibre, effetti igroscopici etc, possono essere eliminati o sono inesistenti. Le strutture in FGM sono ampiamente studiate non solo per possibili applicazioni in problemi di thermal shielding ma anche in altri campi. Questi materiali hanno delle potenzialità pressoché illimitate in diverse altre applicazioni, come ad esempio la realizzazione di protesi bio−compatibili. La presente tesi è stata svolta con lo scopo di studiare le vibrazioni libere di travi tridimensionali rotanti, metalliche e in FGM tenendo in considerazione l'effetto Coriolis. Le travi analizzate presentano differenti geometrie in accordo con la variazione di alcuni parametri d'interesse come il rapporto lunghezza su spessore (slenderness ratio), il rapporto tra le corda di estremità e di radice (taper ratio), l'angolo di svergolamento. Lo studio è stato svolto sfruttando il metodo dell'espansione in power series delle componenti dello spostamento. Questo approccio consente di ottenere delle teorie strutturali rifinite che consentono una descrizione della cinematica variabile. Difatti ciascuna variabile dello spostamento, nel campo degli spostamenti, può essere espansa a un qualsiasi ordine indipendentemente dalle altre, in dipendenza dall'accuratezza richiesta per la soluzione e la capacità di gestire carichi computazionali più o meno elevati. Le equazioni in forma debole sono derivate a partire dal Principio di Hamilton (equivalentemente dal PLV), il metodo di Ritz viene utilizzato come tecnica di soluzione. Nell'analisi sono utilizzate le funzioni algebriche di Ritz. Queste sono state ortogonalizzate sfruttando il metodo di Gram−Schmidt per incrementare in maniera significativa la stabilità del codice. Le equazioni sono scritte in termini di "nuclei fondamentali", questi non variano con l'ordine della teoria. La convergenza e l'accuratezza della formulazione proposta sono esaminate. Si analizza infine l'effetto di parametri

caratteristici della geometria della trave e del problema, come rapporto di snellezza, taper ratio, angolo di svergolamento, e velocit$\grave{a}$ angolare sulle frequenze naturali del sistema, confrontando i risultati con quelli presenti in letteratura e quelli ottenuti tramite l'utilizzo di software commerciali per la FEA.

Contents

List of Tables

List of Figures

Chapter 1

Introduction

1.1 Composite structure with a focus on FGM

Materials play an important role in the advancement of human life. The rapid growth in the development and use of composite materials is due to the advantages that they offer, such as specific strength and stiffness properties, lightweight and corrosion resistance.

Composites comprise two or more phases where normally the constituent materials are processed separately and then bonded. The properties of the composites are different from the constituent materials acting alone. One of the constituents is reinforcing phase in the forms of fibers, particles, or sheets and are embedded in another constituent called matrix.

Furthermore, there are a number of applications in which the use of a single material is not convenient. Such cases may involve the use of one of the solutions listed below.

- *Sandwich structures*:

  sandwich beams, plates and shells are composite structures that consist of at least three different layers. Two or more high-strength stiff layers (faces) are bonded to one or more low-density flexible layer (core). The core, which is usually the cheapest material, mainly has the task of keeping away the two faces from the neutral axes, thus improving bending resistance. Sandwich structures can be defined as composite structures, since they are composed of at least two different materials at a microscopic level. There are many type of sandwich structures in aerospace construction that have not been dealt with detail here.

- *Layer structures for thermal protection purposes*:

  engine components, reentry vehicles and supersonic aircraft often require an adequate thermal protection. In many cases, it is not possible to obtain a

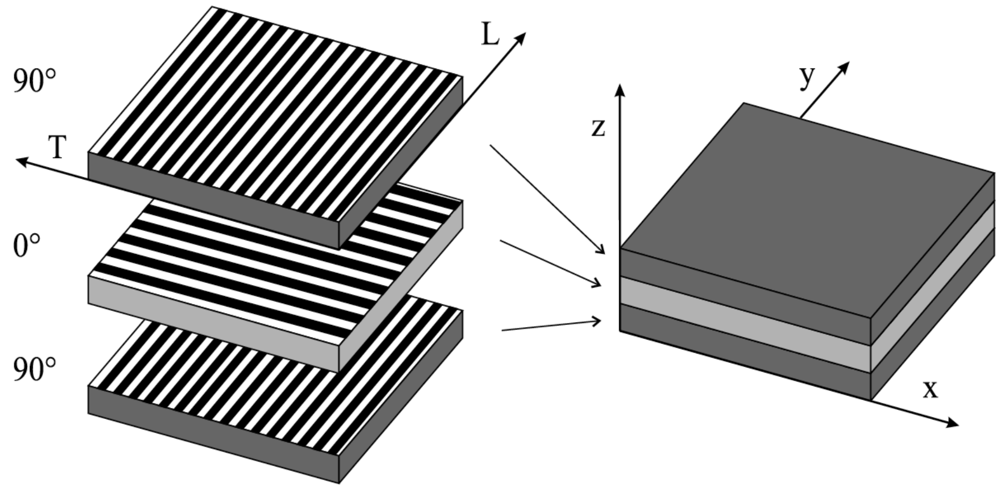

Figure 1.1. Layered plate made of unidirectional laminae.

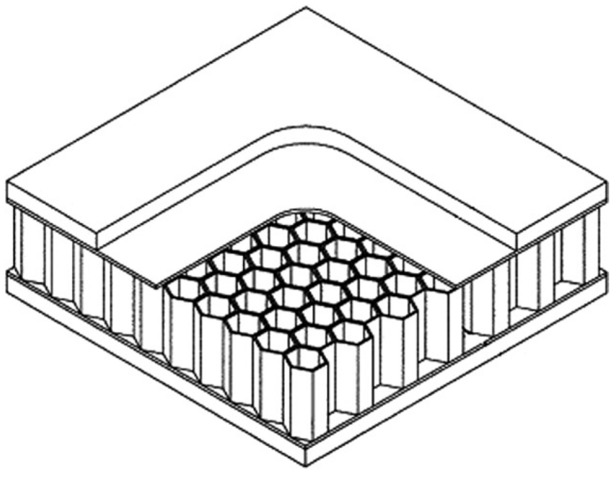

Figure 1.2. Honeycomb core Sandwich.

material that can stand both mechanical and thermal loads at the same time. The solution, in this case, is to build a composite multilayer structure: the mechanical structure is protected by an additional layer that leads to high resistance with respect to thermal loadings.

- *Piezo-layered materials for smart structures*:

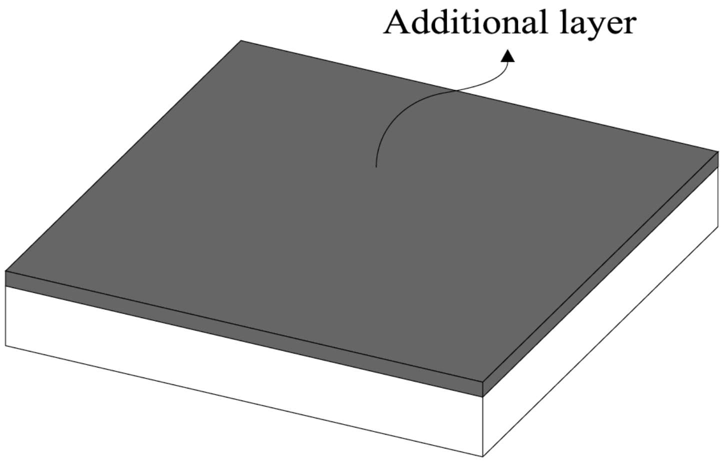

Figure 1.3. Layered plate made of isotropic layers for thermal protection.

the phenomenon of piezoelectricity is a particular feature of certain classes of crystalline materials. The piezoelectric effect consist of a linear energy conversion between the mechanical and electric fields in both direction that define a direct or converse piezoelectric effect. The direct piezoelectric effect generate an electric polarization by applying mechanical stresses. The converse piezoelectric effect instead induces mechanical stress or strain by applying an electric field. Multilayered structures are also obtained when piezo-layers are bonded as sensor or actuators to a given structure.

- *Laminates*:

  the laminate structure is the most common case of composite materials. Composite are multilayered structures (made mostly of flat and curved panels) constituted by several layers or laminate that are bonded perfectly together. Each lamina is composed of fibers embedded in a matrix. These fibers are produced according to a specific technological process that confers high mechanical properties in the longitudinal direction (L) of the fibers. The matrix has the role of holding the fibers together. Carbon, boron and glass fibers are used above, all along with organic products. The matrices are mostly of an epoxy type. There are several possible ways of putting the fibers and matrix together. Uni-directional laminate or laminates made of differently oriented laminae are used in most applications related to the construction of aerospace, automotive or sea vehicles. The laminae are placed one over the other, according to a given lay-out. Such a possibility, which is known as "tailoring",

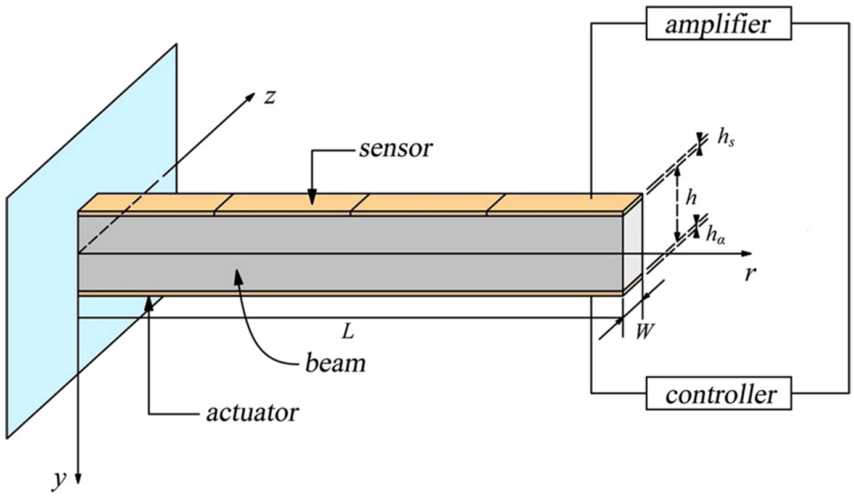

Figure 1.4. Exemple of smart structure: sensor-actuator network for a plate.

permits one to optimize the use of the material for a given set of design requirements.

- *Functionally graded materials*:

  FGMs are advanced composite materials, within which the composition of each constituent varies gradually with respect to spatial coordinates. Therefore the macroscopic material properties in FGMs vary continuously, thus distinguishing them from laminated composites materials in which the abrupt change of the material properties across the layer interfaces leads to large inter-laminar stresses which can lead to damage development. As in the case of laminated composite materials, FGMs combine the desirable properties of the constituent phases to obtain a superior performance. To this aim, functionally graded materials layers can be embedded in multilayered structures.

- *Multiwalled carbon-nanotubes*: carbon nanotubes (CNT) have exceptional mechanical properties (Young's modulus, tensile strength, toughness, etc.), which are due to their molecular structure, which consist of single or multiple sheets of graphite wrapped into seamless hollow cylinders. Owning to the great stiffness, strength and high aspect rateo of CNT's, it is expected that, by dispersing them evenly throughout a polymer matrix, it is possible to produce composites with considerably improved overall effective mechanic properties. Furthermore, CNT's have a relatively low density of about 1.75 $\mathrm{g/cm^3}$ and nanotube reinforced polymers (NRPs), therefore, excel due to their extremely high specific stiffness, strength and toughness [16].

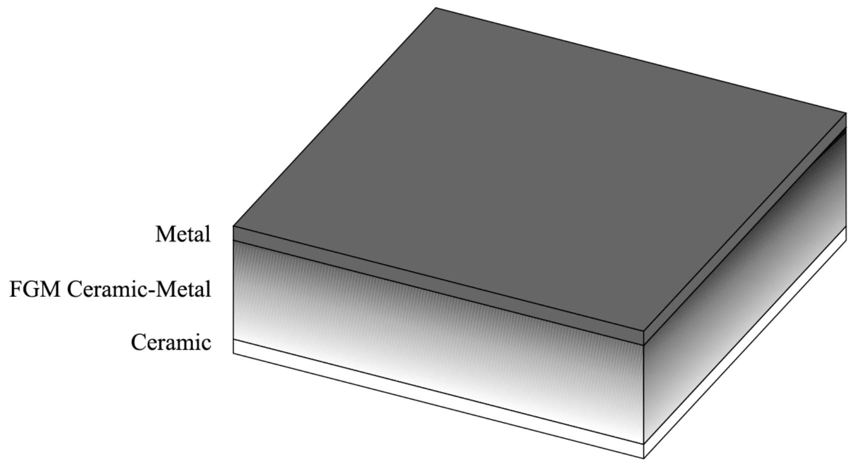

Figure 1.5. Multilayered plate embedding a FGM layer.

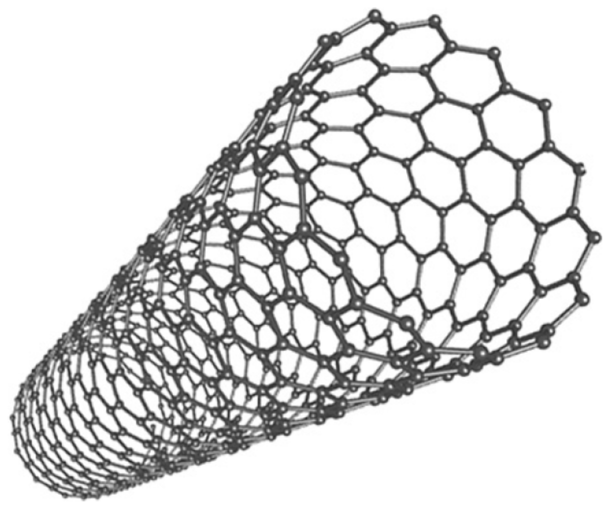

Figure 1.6. Exemple of single-walled carbon nanotube.

In order to meet the demands of new technologies, particularly in microelectronics, aerospace and high temperature applications, the materials science and engineering community is continuously engaged in research to develop new materials with improved properties. The great bulk of the work in this area has been in processing a variety of composites, ceramics, alloys and coatings. The main objective of these efforts generally has been to produce materials which are homogeneous in bulk having controlled microstructure and, hence, controlled thermo-mechanical properties. In the recent past considerable success seems to have been attained in processing materials with desirable properties such as certain nano-composites, metal matrix composites and intermetallics which are macroscopically homogeneous and isotropic, and fiber or filament reinforced composites and unidirectionally solidified eutectics which are highly oriented with regard to their mechanical and strength properties.

At least in one important technological area, namely in high temperature applications, it is becoming more and more difficult to meet the highly stringent design requirements by using materials that are "homogeneous" in their bulk properties. At high temperatures metals and metal alloys appear to be very susceptible to oxidation, creep, and generally to loss of structural integrity. The disadvantage of ceramics has always been low strength and low toughness. Thus, a variety of metal/ceramic composites and ceramic thermal barrier coatings have been developed in an effort to take advantage of the respective favorable properties of these two major groups of materials. However, in composites, to varying degrees, oxidation and low toughness are still a problem, whereas the shortcomings of ceramic coatings seem to be poor interfacial bonding, high residual and thermal stresses, low toughness, and consequent tendency toward cracking and spallation [31].

As regards the FGM concept, it is worth highlighting the fact that it was originated in Japan in 1984 during the space plane project, in the form of a proposed thermal barrier material capable of withstanding a surface temperature of 2000 K and a temperature gradient of 1000 K across a cross section of less than 10 mm [38]. In the light of this concept, the main challenge is to combine irreconcilable properties in the same component, such as high hardness at high temperatures and structural toughness at low temperatures. A possible concept to meet this demand is that of functionally graded materials.

FGMs are essentially two-phase particulate composites synthesized in such a way that the volume fractions of the constituents vary in the thickness direction to give a predetermined composition profile (Hirano and Yamada, 1988; Hirano et al., 1988; Kawasaki and Watanabe, 1990). The composition profile, varying e.g. from 0% ceramic at the interface to 100% near the surface, in turn, is selected in such a way that the resulting non-homogeneous material exhibits the desired thermo-mechanical properties. According to the material combinations, FGM is divided into metal/ceramic, ceramic/ceramic, ceramic/plastic and many other combinations. In accordance with their changing compositions, the overall FGM is divided into functionally graded type (composed of form one side to another gradient side of the structure of gradient materials), functionally graded coating type (the matrix material to form a coating composition gradient), functional gradient Connection type (connecting two interface layer between the substrate gradient changes).

Even though the initial research on FGMs was largely motivated by the practical applications of the concept in a wide variety of thermal shielding problems, materials with graded physical properties have almost unlimited potential in many other technological applications.

1.2 Thin-walled structures background

For about a century many branches of the industry have sought stronger and at the same time lighter structural solutions which optimize the effectiveness and the cost of the structures. This has led to an increasing use of thin-walled structures.

Thin-walled structures made of aluminium and composite materials are widely used in most applications related to the construction of aerospace, automotive or sea vehicles.

Thin-walled beams are characterized by the relative magnitudes of their dimensions. The wall thickness is small relative to the dimensions of the cross-section, and the dimensions of the cross-section are small compared with the length of the beam. It is useful to mention that for a thin-walled beam subjected to bending, torsion or combined loading, the value of direct stress at a point on the cross-section depends on the position of the point, the geometrical properties of the cross-section, and the applied loading. This may be true whether the cross-section of the thin-walled beam is closed or open.

There are many reasons why thin-walled structures must be given special considerations in their analysis and design. Some of them are listed below:

- *Out-of-plane distortion.* The shear stresses and strains are relatively larger than those in a solid rectangular beam. By twisting a thin-walled structure it is easily shown that there is an out-of-plane distortion of the cross section in the longitudinal beam direction (warping).

- *Shear flow.* In the closed cross section the torsional moment is reduced by the action of a shear flow around the cell. Consequently the torsional stiffness is increased considerably as compared to a similar open cross section.

- *Shear lag.* Shear lag occurs when the forces cannot be transmitted directly into the entire cross section. This means that the area that is effective in resisting the force is smaller than the total area.

- *Susceptible to local buckling.* It is well known that thin-walled structures are susceptible to local buckling when subjected to load.

- *Stress distribution.* It is well known that warping and torsion have a great influence on the stress distribution.

- *In-plane distortion.* Due to the thin walls, thin-walled beams are much susceptible to deformation of the cross section, leading to effects of local and general instability that do not exist for a classic not-hollowed beam [2].

Because of the increased slenderness of these structures and the non-linearity of many of the effects linked to the hollowed section, these structures require the development of more comprehensive and accurate mathematical approaches than the application of the thin-walled beams theory developed by Vlasov.

1.3 Literature review

This section is intended to provide a comprehensive review of the investigations to date on vibration analysis *FGM pre-twisted, single or double-tapered, rotating beams.*

The first two subsection reviews the main research on the behavior of isotropic pre-twisted, single and double-tapered and rotating beams. To complete the overview the last two subsections reviews the main research on the behavior of FGMs pre-twisted, single and double-tapered rotating beams.

1.3.1 Pre-twisted, tapered isotropic beams

Non-prismatic beams i.e. beams with cross-section varying continuously or discontinuously along their length are widely used as constitutive elements in complex structures such as aircrafts and space vehicles due to their ability in optimization of weight and strength; consequently the significance of vibration analysis of such elements considerably arises since these structures are regularly exposed to variety of time dependent loads introduced by blast, sonic booms and fuel explosion.

The governing differential equation for transverse vibration of non-prismatic beams is a fourth order non-homogeneous differential equation with variable coefficients. Except for some particular cases [4, 20, 29, 53], there is no exact solution available. Thus, a wide variety of numerical techniques such as Frobenius method [14, 13, 98], Chebyshev series [78] and Rayleigh-Ritz method [5] has been developed through the years. Finite element method is one of the most popular methods among approximate techniques which have been enormously used in analysis of tapered beams. Analyzing a non-prismatic beam using conventional finite element method (CFEM) involves modeling of the original non-uniform beam with uniform elements. It is obvious that by increasing the number of elements the accuracy of the solution improves and dimensions of structural matrices grow larger; hence more time is consumed for computations.

Many researchers have devoted their work to either formulating new exact elements or improving the existing approximate elements. Gallagher and Lee [40] derived approximate structural matrices for dynamic and instability analyses of non-uniform beams. Karabalis and Beskos [51] evaluated approximate consistent mass and geometric stiffness matrices for beam elements with constant width and linearly tapering depth. Banerjee and Williams [14] derived exact dynamic stiffness matrix in terms of Bessel functions for non-prismatic beams whose cross-sectional area and moment of inertia vary along beam as integer powers n and $n + 2$, respectively. Eisenberger [30] derived the exact stiffness matrix for beams with general variation of width and depth via a series solution of the governing differential equation. Mou et al. [65] derived exact dynamic stiffness matrix for general non-prismatic beam elements in term of hyper-geometric functions. Using Bessel, triangular and hyperbolic functions, Li [60] proposed an exact method for determination of natural frequencies of multistep non-prismatic beams with different mass and spring attachments.

Caruntu [21] used hyper-geometric functions to study free vibration of cantilever beams with parabolic thickness variation. Zhou [112] was the first one to introduce differential transform method (DTM). He employed DTM in solution of initial boundary value problems in electric circuit analysis. Later, Chen and Liu [26] applied DTM in solution of two-point boundary-value problems. The concept of DTM has broadened to problems involving partial differential equations and systems of differential equations [6, 7, 50]. Some researchers [9, 22, 48, 69, 70, 105, 104, 111] have applied DTM for analysis of uniform and non-uniform beams. Ozdemir and Kaya [69] calculated natural frequencies for non-prismatic beams whose cross-sectional area and moment of inertia vary in accordance to two arbitrary powers n and $n + 2$, respectively.

Recently, R. Attarnejad, A. Shahba and M. Eslaminia studied free transverse vibration of non-prismatic beams from a mechanical point of view, introducing new functions, namely Basic Displacement Functions (BDFs) [4]. Syed Muhammad Ibrahim, Saleh H Alsayed, Husain Abbas, Erasmo Carrera, Yousef A Al-Salloum and Tarek H Almusalla, presented an accurate frequency solutions of tapered vibrating beams and plates using a simple and efficient displacement based unified beam theory [85].

1.3.2 Rotating isotropic beams

A thorough understanding of the dynamic features of rotating blades serves as a starting point for the study of fatigue effects, forced-response and flutter instability, which occur in airplane engines, helicopters and turbomachinery. Rotating structures where a geometrical dimension is predominant over the others are usually modeled as beams. Many researchers have addressed the problem of the rotating beam by simplifying both the equations of motion and the displacement formulations. For instance, Banerjee [14, 13], Ozge and Kaya [71], Mei [64] and Hodges and Rutkowski [47] limited their studies to the flexural vibrations of both uniform and tapered Euler-Bernoulli rotating beams by using, respectively, the Dynamic

Stiffness Method, the Differential Transform Method and a variable-order finite element. The assumption that the beam deforms only in bending is restrictive, since the coupling between the axial deformation and the lagwise motion can be significant. In order to take into account this coupling the introduction of the Coriolis force becomes mandatory. For this reason, Hsiao et al. solved the complete motion equations of Euler beams by using the power series solution [59] and the Finite Element Method [49]. Further improvements have been introduced by introducing enhanced displacement fields over the blade cross-section. Indeed, in the open literature, there are many papers devoted to the development of theories for the rotating structures based on the Timoshenko model, in which the Coriolis term has [86] or has not been considered [54, 45]. In all papers mentioned, the generic rotating blade is assumed to be a compact structure constituted by isotropic material or by orthotropic laminae.

1.3.3 Pre-twisted, tapered FGM beams

The enhancement in the development of the structural beam models went hand-in-hand with the improvement in the mechanical as well as thermal performances of new advanced materials. Amongst the latter, the functionally graded materials (FGMs) have raised a lot of interest in the research community in the last decade. They showed some outstanding properties, which, in several applications, make them more attractive than classical fibre-reinforced composites. They have turned out to be more advantageous, indeed problems such as delamination, fibre failure, adverse hygroscopic effects etc, are effectively eliminated or non-existent. Thus, due to their potential application in several fields, there is the need to fully understand their mechanical and thermal behavior. In this respect, many scientific articles have been recently published on the static and dynamic analysis of FG beams. In particular, Vo et al. [96] coped with the static and vibration analysis of FG beams using refined shear deformation theories. Thai and Vo [95] dealt with bending and free vibration analysis of FG beams considering various boundary conditions and shear deformation beam theories. Fundamental frequencies of FG beams using different high-order beam theories have been provided by Sismek [82]. The same author [81] studied the free and forced vibration behaviour of bi-directional functionally graded materials (BDFGMs) of Timoshenko beams with various boundary conditions. Chunhua and Wang [28] provided and accurate free vibration analysis of Euler-type FG beams by using the weak-form quadrature element method. Wang et al. [97] analysed the free vibration behaviour of two-directional FG beams. Lu et al. [61] proposed semi-analytical elasticity solutions for bi-directional functionally graded beams. Alshorbagy et al. [1] studied the free vibration characteristics of a functionally graded beam by using FEM formulation. Maganti and Nullari [63] investigated the free vibration analysis of pre-twisted rotating FG beams by using

Rayleigh-Ritz method. The same authors [62] studied the flapwise bending vibration analysis of functionally graded rotating double-tapered beams. Free vibration of FG Timoshenko beams with through-width delamination have been investigated by Li and Fan [57]. Ke et al. [52] coped with the non-linear vibration of edged cracked FG beams using differential quadrature method and Timoshenko beam model. Vibration characteristics of stepped beams made of FGM using differential transformation method were analysed by Wattanasakulpong and Charoensuk [101]. The same authors [100] proposed the study of flexural vibration of imperfect FG beams based on Timoshenko beam theory and Chebyshev collocation method. Shegokar and Lal [79] coped with a stochastic finite element non-linear free vibration analysis of piezoelectric FG beams subjected to thermo-piezoelectric loadings with material uncertainties. Nonlinear forced vibration analysis of clamped functionally graded beams have been analysed by Shooshtari and Rafiee [80]. A combined Fourier series Galerkin method for the analysis of FG beams have been proposed by Zhu and Sankar [113]. Azadi [8] dealt with the free and forced vibration analysis of FG beam considering temperature dependency of material properties. Pradhan and Chackraverty [72] investigated the effects of different shear deformation theories on the free vibration of functionally graded beams. Librescu et al. [56] investigated the free vibration and stability behaviour of thin walled beams made of FGMs and operating in high temperature environment. Giunta et al. [43] proposed hierarchical beam theories for an accurate free vibration analysis of functionally graded beams. The same authors [42] coped with a thermo-mechanical analysis of FG beams via hierarchical modelling. Su and Benerjee [11] proposed a development of dynamic stiffness method for the free vibration analysis of FG Timoshenko beams. Ziane et al. [110] coped with the free vibration analysis of thin and thick-walled FGM box beams by using an exact dynamic stiffness matrix on the basis of first-order shear deformation theory. Xu et al.[102] investigated the stochastic dynamic characteristics of FGM beams with random material properties. Eroglu [32] proposed a study on in-plane free vibrations of circular beams made of FGM in thermal environment. Roque and Martins [77] used the RBF numerical method combined with the differential evolution for optimization of FG beams. Free vibrations of FG spatial curved beams have been analysed by Yousefi and Rastgoo [106]. FGM structures have been widely analysed for free vibration problems by Tornabene et al. [90, 93, 91, 33, 92]. In the latter the attention has been primarily focused on FGM doubly-curved shells with variable radii of curvature. An extensive contribution in the thermo-mechanical analysis of FG beams has been provided by Batra et al. [55, 89]. Fiorenzo A. Fazzolari [37] studied the free vibration of metallic and FGM beams with general boundary conditions by using advanced and refined variable-kinematics quasi-3D beam models developed by using the method of power series expansion of displacement components.

Recently some interesting beam formulations have been provided by Yu, Hodges and co-authors [108, 107, 109]. They proposed the variational asymptotic method which led to the computer program variational asymptotic beam sectional analysis (VABS), which has been successfully used for several structural problems. The radial basis function (RBF)-pseudospectral method has been employed by Ferreira and Fasshauer [39] for the computation of natural frequencies of shear deformable beams and plates. The development of other hierarchical models is given in Ref. [19]. Exact beam formulations based on the dynamic stiffness method (DSM) have been proposed by Banerjee and co-authors [10, 11, 87]. Amin Ghorbani Shenas, Parviz Malekzadeh and Sima Ziaee studied the thermal buckling of pre-twisted FGM beams deriving the governing stability equations based on the third-order shear deformation theory (TSDT) in conjunction with the adjacent equilibrium state criterion under the Von Karman's non-linear assumptions using the Cherbyshev-Ritz method [41].

1.3.4 Rotating composite beams

The design of advanced rotor blades has been strongly affected by the advent of composite materials which combine a high specific strength and stiffness with the capability to be easily modeled. These properties produce light and efficient blades, whose dynamic characteristics usually involve phenomena that cannot be detected by the use of the classical models. For this reason, a considerable number of refined theories have been introduced with the purpose of describing the rotating composite blade behavior. For instance, Song and Librescu presented in [84] a structural model encompassing transverse shear, secondary warping deriving from the assumption of the non-uniform torsion along the longitudinal axis and the effect of the heterogeneity of the materials. They observed that by discarding the Coriolis term, the equations described separately the flap-lag deformation and the extension-twist motion, and within this context, they examined the ply orientation effects. Contrary to this ad hoc formulation, Chandiramani et al. provided a geometrically nonlinear theory for analyzing the rotating composite thin-walled box beam [24], in which the non-classical effects were captured in a general way. The linearized equations of motion were solved with the Modified Galerkin Method and the Coriolis term was disregarded. Furthermore, the authors modified their formulation for extension to pre-twisted composite blades [25]. See [66, 83], for interesting studies on controlling thin-walled composite blades via piezoelectric patches. Jung et al. [68] developed a one-dimensional finite element based on a mixed variational approach in which both displacement and force formulations were used. The walls of the considered structures were modeled as shell and the global deformation was described by the Timoshenko beam model. This model is suitable for composite structures with open and closed contour. The dynamic of the rotating composite blades clearly represents a complex and interesting topic (see [46, 67]), but it seems that a reliable and general method for its complete analysis is not yet available. In order to overcome the limitation of ad-hoc assumptions about the displacement fields, Carrera et al. presented the Carrera Unified Formulation (CUF) applied to the Finite Element Method [17].

Chapter 2

Structural Models

During the 16th century the *strength doctrine* was founded by Galileo Galilei. After his death Robert Hooke, first, and later Coulomb, continued developing the Theory of Elasticity. The *Da Vinci-Eulero-Bernoulli Beam Theory* was first enunciated in 1750 ca [94]. The classic beam theory is based on the assumption that plane cross sections remain plane. Furthermore, the physical assumption of Hooke on linear elasticity is made, which means that the strain distribution will vary linearly over the cross section.

In the early 20th century Stephen Timoshenko developed the *Timoshenko Beam Theory*. This model takes into account shear deformation and rotational bending effects. As a result thus allows to describe the behavior of thick beams, sandwich composite beams or beams subjected to a high-frequency excitation when the wavelength approaches the thickness of the beam.

These theory have represented the vanguard until the advent of modern computers in the end of the 20th century. Their computational power allows the use of high-order theories based on both, the axiomatic hypothesis method and the asymptotic expansion method. This methods permit a 3D problem to be reduced to a 1D problem [18].

The following sections focus on the different beam models and their fields of validity.

2.1 *Da Vinci-Eulero-Bernoulli* Beam Model

A fundamental assumption of the *Da Vinci-Eulero-Bernoulli* theory is that the cross-section of the beam is infinitely rigid in its own plane, *i.e.*, no deformation occur in the plane of the cross-section. Consequently, the in-plane displacement field can be represented by two rigid body translations and one rigid body rotation. This fundamental assumption deals only with in-plane displacements of the cross section. In addition, during deformation, the cross section is assumed to remain plane and normal to the deformed axe of the beam.

Consider a triad with coordinates $x_1, x_2,$ *and* $x_3, I = (\bar{i}_1, \bar{i}_2, \bar{i}_3)$. This set of axis is attached at a point of the beam cross-section. i_1, is along the axis of the beam, i_2 and i_3 define the plane of the cross section. The displacements in the directions $\bar{i}_1, \bar{i}_2$ and $\bar{i}_3$ are $u_1(x_1, x_2, x_3)$, $u_2(x_1, x_2, x_3)$, $u_3(x_1, x_2, x_3)$, respectively.

The first assumption states that the cross-section is undeformable in its own plane. Hence, the displacement field in the plane cross section consist of two rigid body translation, $\overline{u}_2(x_1)$ and $\overline{u}_3(x_1)$:

$$u_2(x_1, x_2, x_3) = \overline{u}_2(x_1) \qquad u_3(x_1, x_2, x_3) = \overline{u}_3(x_1) \tag{2.1}$$

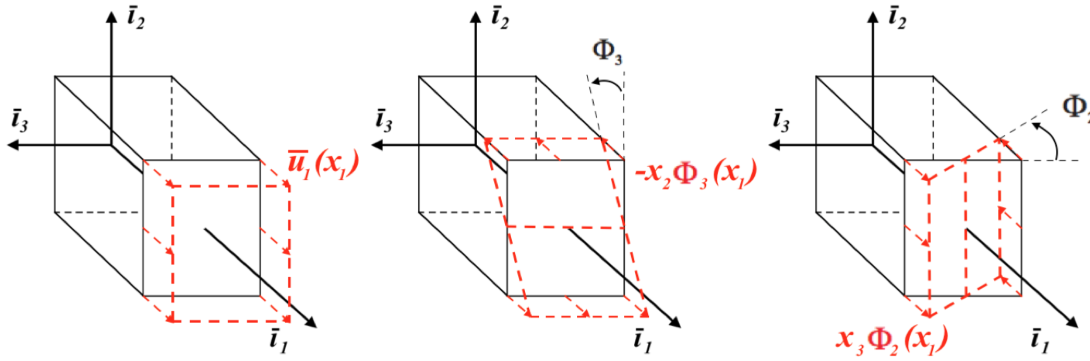

Figure 2.1. Schematic representation of the displacement field.

The second assumption states that the cross-section remain plane after deformation. This implies an axial displacement field consisting of a rigid body translation $\overline{u}_1(x_1)$, and two rigid body rotations $\Phi_2(x_1)$ and $\Phi_3(x_1)$. The axial displacement is than:

$$u_1(x_1, x_2, x_3) = \overline{u}_1(x_1) + x_3\Phi_2(x_1) - x_2\Phi_3(x_1) \tag{2.2}$$

Note the sign convention: the rigid body translations of the cross-section $\overline{u}_1(x_1)$, $\overline{u}_2(x_1)$, $\overline{u}_3(x_1)$, are positive in the direction of the axes $\bar{i}_1$, $\bar{i}_2$ and $\bar{i}_3$ respectively; the rigid rotations of the cross-section, $\Phi_2(x_1)$ and $\Phi_2(x_1)$, are positive abut the axes $\bar{i}_2$ and $\bar{i}_3$, respectively. The Fig. 2.2 depicts these various sign conventions.

The third assumption states that the cross-section remains normal to the deformed axis of the beam. As depicted in Fig. 2.3 this implies the equality of the slope of the beam and of the rotation of the section:

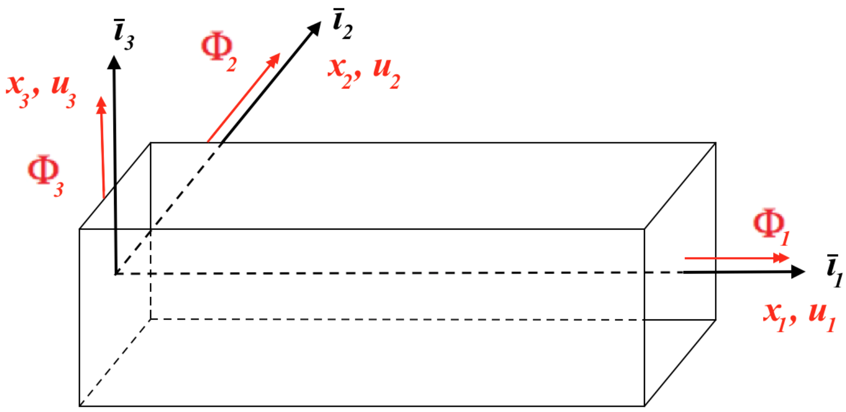

Figure 2.2. Sign convention for displacements and rotations of a beam.

$$\Phi_3(x_1) = \frac{\mathrm{d}\overline{u}_2(x_1)}{\mathrm{d}x_1} \qquad \Phi_2(x_1) = -\frac{\mathrm{d}\overline{u}_3(x_1)}{\mathrm{d}x_1} \tag{2.3}$$

The minus in the second equation is a consequence of the sign convention for the sectional displacements and rotations.

The equation (2.3) can be used to eliminate the sectional rotation from the axial displacement field. The complete displacement field for the *Da Vinci-Eulero-Bernoulli* beam model is:

$$\begin{cases} u_1(x_1, x_2, x_3) = \overline{u}_1(x_1) - x_3 \dfrac{\mathrm{d}\overline{u}_3(x_1)}{\mathrm{d}x_1} - x_2 \dfrac{\mathrm{d}\overline{u}_2(x_1)}{\mathrm{d}x_1} \\ u_2(x_1, x_2, x_3) = \overline{u}_2(x_1) \\ u_3(x_1, x_2, x_3) = \overline{u}_3(x_1) \end{cases} \tag{2.4}$$

The complete three-dimensional displacement field of the beam can therefore be expressed in terms of three sectional displacements, $\overline{u}_1(x_1)$, $\overline{u}_2(x_1)$, $\overline{u}_3(x_1)$ and their derivative with respect to x_1. This important simplification result from the assumptions made and allows the development of a one-dimensional beam theory, *i.e.*, a theory in which the unknown displacements are functions only of the span-wise coordinate, x_1.

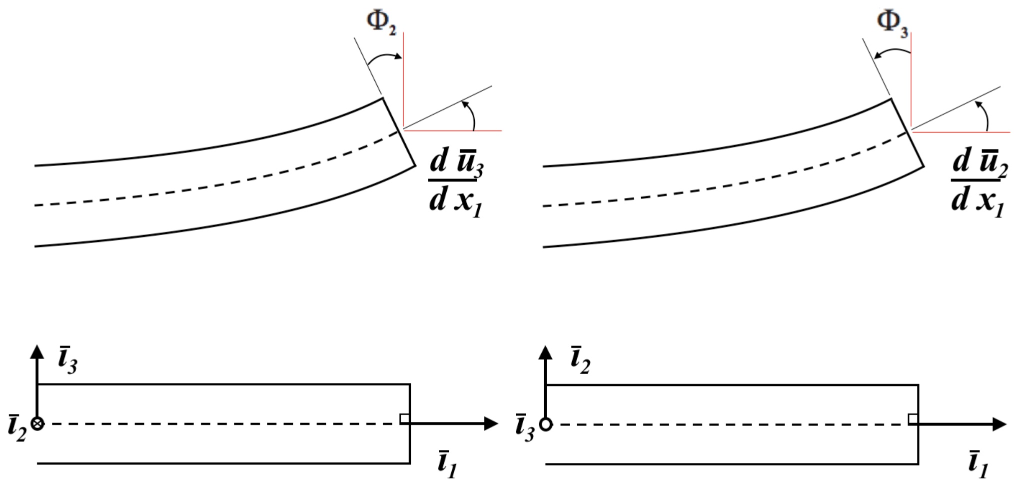

Figure 2.3. Beam slope and cross-sectional rotation for a *Eulero-Bernoulli* beam.

2.2 *Timoshenko* Beam Model

As for the *Da Vinci-Eulero-Bernoulli's* beam model, fundamental assumptions of the *Timoshenko's* theory are that the cross-section of the beam is infinitely rigid in its own plane, *i.e.*, no deformation occur in the plane of the cross-section, and that the cross-section of the beam remains plane after deformation. Consequently, the in-plane displacement field can be represented by two rigid body translations and one rigid body rotation. This fundamental assumption deals only with in-plane displacements of the cross section.

In contrast with the *Eulero-Bernoulli's* theory, in the *Timoshenko's* theory the plane of the cross-section can rotate with respect to the axe of the deformed beam. This rotation is due to a shear deformation, which is not included in the *Eulero-Bernoulli's* theory. Therefore the *Eulero-Bernoulli's* beam is stiffer.

As in the previous section, consider a triad with coordinates $x_1, x_2,\ and\ x_3, I = (\bar{i}_1, \bar{i}_2, \bar{i}_3)$. This set of axis is attached at a point of the beam cross-section. i_1, is along the axis of the beam, i_2 and i_3 define the plane of the cross section. The displacements in the directions $\bar{i}_1, \bar{i}_2$ and $\bar{i}_3$ are $u_1(x_1, x_2, x_3)$, $u_2(x_1, x_2, x_3)$, $u_3(x_1, x_2, x_3)$, respectively.

The first assumption states that the cross-section is undeformable in its own plane. Hence, the displacement field in the plane cross section consist of two rigid body translation, $\overline{u}_2(x_1)$ and $\overline{u}_3(x_1)$:

$$u_2(x_1, x_2, x_3) = \overline{u}_2(x_1) \qquad u_3(x_1, x_2, x_3) = \overline{u}_3(x_1) \tag{2.5}$$

The second assumption implies an axial displacement field consisting of a rigid body translation $\overline{u}_1(x_1)$, and two rigid body rotations $\Phi_2(x_1)$ and $\Phi_3(x_1)$. The axial displacement is than:

$$u_1(x_1, x_2, x_3) = \overline{u}_1(x_1) + x_3\Phi_2(x_1) - x_2\Phi_3(x_1) \tag{2.6}$$

The sign conventions and the decomposition of the axial displacement field are depicted, respectively, in Figure 2.1 and Figure 2.2.

In the *Timoshenko's* theory, the cross-section can rotate with respect to the axe of the deformed beam. Therefore the complete displacement field for the *Timoshenko* beam model is:

$$\begin{cases} u_1(x_1, x_2, x_3) = \overline{u}_1(x_1) + x_3\Phi_2(x_1) - x_2\Phi_3(x_1) \\ \\ u_2(x_1, x_2, x_3) = \overline{u}_2(x_1) \\ \\ u_3(x_1, x_2, x_3) = \overline{u}_3(x_1) \end{cases} \tag{2.7}$$

As a result of the last assumption, in this model the number of variables becomes five. In addition to the variables of the *Eulero-Bernoulli's* theory, $\overline{u}_1(x_1)$, $\overline{u}_2(x_1)$ and $\overline{u}_3(x_1)$, the model present two more variables, $\Phi_2(x_1)$ and $\Phi_3(x_1)$.

The Figure 2.4 depicts the beam slope and the cross-sectional rotation for a *Timoshenko* beam.

2.3 *Reddy's* Third-Order Beam Model

The third-order beam theory to be developed is based on the same assumptions as the classical and first-order beam theories, except that we relax the assumption on the straightness and normality of a transverse normal after deformation by expanding the displacements as cubic functions of the thickness coordinate.

In the *Reddy's* model the displacement field accommodates quadratic variations of the transverse shear strains (and hence stresses) and vanishing of traverse shear stresses on the top and bottom of a general laminate composed of monoclinic layers. Thus there is no need to use correction factors in a third-order theory. The number of dependent unknowns is reduced imposing traction-free boundary conditions on the top and bottom faces of the laminate ($\sigma_{x_1x_3}(x, y, \pm h/2, t) = 0$, $\sigma_{x_2x_3}(x, y, \pm h/2, t) = 0$). The third-order theories provide a slight increase in accuracy relative to the FSDT-*First order Shear Deformation Theory* (Timoshenko's Theory) solution, at the expense of an increase of computational effort [75].

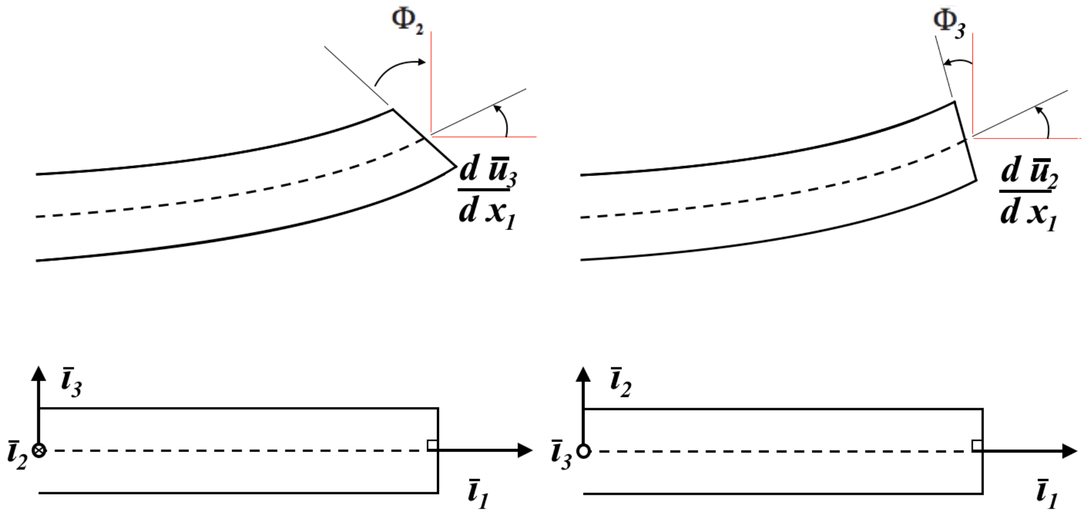

Figure 2.4. Beam slope and cross-sectional rotation for a *Timoshenko* beam.

The *Third-Order Beam Theory of Reddy* with transverse inextensibility is based on the following displacement field:

$$\begin{cases} u_1(x_1,x_2,x_3) = \overline{u}_1(x_1) + x_3\Phi_2(x_1) - x_3^3\dfrac{4}{3h^2}\left(\phi_2(x_1) + \dfrac{\partial\overline{u}_3(x_1)}{\partial x_1}\right) \\ \qquad\qquad -x_2\Phi_3(x_1) - x_2^3\dfrac{4}{3h^2}\left(\phi_3(x_1) + \dfrac{\partial\overline{u}_2(x_1)}{\partial x_1}\right) \\ u_2(x_1,x_2,x_3) = \overline{u}_2(x_1) \\ u_3(x_1,x_2,x_3) = \overline{u}_3(x_1) \end{cases} \tag{2.8}$$

As a result of the assumed displacement field, the cross-section can warp and rotate with respect to the axe of the deformed beam. Fig. 2.6 depicts the beam slope and cross-sectional rotation for a *Reddy's* beam.

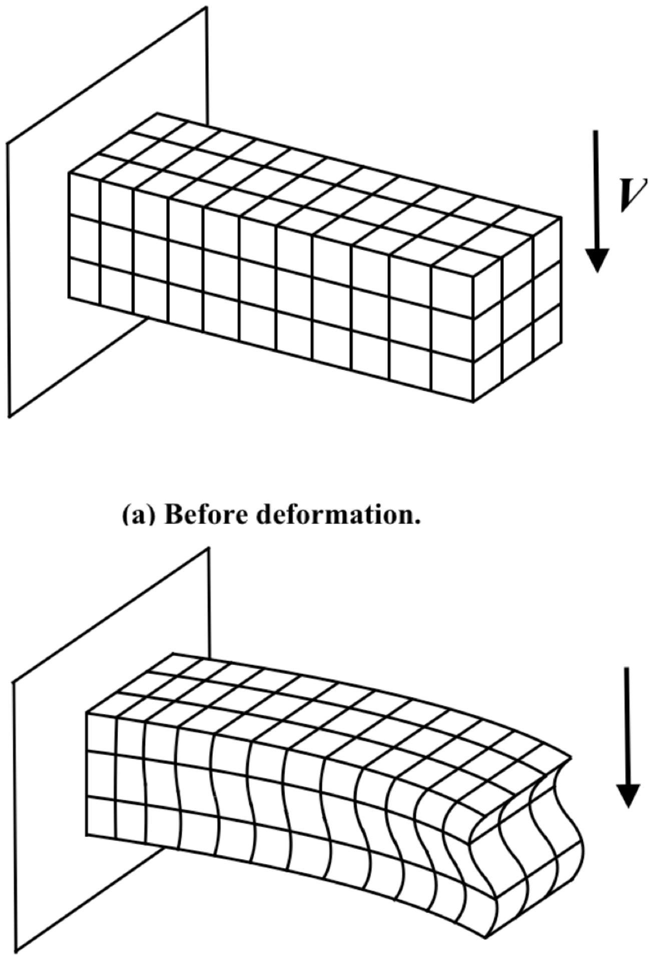

(a) Before deformation.

(b) After deformation.

Figure 2.5. Cross-sectional warping for a *Reddy* beam.

2.4 ***High Order*** Beam Model

The higher order beam theories allows a more accurate description of the beam kinematics, which is needed above all in unconventional structural mechanics applications such as static and dynamic analysis of beams subjected to multi-field loadings. By the use of the CUF-*Carrera Unified Formulation*, it is possible to develop a 1D structural model that requires in an axiomatic framework a 2D expansion of the generic function F_τ above the cross-section domain. In a compact

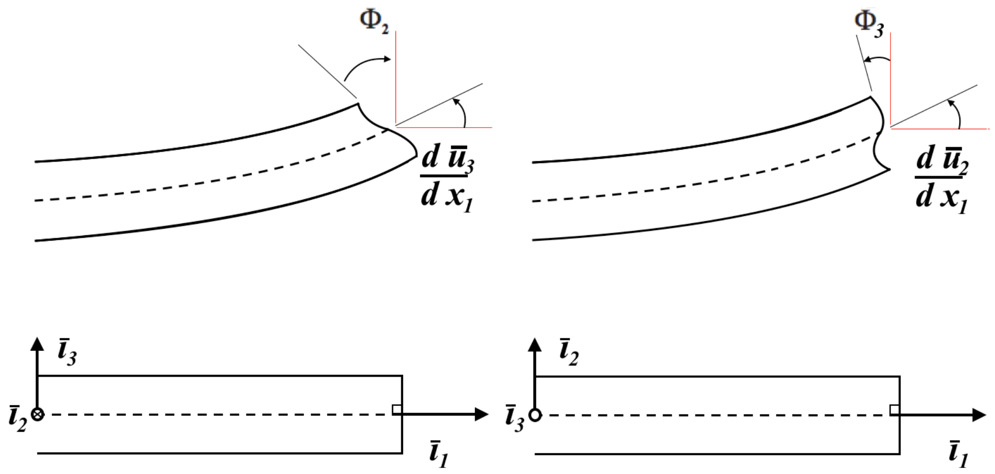

Figure 2.6. Beam slope and cross-sectional rotation for a *Reddy* beam.

notation the displacement field can be written as:

$$\boldsymbol{u}(x,y,z,t) = F_\tau(x,y)\ \boldsymbol{u}_\tau(z,t) \qquad \tau = 1,...,M \tag{2.9}$$

where F_τ is the expansion function, $\boldsymbol{u}_\tau$ is the vector of the unknown displacements and M is the number of the expansion terms[16]. The following aspects are of fundamental importance:

- F_τ can be of any-type. This means that one can assume polynomial expansions, Lagrange/Legendre polynomials, harmonics, exponentials, combinations of different expansions types, etc.

- M can be arbitrary. This means that the number of terms can be increased to any extent. According to [99], as $M \to \infty$, the 1D model solution coincides with the exact $3D$ solution independently of the problem characteristics.

For instance, a second-order model based on Taylor-like expansions ($N = 2$, $M = 6$) produce the following displacement fields:

$$u_x(x,y,z,t) = u_{x_1} + xu_{x_2} + yu_{x_3} + x^2u_{x_4} + xyu_{x_5} + y^2u_{x_6}$$
$$u_y(x,y,z,t) = u_{y_1} + xu_{y_2} + yu_{y_3} + x^2u_{y_4} + xyu_{y_5} + y^2u_{y_6} \tag{2.10}$$
$$u_z(x,y,z,t) = u_{z_1} + xu_{z_2} + yu_{z_3} + x^2u_{z_4} + xyu_{z_5} + y^2u_{z_6}$$

Refined Formulation

The proposed advanced computational technique is able to generate a class of beams theories in a systematic way. In particular each displacement variable in the displacement field is expanded at any desired order independently from the others and regarding on the results and computational cost. Thereby, the most general displacement field can be written as follows:

$$\begin{aligned} u_x(x,y,z,t) &= F_{\tau_{u_x}}(x,y)\ u_{x\tau_{u_x}}(z,t) \qquad && \tau_{u_x} = 1, ..., N_{u_x} \\ u_y(x,y,z,t) &= F_{\tau_{u_y}}(x,y)\ u_{y\tau_{u_y}}(z,t) \qquad && \tau_{u_y} = 1, ..., N_{u_y} \\ u_z(x,y,z,t) &= F_{\tau_{u_z}}(x,y)\ u_{z\tau_{u_z}}(z,t) \qquad && \tau_{u_z} = 1, ..., N_{u_z} \end{aligned} \tag{2.11}$$

The compact form of this expression is the Eq.2.9 where:

$$\boldsymbol{u}_\tau(z,t) = \begin{Bmatrix} u_{x\tau_{u_x}}(z,t) \\ u_{y\tau_{u_y}}(z,t) \\ u_{z\tau_{u_z}}(z,t) \end{Bmatrix} \qquad \boldsymbol{F}_\tau(x,y) = \begin{bmatrix} F_{\tau_{u_x}}(x,y) & 0 & 0 \\ 0 & F_{\tau_{u_y}}(x,y) & 0 \\ 0 & 0 & F_{\tau_{u_z}}(x,y) \end{bmatrix} \tag{2.12}$$

$F_{\tau_{u_x}}(x,y),\ F_{\tau_{u_y}}(x,y),\ F_{\tau_{u_z}}(x,y)$ are the cross section function; $u_{x\tau_{u_x}}(z,t)$, $u_{y\tau_{u_y}}(z,t)$, $u_{z\tau_{u_z}}(z,t)$ are the displacement vector components and and $N_{u_x},\ N_{u_y},\ N_{u_z}$ are the order of the expansions along the axes $x,\ y,\ z$, respectively. According to Einstein's notation, the repeated subscripts $\tau_{u_x},\ \tau_{u_y},\ \tau_{u_z}$ indicate summation. In addition, choosing the cross-section functions to be Taylor's series expansion the Eq.2.11 can be rewritten as:

$$
\begin{aligned}
u_x(x,y,z,t) &= \sum_{n_{u_x}=0}^{N_{u_x}} \left[\sum_{n^*_{u_x}=0}^{n_{u_x}} x^{(n_{u_x}-n^*_{u_x})} y^{n^*_{u_x}} u_{x_{\overline{N}_{u_x}}}(z,t) \right] \\
u_y(x,y,z,t) &= \sum_{n_{u_y}=0}^{N_{u_y}} \left[\sum_{n^*_{u_y}=0}^{n_{u_y}} x^{(n_{u_y}-n^*_{u_y})} y^{n^*_{u_y}} u_{y_{\overline{N}_{u_y}}}(z,t) \right] \\
u_z(x,y,z,t) &= \sum_{n_{u_z}=0}^{N_{u_z}} \left[\sum_{n^*_{u_z}=0}^{n_{u_z}} x^{(n_{u_z}-n^*_{u_z})} y^{n^*_{u_z}} u_{z_{\overline{N}_{u_z}}}(z,t) \right]
\end{aligned}
\tag{2.13}
$$

where $\overline{N}_u = \frac{n_u(n_u+1)+2(n^*_u+1)}{2}$.The total number of degree of freedoms (DOFs) involved in a generic analysis when using the present model is:

$$
DOFs^{TE} = \left[\frac{(N_{u_x}+1)(N_{u_x}+2)}{2} + \frac{(N_{u_y}+1)(N_{u_y}+2)}{2} + \frac{(N_{u_z}+1)(N_{u_z}+2)}{2} \right]
\tag{2.14}
$$

An example of a possible displacement field with a second-order model based on Taylor-like expansions ($N_{u_x} = 2$, $N_{u_y} = 2$ and $N_{u_z} = 1$) follows:

$$
\begin{aligned}
u_x(x,y,z,t) &= u_{x_1} + x u_{x_2} + y u_{x_3} + x^2 u_{x_4} + xy u_{x_5} + y^2 u_{x_6} \\
u_y(x,y,z,t) &= u_{y_1} + x u_{y_2} + y u_{y_3} + x^2 u_{y_4} + xy u_{y_5} + y^2 u_{y_6} \\
u_z(x,y,z,t) &= u_{z_1} + x u_{z_2} + y u_{z_3}
\end{aligned}
\tag{2.15}
$$

In this case, the 1D model has 18 unknown displacement variables.

An other example of possible functions that could be used to approximate the beam cross-section kinematics are the exponential functions. According to this functions choice, the expansion takes the following form:

$$
\begin{aligned}
u_x(x,y,z,t) &= u_{x_0}(z,t) + \sum_{m=1}^{N_{u_x}} \left[e^{\left(\frac{mx}{h}\right)} u_{x_{2m}}(z,t) + e^{\left(\frac{my}{b}\right)} u_{x_{2m+1}}(z,t) \right] \\
u_y(x,y,z,t) &= u_{y_0}(z,t) + \sum_{m=1}^{N_{u_y}} \left[e^{\left(\frac{mx}{h}\right)} u_{y_{2m}}(z,t) + e^{\left(\frac{my}{b}\right)} u_{y_{2m+1}}(z,t) \right] \\
u_z(x,y,z,t) &= u_{z_0}(z,t) + \sum_{m=1}^{N_{u_z}} \left[e^{\left(\frac{mx}{h}\right)} u_{z_{2m}}(z,t) + e^{\left(\frac{my}{b}\right)} u_{z_{2m+1}}(z,t) \right]
\end{aligned}
\tag{2.16}
$$

Using the present model the total number of DOFs involved is:

$$
DOFs^{TE} = \left[(2N_{u_x} + 1) + \left(2N_{u_y} + 1\right) + (2N_{u_z} + 1) \right] \tag{2.17}
$$

For instance, a possible displacement field according to the present approach and by using expansion orders $N_{u_x} = 2$, $N_{u_y} = 2$ and $N_{u_z} = 1$ is given in Eq.2.18:

$$
\begin{aligned}
u_x(x,y,z,t) &= u_{x_0}(z,t) + e^{\left(\frac{x}{h}\right)} u_{x_1}(z,t) + e^{\left(\frac{y}{b}\right)} u_{x_2}(z,t) + e^{\left(\frac{2x}{h}\right)} u_{x_3}(z,t) + e^{\left(\frac{2y}{b}\right)} u_{x_4}(z,t) \\
u_y(x,y,z,t) &= u_{y_0}(z,t) + e^{\left(\frac{x}{h}\right)} u_{y_1}(z,t) + e^{\left(\frac{y}{b}\right)} u_{y_2}(z,t) + e^{\left(\frac{2x}{h}\right)} u_{y_3}(z,t) + e^{\left(\frac{2y}{b}\right)} u_{y_4}(z,t) \\
u_z(x,y,z,t) &= u_{z_0}(z,t) + e^{\left(\frac{x}{h}\right)} u_{z_1}(z,t) + e^{\left(\frac{y}{b}\right)} u_{z_2}(z,t)
\end{aligned}
\tag{2.18}
$$

Then when the cross-section functions are chosen to be trigonometric functions, the displacement field can be expanded accordingly as follows:

$$u_x(x,y,z,t) = u_{x_0}(z,t) + \sum_{m=1}^{N_{u_x}} [sin\left(\frac{mx}{h}\right) u_{x_{4m-2}}(z,t) + sin\left(\frac{my}{b}\right) u_{x_{4m-1}}(z,t) +$$
$$+cos\left(\frac{mx}{h}\right) u_{x_{4m}}(z,t) + cos\left(\frac{my}{b}\right) u_{x_{4m+1}}(z,t)]$$
$$u_y(x,y,z,t) = u_{y_0}(z,t) + \sum_{m=1}^{N_{u_y}} [sin\left(\frac{mx}{h}\right) u_{x_{4m-2}}(z,t) + sin\left(\frac{my}{b}\right) u_{y_{4m-1}}(z,t) +$$
$$+cos\left(\frac{mx}{h}\right) u_{y_{4m}}(z,t) + cos\left(\frac{my}{b}\right) u_{y_{4m+1}}(z,t)]$$
$$u_z(x,y,z,t) = u_{z_0}(z,t) + \sum_{m=1}^{N_{u_z}} [sin\left(\frac{mx}{h}\right) u_{z_{4m-2}}(z,t) + sin\left(\frac{my}{b}\right) u_{z_{4m-1}}(z,t) +$$
$$+cos\left(\frac{mx}{h}\right) u_{z_{4m}}(z,t) + cos\left(\frac{my}{b}\right) u_{z_{4m+1}}(z,t)] \tag{2.19}$$

The total number of DOFs involved in the expansion is:

$$DOFs^{TE} = \left[(4N_{u_x}+1) + \left(4N_{u_y}+1\right) + (4N_{u_z}+1)\right] \tag{2.20}$$

As for the previous case, according to the here developed beam model and by selecting the expansion orders as $N_{u_x} = 2$, $N_{u_y} = 2$ and $N_{u_z} = 1$ the displacement field takes the following form:

$$u_x(x,y,z,t) = u_{x_0}(z,t) + sin\left(\frac{x}{h}\right) u_{x_1}(z,t) + sin\left(\frac{y}{b}\right) u_{x_2}(z,t) + cos\left(\frac{x}{h}\right) u_{x_3}(z,t) +$$
$$+cos\left(\frac{y}{b}\right) u_{x_4}(z,t) + sin\left(\frac{2x}{h}\right) u_{x_5}(z,t) + sin\left(\frac{2y}{b}\right) u_{x_6}(z,t) +$$
$$+cos\left(\frac{2x}{h}\right) u_{x_7}(z,t) + +cos\left(\frac{2y}{b}\right) u_{x_8}(z,t)$$
$$u_y(x,y,z,t) = u_{y_0}(z,t) + sin\left(\frac{x}{h}\right) u_{y_1}(z,t) + sin\left(\frac{y}{b}\right) u_{y_2}(z,t) + cos\left(\frac{x}{h}\right) u_{y_3}(z,t) +$$
$$+cos\left(\frac{y}{b}\right) u_{y_4}(z,t) + sin\left(\frac{2x}{h}\right) u_{y_5}(z,t) + sin\left(\frac{2y}{b}\right) u_{y_6}(z,t) +$$
$$+cos\left(\frac{2x}{h}\right) u_{y_7}(z,t) + +cos\left(\frac{2y}{b}\right) u_{y_8}(z,t)$$
$$u_z(x,y,z,t) = u_{z_0}(z,t) + sin\left(\frac{x}{h}\right) u_{z_1}(z,t) + sin\left(\frac{y}{b}\right) u_{z_2}(z,t) + cos\left(\frac{x}{h}\right) u_{z_3}(z,t) +$$
$$+cos\left(\frac{y}{b}\right) u_{z_4}(z,t) \tag{2.21}$$

Among all the functions presented in this section, the Taylor-like expansions own a good computational stability, allowing generally to reach a high level of accuracy in various structural applications featured by $3D$ effects [36]. Thus these have been adopted in the *Refined Method.*

Chapter 3

Governing Equations-weak form, Ritz Method and admissible functions

In order obtain the weak form of the governing equations, the Principle of Virtual Displacements (PVD) is employed to derive the Hierarchical Ritz Formulation (HRF).

The PVD variational statement, in its classical form, can be written as follow:

$$\delta L_{int} = \delta L_{ext} - \delta L_{ine} \tag{3.1}$$

where $\delta L_{int}, \delta L_{ext}, \delta L_{ine}$, are the virtual internal work, the virtual external work and the virtual inertial work, respectively.

When dealing with dynamics problems, Hamilton's principle can be alternatively used. The latter can be expressed as:

$$\int_{t_1}^{t_2} \delta \mathcal{L} \; dt = 0 \tag{3.2}$$

where t_1 *and* t_2 are the initial and the generic instant of time; $\mathcal{L}$ is the Lagrangian which assumes the following form:

$$\mathcal{L} = T - \Pi, \quad with \;\; \Pi = U + V \tag{3.3}$$

T is the kinetic energy and Π is the total potential energy of the system; U and V are the potential strain energy and the potential energy due to the eternal forces, respectively.

The PVD can be easily derived by Hamilton's principle [34], indeed the following relations hold:

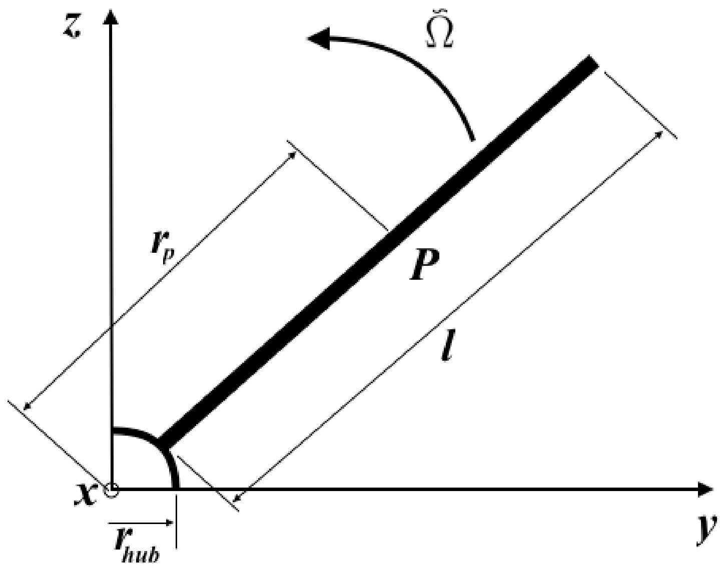

Figure 3.1. Schematic representation of the rotating reference frame.

$$\delta L_{int} = \delta U \qquad \delta L_{ext} = -\delta V \qquad \delta L_{ine} = -\delta T \tag{3.4}$$

The variation of the kinetic energy, T, is:

$$\delta T = \delta \int_V \frac{1}{2}\rho(\boldsymbol{v}^T\boldsymbol{v})dV = \delta \int_V \frac{1}{2}\rho[\dot{\boldsymbol{u}} + \tilde{\boldsymbol{\Omega}}(\boldsymbol{u}+\boldsymbol{r})]^T[\dot{\boldsymbol{u}} + \tilde{\boldsymbol{\Omega}}(\boldsymbol{u}+\boldsymbol{r})]dV \tag{3.5}$$

where $\boldsymbol{v} = \dot{\boldsymbol{u}} + \tilde{\boldsymbol{\Omega}}(\boldsymbol{u}+\boldsymbol{r})$ is the absolute velocity of the generic point P, $\tilde{\boldsymbol{\Omega}}$ is the angolar velocity and $\boldsymbol{r}$ is the distance from the rotation axe:

$$\tilde{\boldsymbol{\Omega}} = \begin{bmatrix} 0 & 0 & 0 \\ 0 & 0 & \tilde{\Omega} \\ 0 & -\tilde{\Omega} & 0 \end{bmatrix} \qquad \boldsymbol{r} = \begin{Bmatrix} 0 \\ y_p + r_{hub} \\ z_p + r_{hub} \end{Bmatrix} \tag{3.6}$$

r_{hub} is the radius of the hub (see Fig.3.1).

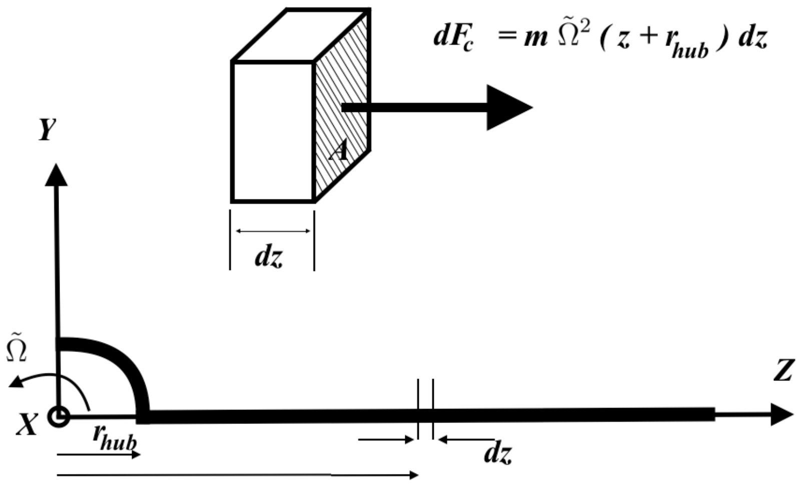

Figure 3.2. Centrifugal force on a beam element.

The body can be loaded by static stresses, such as the the centrifugal stress σ_0. In order to take into account this effect, according with the linearized theory, the potential energy can be written in the following form:

$$U = \int_V \frac{1}{2}(\boldsymbol{\varepsilon}^T \boldsymbol{\sigma})dV + \int_V \frac{1}{2}(\boldsymbol{\varepsilon}_{\boldsymbol{nl}}^T \boldsymbol{\sigma_0})dV \tag{3.7}$$

The centrifugal force to which an infinitesimal element of a beam is subjected is given by:

$$dF_c = m\tilde{\Omega}^2(z + r_{hub})dz = \rho A\tilde{\Omega}^2(z + r_{hub})dz \tag{3.8}$$

where dz is the length of the element, $(z + r_{hub})$ is the distance of the element from the axe of rotation, $\tilde{\Omega}$ is the angular velocity and m is the mass for unit of length. Dividing the elementary centrifugal force for the cross-section area of the element, it is possible to obtain the elementary centrifugal stress:

$$d\sigma_0 = \frac{dF_c}{A} = \rho\tilde{\Omega}^2(z + r_{hub})dz \tag{3.9}$$

Integrating along the axe of the beam between a generic position z and the length of the beam l, the centrifugal stress on a generic section of the rotating beam:

$$\sigma_0 = \int_\sigma d\sigma_0 = \int_l \rho\tilde{\Omega}^2(z + r_{hub})dz = \rho\tilde{\Omega}^2 \left[\frac{l^2}{2} - \frac{z^2}{2} + r_{hub}(l - z)\right] \tag{3.10}$$

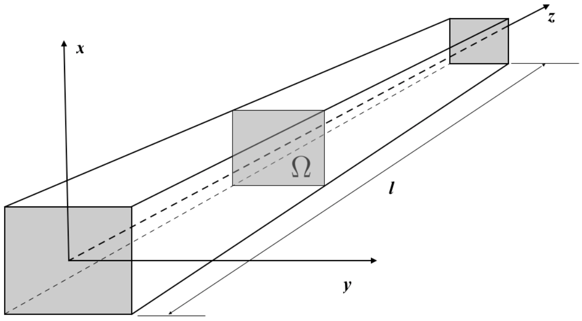

Figure 3.3. Tapered beam structure and coordinate system.

As a consequence the Eq.3.1 can be expressed, in case of a variable cross-section beam, Ω, along the beam spam (see Fig.3.3):

$$\begin{aligned}&\int_l\int_\Omega \delta\boldsymbol{\varepsilon}^T\boldsymbol{\sigma}\ d\Omega\ dl + \int_l\int_\Omega \delta\boldsymbol{\varepsilon}_{\boldsymbol{nl}}^T\boldsymbol{\sigma_0}\ d\Omega\ dl = \delta L_{ext} - \int_l\int_\Omega \rho\delta\boldsymbol{u}^T\ddot{\boldsymbol{u}}\ d\Omega\ dl + \\ &-\int_l\int_\Omega \rho\delta\boldsymbol{u}^T\tilde{\boldsymbol{\Omega}}^T\dot{\boldsymbol{u}}\ d\Omega\ dl + \int_l\int_\Omega \tfrac{1}{2}\rho\delta\boldsymbol{u}^T\tilde{\boldsymbol{\Omega}}^T\tilde{\boldsymbol{\Omega}}\boldsymbol{u}\ d\Omega\ dl + \int_l\int_\Omega \rho\delta\boldsymbol{u}^T\tilde{\boldsymbol{\Omega}}^T\tilde{\boldsymbol{\Omega}}\boldsymbol{r}\ d\Omega\ dl\end{aligned} \tag{3.11}$$

According to the Hooke's law $\boldsymbol{\sigma} = \boldsymbol{C}\boldsymbol{\varepsilon}$, thus:

$$\begin{aligned}&\int_l\int_\Omega \delta\boldsymbol{\varepsilon}^T\boldsymbol{C}\boldsymbol{\varepsilon}\ d\Omega\ dl + \int_l\int_\Omega \delta\boldsymbol{\varepsilon}_{\boldsymbol{nl}}^T\boldsymbol{\sigma_0}\ d\Omega\ dl = \delta L_{ext} - \int_l\int_\Omega \rho\delta\boldsymbol{u}^T\ddot{\boldsymbol{u}}\ d\Omega\ dl + \\ &-\int_l\int_\Omega \rho\delta\boldsymbol{u}^T\tilde{\boldsymbol{\Omega}}^T\dot{\boldsymbol{u}}\ d\Omega\ dl + \int_l\int_\Omega \tfrac{1}{2}\rho\delta\boldsymbol{u}^T\tilde{\boldsymbol{\Omega}}^T\tilde{\boldsymbol{\Omega}}\boldsymbol{u}\ d\Omega\ dl + \int_l\int_\Omega \rho\delta\boldsymbol{u}^T\tilde{\boldsymbol{\Omega}}^T\tilde{\boldsymbol{\Omega}}\boldsymbol{r}\ d\Omega\ dl\end{aligned} \tag{3.12}$$

In the Ritz method the displacement amplitude vector components $u_{x\tau_{u_x}}$, $u_{y\tau_{u_y}}$ and $u_{z\tau_{u_z}}$, are expressed in series expansion, assuming N as as the order of expansion in the approximation:

$$
\begin{aligned}
u_{x\tau_{u_x}}(z,t) &= \sum_{i}^{N} U_{x\tau_{u_x}i}\psi_{x_i}(z)e^{\bar{i}\omega_{ij}t} \\
u_{y\tau_{u_y}}(z,t) &= \sum_{i}^{N} U_{y\tau_{u_y}i}\psi_{y_i}(z)e^{\bar{i}\omega_{ij}t} \\
u_{z\tau_{u_z}}(z,t) &= \sum_{i}^{N} U_{z\tau_{u_z}i}\psi_{z_i}(z)e^{\bar{i}\omega_{ij}t}
\end{aligned}
\tag{3.13}
$$

where $\bar{i} = \sqrt{-1}$, t is the time and ω_{ij} the circular frequency; $U_{x\tau_{u_x}i}$, $U_{y\tau_{u_y}i}$ $U_{z\tau_{u_z}i}$ are the unknown coefficients and $\psi_{x_i}, \psi_{y_i}, \psi_{z_i}$ are the Ritz functions selected with respect to the features of the problem under investigation.

The convergence to the exact solution is guaranteed if the Ritz functions are admissible functions in the used variational principle [34, 76, 74, 35].

The Ritz functions used are a set of algebraic functions which satisfy the geometric boundary conditions. In particular, setting N as the order in the Ritz approximation, they assume the following form:

$$
\begin{aligned}
\psi_{x_i}(z) &= z^{p_x}(l-z)^{q_x}z^i - 1 \qquad i = 1,2,3,...,N \\
\psi_{y_i}(z) &= z^{p_y}(l-z)^{q_y}z^i - 1 \qquad i = 1,2,3,...,N \\
\psi_{z_i}(z) &= z^{p_x}(l-z)^{q_z}z^i - 1 \qquad i = 1,2,3,...,N
\end{aligned}
\tag{3.14}
$$

where l is the length of the beam, p_k and q_k, with $k = x, y, z$, assume the values 0,1,2 for free (F), simply supported (SS) and clamped (C) boundary conditions, respectively.

In order to enhance the computational stability, the Ritz functions have been orthogonalized in the domain $[0, l]$ via the Gram-Smith process [44]. The first member of the orthogonal polynomial set $\psi_{k_1}(z)$ is chosen as the simplest polynomial of the last order that satisfies the natural boundary conditions of the beam. The other members of the orthogonal set in the interval $[0, l]$ are generated by using the following recursive procedure:

$$
\begin{aligned}
\psi_{k_2}(z) &= (z - B_2)\psi_{k_1}(z) \\
\psi_{k_3}(z) &= (z - B_3)\psi_{k_2}(z) - C_3\psi_{k_1}(z) \\
&\vdots \\
\psi_{k_i}(z) &= (z - B_i)\psi_{k_{i-1}}(z) - C_3\psi_{k_{i-2}}(z) \\
&\vdots \\
\psi_{k_N}(z) &= (z - B_{N-1})\psi_{k_{N-1}}(z) - C_N\psi_{k_{N-2}}(z)
\end{aligned}
\tag{3.15}
$$

where

$$
\begin{aligned}
B_i &= \frac{\int_0^l w(z) z \phi_{k_{i-1}}^2(z)\ dz}{\int_0^l w(z)\phi_{k_{i-1}}^2(z)\ dz} \\
C_i &= \frac{\int_0^l w(z) z \phi_{k_{i-1}}(z)\phi_{k_{i-2}}(z)\ dz}{\int_0^l w(z)\phi_{k_{i-2}}^2(z)\ dz}
\end{aligned}
\tag{3.16}
$$

with $k = x, y, z$.

The polynomials ϕ_{k_i} satisfy the orthogonality condition:

$$
\int_0^l w(z)\phi_{k_i}(z)\phi_{k_j}(z)dz = \Lambda_{ij}\begin{cases} = 0\ for\ i \neq j \\ \neq 0\ for\ i = j \end{cases}
\tag{3.17}
$$

with $i, j = 1, ..., N$, $w(z)$ is the weight function. In the particular case of uniform beams $w(z) = 1$. In the case of study, $w(z)$, is a specific function of z.

The displacement field is then given, substituting the Eq.3.13 in the Eq.2.11:

$$\begin{cases} u_x(x,y,z,t) = \sum_i^N U_{x\tau_{ux}i} F_{\tau_{ux}} \psi_{x_i}(z) e^{\bar{i}\omega_{ij}t} \\ \\ u_y(x,y,z,t) = \sum_i^N U_{y\tau_{uy}i} F_{\tau_{uy}} \psi_{y_i}(z) e^{\bar{i}\omega_{ij}t} \\ \\ u_z(x,y,z,t) = \sum_i^N U_{z\tau_{uz}i} F_{\tau_{uz}} \psi_{z_i}(z) e^{\bar{i}\omega_{ij}t} \end{cases} \tag{3.18}$$

In a compact form:

$$\mathbf{u} = \mathbf{F}_\tau \mathbf{U}_{\tau i} \Psi_i \tag{3.19}$$

where:

$$\mathbf{U}_{\tau i}(t) = e^{\bar{i}\omega_{ij}t} \begin{Bmatrix} U_{x\tau_{ux}i} \\ U_{y\tau_{uy}i} \\ U_{z\tau_{uz}i} \end{Bmatrix}, \quad \Psi_i(z) = \begin{bmatrix} \psi_{x_i}(z) & 0 & 0 \\ 0 & \psi_{y_i}(z) & 0 \\ 0 & 0 & \psi_{z_i}(z) \end{bmatrix} \tag{3.20}$$

The stresses, $\boldsymbol{\sigma}$, and strains, $\boldsymbol{\varepsilon}$, are grouped as follows:

$$\begin{aligned} \boldsymbol{\sigma}_{pH} &= \begin{Bmatrix} \sigma_{xx} \\ \\ \sigma_{yy} \\ \\ \tau_{xy} \end{Bmatrix} \qquad & \boldsymbol{\varepsilon}_{pG} &= \begin{Bmatrix} \varepsilon_{xx} \\ \\ \varepsilon_{yy} \\ \\ \gamma_{xy} \end{Bmatrix} \\ \boldsymbol{\sigma}_{nG} &= \begin{Bmatrix} \tau_{xz} \\ \\ \tau_{yz} \\ \\ \gamma_{zz} \end{Bmatrix} \qquad & \boldsymbol{\varepsilon}_{nG} &= \begin{Bmatrix} \gamma_{xz} \\ \\ \gamma_{yz} \\ \\ \varepsilon_{zz} \end{Bmatrix} \end{aligned} \tag{3.21}$$

The subscripts n and p denote out-of-plane and in-plane components, respectively, whilst the subscripts H and G state the Hooke's law and Geometric relations are used. The strain-displacement relations are:

$$\begin{aligned} \boldsymbol{\varepsilon}_{pG} &= \boldsymbol{D}_p \boldsymbol{u} \\ \boldsymbol{\varepsilon}_{nG} &= \boldsymbol{D}_n \boldsymbol{u} = (\boldsymbol{D}_{np} + \boldsymbol{D}_{nz}) \boldsymbol{u} \end{aligned} \tag{3.22}$$

where $\boldsymbol{D}_p, \boldsymbol{D}_n, \boldsymbol{D}_{np}, \boldsymbol{D}_{nz}$ are differential matrix operators defined as follows:

$$\boldsymbol{D}_p = \begin{bmatrix} \frac{\partial}{\partial x} & 0 & 0 \\ 0 & \frac{\partial}{\partial y} & 0 \\ \frac{\partial}{\partial y} & \frac{\partial}{\partial x} & 0 \end{bmatrix} \qquad \boldsymbol{D}_n = \begin{bmatrix} \frac{\partial}{\partial z} & 0 & \frac{\partial}{\partial x} \\ 0 & \frac{\partial}{\partial z} & \frac{\partial}{\partial y} \\ 0 & 0 & \frac{\partial}{\partial z} \end{bmatrix}$$
$$\boldsymbol{D}_{np} = \begin{bmatrix} 0 & 0 & \frac{\partial}{\partial x} \\ 0 & 0 & \frac{\partial}{\partial y} \\ 0 & 0 & 0 \end{bmatrix} \qquad \boldsymbol{D}_{nz} = \begin{bmatrix} \frac{\partial}{\partial z} & 0 & 0 \\ 0 & \frac{\partial}{\partial z} & 0 \\ 0 & 0 & \frac{\partial}{\partial z} \end{bmatrix} \tag{3.23}$$

According to Hooke's law, the 3D constitutive equations are given as:

$$\boldsymbol{\sigma} = \boldsymbol{C}(x)\ \boldsymbol{\varepsilon} \tag{3.24}$$

By using Eq.3.21, the Above equation becames:

$$\begin{aligned} \boldsymbol{\sigma}_{pH} &= \boldsymbol{C}_{pp}(x)\boldsymbol{\varepsilon}_{pG} + \boldsymbol{C}_{pn}(x)\boldsymbol{\varepsilon}_{nG} \\ \boldsymbol{\sigma}_{nH} &= \boldsymbol{C}_{np}(x)\boldsymbol{\varepsilon}_{pG} + \boldsymbol{C}_{nn}(x)\boldsymbol{\varepsilon}_{nG} \end{aligned} \tag{3.25}$$

where matrices $\boldsymbol{C}_{pp}(x), \boldsymbol{C}_{pn}(x), \boldsymbol{C}_{pn}(x), \boldsymbol{C}_{np}(x), \boldsymbol{C}_{nn}(x)$ are:

$$\boldsymbol{C}_{pp}(x) = \begin{bmatrix} C_{11}(x) & C_{12}(x) & 0 \\ C_{12}(x) & C_{22}(x) & 0 \\ 0 & 0 & C_{66}(x) \end{bmatrix} \qquad \boldsymbol{C}_{pn}(x) = \begin{bmatrix} 0 & 0 & C_{13}(x) \\ 0 & 0 & C_{23}(x) \\ 0 & 0 & 0 \end{bmatrix}$$

$$\boldsymbol{C}_{np}(x) = \begin{bmatrix} 0 & 0 & 0 \\ 0 & 0 & 0 \\ C_{13}(x) & C_{23}(x) & 0 \end{bmatrix} \qquad \boldsymbol{C}_{nn}(x) = \begin{bmatrix} C_{55}(x) & 0 & 0 \\ 0 & C_{44}(x) & 0 \\ 0 & 0 & C_{33}(x) \end{bmatrix} \tag{3.26}$$

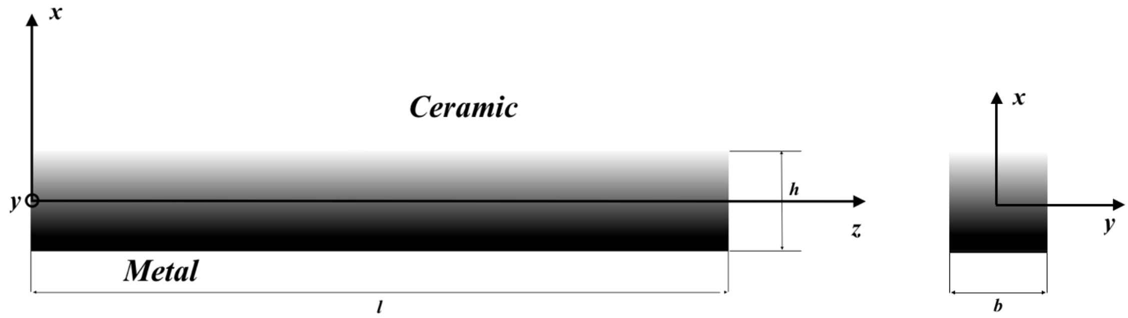

Figure 3.4. FG beam structure.

Referring to Fig.3.4, the volume fraction of the ceramic phase is defined according to the following power-low:

$$V_c(x) = \left(\frac{1}{2} + \frac{x}{h}\right)^p \qquad x \in \left[-\frac{h}{2}, \frac{h}{2}\right] \tag{3.27}$$

where h is the thickness of the beam and the exponent p is the volume fraction index indicating the material variation through the thickness direction.

The volume fraction of the metal phase is given as $V_m(x) = 1 - V_c(x)$. Young's modulus E, Poisson's coefficient ν, and density ρ are computed by means of the following *Rule-Of-Mixture* (ROM):

$$\begin{cases} E(x) = (E_c - E_m)V_c(x) + E_m \\ \nu(x) = (\nu_c - \nu_m)V_c(x) + \nu_m \\ \rho(x) = (\rho_c - \rho_m)V_c(x) + \rho_m \end{cases} \tag{3.28}$$

Finally the effective FG material coefficients $C_{ij}(x)$, derived after careful considerations based on micro-mechanical approaches [37], are given as follows:

$$\begin{cases} C_{11} = C_{22} = C_{33} = \lambda(x) + 2G(x) \\ C_{12} = C_{13} = C_{23} = \lambda(x) \\ C_{44} = C_{55} = C_{66} = G(x) \end{cases} \tag{3.29}$$

where λ is the Lam$\acute{e}$ coefficients, and G is the shear modulus. For the sake of completeness their explicit expressions are given below:

$$\begin{aligned} \lambda(x) &= \frac{\nu(x)E(x)}{(1+\nu)(1-2\nu)} \\ G(x) &= \frac{E(x)}{2(1+\nu)} \end{aligned} \tag{3.30}$$

Combining the strain-displacement relation Eq.3.22 and Eq.3.19, the geometric relations can be written in terms of Ritz functions:

$$\begin{aligned} \varepsilon_{pG} &= \mathbf{D}_p(\mathbf{F}_\tau \Psi_i)\mathbf{U}_{\tau i} \\ \varepsilon_{nG} &= \mathbf{D}_{np}(\mathbf{F}_\tau \Psi_i)\mathbf{U}_{\tau i} + \mathbf{D}_{nz}(\mathbf{F}_\tau \Psi_i)\mathbf{U}_{\tau i} \end{aligned} \tag{3.31}$$

By substituting the previous expression in Eq.3.12 the explicit expressions of the internal work, split in its four contributions, can be obtained as:

$$
\begin{aligned}
&\delta(L_{int})_{pp} = \int_l \int_\Omega \delta\boldsymbol{\varepsilon}_{pG}^T \boldsymbol{C}_{pp} \boldsymbol{\varepsilon}_{pG} \; d\Omega \; dl = \\
&= \delta\mathbf{U}_{\tau i}^T \left(\int_l \int_\Omega ([\mathbf{D}_p(\mathbf{F}_\tau \Psi_i)]^T \; \boldsymbol{C}_{pp} \; \mathbf{D}_p(\mathbf{F}_s \Psi_j)) \; d\Omega \; dl \right) \mathbf{U}_{sj} \\
&\delta(L_{int})_{pn} = \int_l \int_\Omega \delta\boldsymbol{\varepsilon}_{pG}^T \boldsymbol{C}_{pn} \boldsymbol{\varepsilon}_{nG} \; d\Omega \; dl = \\
&= \delta\mathbf{U}_{\tau i}^T (\int_l \int_\Omega ([\mathbf{D}_p(\mathbf{F}_\tau \Psi_i)]^T \; \boldsymbol{C}_{pn} \; \mathbf{D}_{np}(\mathbf{F}_s \Psi_j) + \\
&+ [\mathbf{D}_p(\mathbf{F}_\tau \Psi_i)]^T \; \boldsymbol{C}_{pn} \; \mathbf{D}_{nz}(\mathbf{F}_s \Psi_j)) \; d\Omega \; dl) \mathbf{U}_{sj} \\
&\delta(L_{int})_{np} = \int_l \int_\Omega \delta\boldsymbol{\varepsilon}_{nG}^T \boldsymbol{C}_{pn} \boldsymbol{\varepsilon}_{pG} \; d\Omega \; dl = \\
&= \delta\mathbf{U}_{\tau i}^T (\int_l \int_\Omega ([\mathbf{D}_{np}(\mathbf{F}_\tau \Psi_i)]^T \; \boldsymbol{C}_{np} \; \mathbf{D}_p(\mathbf{F}_s \Psi_j) + \\
&+ [\mathbf{D}_{nz}(\mathbf{F}_\tau \Psi_i)]^T \; \boldsymbol{C}_{np} \; \mathbf{D}_p(\mathbf{F}_s \Psi_j)) \; d\Omega \; dl) \mathbf{U}_{sj} \\
&\delta(L_{int})_{nn} = \int_l \int_\Omega \delta\boldsymbol{\varepsilon}_{nG}^T \boldsymbol{C}_{nn} \boldsymbol{\varepsilon}_{nG} \; d\Omega \; dl = \\
&= \delta\mathbf{U}_{\tau i}^T (\int_l \int_\Omega ([\mathbf{D}_{np}(\mathbf{F}_\tau \Psi_i)]^T \; \boldsymbol{C}_{nn} \; \mathbf{D}_{nz}(\mathbf{F}_s \Psi_j) + \\
&+ [\mathbf{D}_{nz}(\mathbf{F}_\tau \Psi_i)]^T \; \boldsymbol{C}_{nn} \; \mathbf{D}_{np}(\mathbf{F}_s \Psi_j) + \\
&+ [\mathbf{D}_{nz}(\mathbf{F}_\tau \Psi_i)]^T \; \boldsymbol{C}_{nn} \; \mathbf{D}_{nz}(\mathbf{F}_s \Psi_j)) \; d\Omega \; dl) \mathbf{U}_{sj}
\end{aligned}
\tag{3.32}
$$

In addition, the explicit expressions of the internal work due to the centrifugal stress can be obtained as:

$$
\begin{aligned}
&\delta(L_{int})_{\sigma_0} = \int_l \int_\Omega \delta\boldsymbol{\varepsilon}_{nl}^T \boldsymbol{\sigma}_0 \; d\Omega \; dl = \\
&= \delta\mathbf{U}_{\tau i}^T \int_l \int_\Omega \tilde{\sigma}_0([\mathbf{D}_{nl}(\mathbf{F}_\tau \Psi_i)]^T \quad \tilde{\boldsymbol{\Omega}}^T \; \tilde{\boldsymbol{\Omega}} \; \mathbf{D}_{nl}(\mathbf{F}_s \Psi_j) d\Omega \; dl) \mathbf{U}_{sj}
\end{aligned}
\tag{3.33}
$$

Where the differential matrix operator $\mathbf{D}_{nl}$ is given as:

$$\boldsymbol{D}_{nl} = \begin{bmatrix} \frac{\partial}{\partial x} & 0 & 0 \\ 0 & \frac{\partial}{\partial y} & 0 \\ 0 & 0 & \frac{\partial}{\partial z} \end{bmatrix} \tag{3.34}$$

Moreover with the same process the expression of the inertial work became:

$$\begin{aligned} \delta L_{ine} = \delta \mathbf{U}_{\tau i}^T \left[\int_l \int_\Omega \rho (\mathbf{F}_\tau \Psi_i)^T (\mathbf{F}_s \Psi_j)\ d\Omega\ dl\right] \ddot{\boldsymbol{U}}_{sj} + \\ -\delta \mathbf{U}_{\tau i}^T \left[\int_l \int_\Omega \rho (\mathbf{F}_\tau \Psi_i)^T \tilde{\boldsymbol{\Omega}}^T (\mathbf{F}_s \Psi_j)\ d\Omega\ dl\right] \dot{\boldsymbol{U}}_{sj} + \\ -\delta \mathbf{U}_{\tau i}^T \left[\int_l \int_\Omega \rho (\mathbf{F}_\tau \Psi_i)^T \tilde{\boldsymbol{\Omega}}^T \tilde{\boldsymbol{\Omega}} (\mathbf{F}_s \Psi_j)\ d\Omega\ dl\right] \boldsymbol{U}_{sj} + \\ -\delta \mathbf{U}_{\tau i}^T \left[\int_l \int_\Omega \rho (\mathbf{F}_\tau \Psi_i)^T \tilde{\boldsymbol{\Omega}}^T \tilde{\boldsymbol{\Omega}}\ \boldsymbol{r}\ d\Omega\ dl\right] \end{aligned} \tag{3.35}$$

The internal and inertial virtual works can also be be written in a more compact form such as the following one:

$$\begin{aligned} \delta L_{int} = \delta (L_{int})_{pp} + \delta (L_{int})_{pn} + \delta (L_{int})_{np} + \delta (L_{int})_{nn} = \\ = \delta \mathbf{U}_{\tau i}^T (\boldsymbol{K}_{pp}^{\tau sij} + \boldsymbol{K}_{pn}^{\tau sij} + \boldsymbol{K}_{np}^{\tau sij} + \boldsymbol{K}_{nn}^{\tau sij}) \mathbf{U}_{sj} = \\ = \delta \mathbf{U}_{\tau i}^T\ \boldsymbol{K}^{\tau sij}\ \mathbf{U}_{sj} \end{aligned} \tag{3.36}$$

$$\delta L_{ine} = \delta \mathbf{U}_{\tau i}^T\ \mathbf{M}^{\tau sij}\ \mathbf{U}_{sj} + \delta \mathbf{U}_{\tau i}^T\ \boldsymbol{D}_{\boldsymbol{\Omega}}^{\tau sij}\ \mathbf{U}_{sj} + \delta \mathbf{U}_{\tau i}^T\ \boldsymbol{K}_{\boldsymbol{\Omega}}^{\tau sij}\ \mathbf{U}_{sj} \tag{3.37}$$

Furthermore comparing Eqs.3.32 and 3.36 the Ritz fundamental primary stiffness nucleus can be derived:

$$\boldsymbol{K}_{pp}^{\tau sij} = \int_l \int_\Omega([\mathbf{D}_p(\mathbf{F}_\tau \Psi_i)]^T \ \boldsymbol{C}_{pp} \ \mathbf{D}_p(\mathbf{F}_s\Psi_j)) \ d\Omega \ dl$$

$$\boldsymbol{K}_{pn}^{\tau sij} = \int_l \int_\Omega([\mathbf{D}_p(\mathbf{F}_\tau \Psi_i)]^T \ \boldsymbol{C}_{pn} \ \mathbf{D}_{np}(\mathbf{F}_s\Psi_j) + [\mathbf{D}_p(\mathbf{F}_\tau \Psi_i)]^T \ \boldsymbol{C}_{pn} \ \mathbf{D}_{nz}(\mathbf{F}_s\Psi_j)) \ d\Omega \ dl$$

$$\boldsymbol{K}_{np}^{\tau sij} = \int_l \int_\Omega([\mathbf{D}_{np}(\mathbf{F}_\tau \Psi_i)]^T \ \boldsymbol{C}_{np} \ \mathbf{D}_{p}(\mathbf{F}_s\Psi_j) + [\mathbf{D}_{nz}(\mathbf{F}_\tau \Psi_i)]^T \ \boldsymbol{C}_{np} \ \mathbf{D}_{p}(\mathbf{F}_s\Psi_j)) \ d\Omega \ dl$$

$$\boldsymbol{K}_{nn}^{\tau sij} = \int_l \int_\Omega([\mathbf{D}_{np}(\mathbf{F}_\tau \Psi_i)]^T \ \boldsymbol{C}_{nn} \ \mathbf{D}_{nz}(\mathbf{F}_s\Psi_j) + [\mathbf{D}_{nz}(\mathbf{F}_\tau \Psi_i)]^T \ \boldsymbol{C}_{nn} \ \mathbf{D}_{np}(\mathbf{F}_s\Psi_j) +$$

$$+[\mathbf{D}_{nz}(\mathbf{F}_\tau \Psi_i)]^T \ \boldsymbol{C}_{nn} \ \mathbf{D}_{nz}(\mathbf{F}_s\Psi_j)) \ d\Omega \ dl \tag{3.38}$$

Thus:

$$\boldsymbol{K}^{\tau sij} = \boldsymbol{K}_{pp}^{\tau sij} + \boldsymbol{K}_{pn}^{\tau sij} + \boldsymbol{K}_{np}^{\tau sij} + \boldsymbol{K}_{nn}^{\tau sij} =$$

$$= \int_l \int_\Omega([\mathbf{D}_p(\mathbf{F}_\tau \Psi_i)]^T[\boldsymbol{C}_{pp} \ \mathbf{D}_p(\mathbf{F}_s\Psi_j) + \boldsymbol{C}_{pn} \ \mathbf{D}_{np}(\mathbf{F}_s\Psi_j) + \boldsymbol{C}_{pn} \ \mathbf{D}_{nz}(\mathbf{F}_s\Psi_j)] +$$

$$+[\mathbf{D}_{np}(\mathbf{F}_\tau \Psi_i)]^T[\boldsymbol{C}_{np} \ \mathbf{D}_p(\mathbf{F}_s\Psi_j) + \boldsymbol{C}_{nn} \ \mathbf{D}_{np}(\mathbf{F}_s\Psi_j) + \boldsymbol{C}_{nn} \ \mathbf{D}_{nz}(\mathbf{F}_s\Psi_j)] +$$

$$+[\mathbf{D}_{nz}(\mathbf{F}_\tau \Psi_i)]^T[\boldsymbol{C}_{np} \ \mathbf{D}_p(\mathbf{F}_s\Psi_j) + \boldsymbol{C}_{nn} \ \mathbf{D}_{np}(\mathbf{F}_s\Psi_j) + \boldsymbol{C}_{nn} \ \mathbf{D}_{nz}(\mathbf{F}_s\Psi_j)]) \ d\Omega \ dl \tag{3.39}$$

The Ritz fundamental primary stiffening nucleus, following the same procedure:

$$\boldsymbol{K}_{\sigma_0}^{\tau sij} = \int_\Omega \tilde{\sigma}_0 \ [\mathbf{D}_{nl}(\mathbf{F}_\tau \Psi_i)]^T \ \ \tilde{\mathbf{\Omega}}^T \ \tilde{\mathbf{\Omega}} \ \mathbf{D}_{nl}(\mathbf{F}_s\Psi_j) d\Omega \ dl \tag{3.40}$$

Comparing Eqs. 3.35 and 3.37 it is possible to obtain the fundamental primary mass nucleus, the damping and stiffness nucleus and the vector of body forces associated to the inertial work, rispectively:

$$\boldsymbol{M}^{\tau sij} = \int_l \int_\Omega(\rho(\mathbf{F}_\tau \Psi_i)^T(\mathbf{F}_s\Psi_j)) \ d\Omega \ dl \tag{3.41}$$

$$\boldsymbol{D}_{\boldsymbol{\Omega}}^{\tau sij} = -\int_l \int_\Omega (\rho(\mathbf{F}_\tau \Psi_i)^T \tilde{\boldsymbol{\Omega}}^T (\mathbf{F}_s \Psi_j)) \; d\Omega \; dl \tag{3.42}$$

$$\boldsymbol{K}_{\boldsymbol{\Omega}}^{\tau sij} = -\int_l \int_\Omega (\rho(\mathbf{F}_\tau \Psi_i)^T \tilde{\boldsymbol{\Omega}}^T \tilde{\boldsymbol{\Omega}} (\mathbf{F}_s \Psi_j)) \; d\Omega \; dl \tag{3.43}$$

$$\boldsymbol{F}_{\boldsymbol{\Omega}}^{\tau i} = -\int_l \int_\Omega (\rho(\mathbf{F}_\tau \Psi_i)^T \tilde{\boldsymbol{\Omega}}^T \tilde{\boldsymbol{\Omega}} \; \boldsymbol{r}) \; d\Omega \; dl \tag{3.44}$$

After performing the matrix calculus in Eq.3.40 the nine secondary stiffness nuclei are obtained:

$$\begin{aligned}
K_{u_x u_x}^{\tau_{u_x} s_{u_x}} = & \int_l \psi_{x_i} \; \psi_{x_j} \; [\int_\Omega C_{11} \; F_{\tau_{u_x,x}} F_{s_{u_x,x}} \; d\Omega] dz + \\
& + \int_l \psi_{x_i} \; \psi_{x_j} \; [\int_\Omega C_{16} \; F_{\tau_{u_x,y}} F_{s_{u_x,x}} \; d\Omega] dz + \\
& + \int_l \psi_{x_i} \; \psi_{x_j} \; [\int_\Omega C_{16} \; F_{\tau_{u_x,x}} F_{s_{u_x,y}} \; d\Omega] dz + \\
& + \int_l \psi_{x_i} \; \psi_{x_j} \; [\int_\Omega C_{66} \; F_{\tau_{u_x,y}} F_{s_{u_x,y}} \; d\Omega] dz + \\
& + \int_l \psi_{x_{i,z}} \; \psi_{x_{j,z}} \; [\int_\Omega C_{55} \; F_{\tau_{u_x}} F_{s_{u_x}} \; d\Omega] dz
\end{aligned} \tag{3.45}$$

$$\begin{aligned}
K_{u_x u_y}^{\tau_{u_x} s_{u_y}} = & \int_l \psi_{x_i} \; \psi_{y_j} \; [\int_\Omega C_{12} \; F_{\tau_{u_x,x}} F_{s_{u_y,y}} \; d\Omega] dz + \\
& + \int_l \psi_{x_i} \; \psi_{y_j} \; [\int_\Omega C_{26} \; F_{\tau_{u_x,y}} F_{s_{u_y,y}} \; d\Omega] dz + \\
& + \int_l \psi_{x_i} \; \psi_{y_j} \; [\int_\Omega C_{16} \; F_{\tau_{u_x,x}} F_{s_{u_y,x}} \; d\Omega] dz + \\
& + \int_l \psi_{x_i} \; \psi_{y_j} \; [\int_\Omega C_{66} \; F_{\tau_{u_x,y}} F_{s_{u_y,x}} \; d\Omega] dz + \\
& + \int_l \psi_{x_{i,z}} \; \psi_{y_{j,z}} \; [\int_\Omega C_{45} \; F_{\tau_{u_x}} F_{s_{u_y}} \; d\Omega] dz
\end{aligned} \tag{3.46}$$

$$\begin{aligned}
K_{u_x u_z}^{\tau_{u_x} s_{u_z}} = & \int_l \psi_{x_i} \; \psi_{z_{j,z}} \; [\int_\Omega C_{13} \; F_{\tau_{u_x,x}} F_{s_{u_z}} \; d\Omega] dz + \\
& + \int_l \psi_{x_i} \; \psi_{z_{j,z}} \; [\int_\Omega C_{36} \; F_{\tau_{u_x,y}} F_{s_{u_z}} \; d\Omega] dz + \\
& + \int_l \psi_{x_{i,z}} \; \psi_{z_j} \; [\int_\Omega C_{55} \; F_{\tau_{u_x}} F_{s_{u_z,x}} \; d\Omega] dz + \\
& + \int_l \psi_{x_{i,z}} \; \psi_{z_j} \; [\int_\Omega C_{45} \; F_{\tau_{u_x}} F_{s_{u_z,y}} \; d\Omega] dz
\end{aligned} \tag{3.47}$$

$$
\begin{aligned}
K_{u_y u_x}^{\tau_{u_y} s_{u_x}} &= \int_l \psi_{y_i}\ \psi_{x_j}\ [\int_\Omega C_{12}\ F_{\tau_{u_y,y}} F_{s_{u_x,x}}\ d\Omega] dz+ \\
&+ \int_l \psi_{y_i}\ \psi_{x_j}\ [\int_\Omega C_{16}\ F_{\tau_{u_y,x}} F_{s_{u_x,x}}\ d\Omega] dz+ \\
&+ \int_l \psi_{y_i}\ \psi_{x_j}\ [\int_\Omega C_{26}\ F_{\tau_{u_y,y}} F_{s_{u_x,y}}\ d\Omega] dz+ \\
&+ \int_l \psi_{y_i}\ \psi_{x_j}\ [\int_\Omega C_{66}\ F_{\tau_{u_y,x}} F_{s_{u_x,y}}\ d\Omega] dz+ \\
&+ \int_l \psi_{y_{i,z}}\ \psi_{x_{j,z}}\ [\int_\Omega C_{45}\ F_{\tau_{u_y}} F_{s_{u_x}}\ d\Omega] dz
\end{aligned}
\tag{3.48}
$$

$$
\begin{aligned}
K_{u_y u_y}^{\tau_{u_y} s_{u_y}} &= \int_l \psi_{y_i}\ \psi_{y_j}\ [\int_\Omega C_{22}\ F_{\tau_{u_y,y}} F_{s_{u_y,y}}\ d\Omega] dz+ \\
&+ \int_l \psi_{y_i}\ \psi_{y_j}\ [\int_\Omega C_{26}\ F_{\tau_{u_y,x}} F_{s_{u_y,y}}\ d\Omega] dz+ \\
&+ \int_l \psi_{y_i}\ \psi_{y_j}\ [\int_\Omega C_{26}\ F_{\tau_{u_y,y}} F_{s_{u_y,x}}\ d\Omega] dz+ \\
&+ \int_l \psi_{y_i}\ \psi_{y_j}\ [\int_\Omega C_{66}\ F_{\tau_{u_y,x}} F_{s_{u_y,x}}\ d\Omega] dz+ \\
&+ \int_l \psi_{y_{i,z}}\ \psi_{y_{j,z}}\ [\int_\Omega C_{44}\ F_{\tau_{u_y}} F_{s_{u_y}}\ d\Omega] dz
\end{aligned}
\tag{3.49}
$$

$$
\begin{aligned}
K_{u_y u_z}^{\tau_{u_y} s_{u_z}} &= \int_l \psi_{y_i}\ \psi_{z_{j,z}}\ [\int_\Omega C_{23}\ F_{\tau_{u_y,y}} F_{s_{u_z}}\ d\Omega] dz+ \\
&+ \int_l \psi_{y_i}\ \psi_{z_{j,z}}\ [\int_\Omega C_{36}\ F_{\tau_{u_y,x}} F_{s_{u_z}}\ d\Omega] dz+ \\
&+ \int_l \psi_{y_{i,z}}\ \psi_{z_j}\ [\int_\Omega C_{45}\ F_{\tau_{u_y}} F_{s_{u_z,x}}\ d\Omega] dz+ \\
&+ \int_l \psi_{y_{i,z}}\ \psi_{z_j}\ [\int_\Omega C_{44}\ F_{\tau_{u_y}} F_{s_{u_z,y}}\ d\Omega] dz
\end{aligned}
\tag{3.50}
$$

$$
\begin{aligned}
K_{u_z u_x}^{\tau_{u_z} s_{u_x}} &= \int_l \psi_{z_i}\ \psi_{x_{j,z}}\ [\int_\Omega C_{55}\ F_{\tau_{u_z,x}} F_{s_{u_x}}\ d\Omega] dz+ \\
&+ \int_l \psi_{z_i}\ \psi_{x_{j,z}}\ [\int_\Omega C_{45}\ F_{\tau_{u_z,y}} F_{s_{u_x}}\ d\Omega] dz+ \\
&+ \int_l \psi_{z_{i,z}}\ \psi_{x_j}\ [\int_\Omega C_{13}\ F_{\tau_{u_z}} F_{s_{u_x,x}}\ d\Omega] dz+ \\
&+ \int_l \psi_{z_{i,z}}\ \psi_{x_j}\ [\int_\Omega C_{36}\ F_{\tau_{u_z}} F_{s_{u_x,y}}\ d\Omega] dz
\end{aligned}
\tag{3.51}
$$

$$\begin{aligned} K^{\tau_{u_z} s_{u_y}}_{u_z u_y} &= \int_l \psi_{z_i}\ \psi_{y_{j,z}}\ [\int_\Omega C_{45}\ F_{\tau_{u_z,x}} F_{s_{u_y}}\ d\Omega] dz + \\ &+ \int_l \psi_{z_i}\ \psi_{y_{j,z}}\ [\int_\Omega C_{44}\ F_{\tau_{u_z,y}} F_{s_{u_y}}\ d\Omega] dz + \\ &+ \int_l \psi_{z_{i,z}}\ \psi_{y_j}\ [\int_\Omega C_{23}\ F_{\tau_{u_z}} F_{s_{u_y,y}}\ d\Omega] dz + \\ &+ \int_l \psi_{z_{i,z}}\ \psi_{y_j}\ [\int_\Omega C_{36}\ F_{\tau_{u_z}} F_{s_{u_y,x}}\ d\Omega] dz \end{aligned} \tag{3.52}$$

$$\begin{aligned} K^{\tau_{u_z} s_{u_z}}_{u_z u_z} &= \int_l \psi_{z_i}\ \psi_{z_j}\ [\int_\Omega C_{55}\ F_{\tau_{u_z,x}} F_{s_{u_z,x}}\ d\Omega] dz + \\ &+ \int_l \psi_{z_i}\ \psi_{z_j}\ [\int_\Omega C_{45}\ F_{\tau_{u_z,y}} F_{s_{u_z,x}}\ d\Omega] dz + \\ &+ \int_l \psi_{z_i}\ \psi_{z_j}\ [\int_\Omega C_{45}\ F_{\tau_{u_z,x}} F_{s_{u_z,y}}\ d\Omega] dz + \\ &+ \int_l \psi_{z_i}\ \psi_{z_j}\ [\int_\Omega C_{44}\ F_{\tau_{u_z,y}} F_{s_{u_z,y}}\ d\Omega] dz + \\ &+ \int_l \psi_{z_{i,z}}\ \psi_{z_{j,z}}\ [\int_\Omega C_{33}\ F_{\tau_{u_z}} F_{s_{u_z}}\ d\Omega] dz \end{aligned} \tag{3.53}$$

In case of isotropic beam the elastic coefficients are constant, thus they do not need to be integrated along with the cross-section functions. Furthermore in case of beam with constant cross-section the integral on the cross-section, Ω, does not depend on the coordinate z.

Following a similar approach, the nine components of the primary stiffening nucleus:

$$\begin{aligned} K^{\tau_{u_y} s_{u_y}}_{\sigma_0 u_y u_y} &= \rho\ \tilde{\Omega}^2 \int_l \psi_{y_i,z}\ \psi_{y_j,z} \left[\frac{l^2}{2} - \frac{z^2}{2} + r_{hub}(l-z)\right]\ \left[\int_\Omega F_{\tau_{u_y}} F_{s_{u_y}}\ d\Omega\right] dz, \\ K^{\tau_{u_z} s_{u_z}}_{\sigma_0 u_z u_z} &= \rho\ \tilde{\Omega}^2 \int_l \psi_{z_i,z}\ \psi_{z_j,z} \left[\frac{l^2}{2} - \frac{z^2}{2} + r_{hub}(l-z)\right]\ \left[\int_\Omega F_{\tau_{u_z}} F_{s_{u_z}}\ d\Omega\right] dz, \\ K^{\tau_{u_y} s_{u_y}}_{\sigma_0 u_x u_x} &= 0, \qquad K^{\tau_{u_x} s_{u_y}}_{\sigma_0 u_x u_y} = 0, \\ K^{\tau_{u_x} s_{u_z}}_{\sigma_0 u_x u_z} &= 0, \qquad K^{\tau_{u_y} s_{u_x}}_{\sigma_0 u_y u_x} = 0, \\ K^{\tau_{u_y} s_{u_z}}_{\sigma_0 u_y u_z} &= 0, \qquad K^{\tau_{u_z} s_{u_x}}_{\sigma_0 u_z u_x} = 0, \\ K^{\tau_{u_z} s_{u_y}}_{\sigma_0 u_z u_y} &= 0, \end{aligned} \tag{3.54}$$

the nine components of the primary mass nucleus:

$$
\begin{aligned}
& M_{u_x u_x}^{\tau_{u_x} s_{u_x}} = \rho \int_l \psi_{x_i} \ \psi_{x_j} \ [\int_\Omega F_{\tau_{u_x}} F_{s_{u_x}} \ d\Omega] dz, \\
& M_{u_y u_y}^{\tau_{u_y} s_{u_y}} = \rho \int_l \psi_{y_i} \ \psi_{y_j} \ [\int_\Omega F_{\tau_{u_y}} F_{s_{u_y}} \ d\Omega] dz, \\
& M_{u_z u_z}^{\tau_{u_z} s_{u_z}} = \rho \int_l \psi_{z_i} \ \psi_{z_j} \ [\int_\Omega F_{\tau_{u_z}} F_{s_{u_z}} \ d\Omega] dz, \\
& M_{u_x u_y}^{\tau_{u_x} s_{u_y}} = 0, \qquad M_{u_x u_z}^{\tau_{u_x} s_{u_z}} = 0, \\
& M_{u_y u_x}^{\tau_{u_y} s_{u_x}} = 0, \qquad M_{u_y u_z}^{\tau_{u_y} s_{u_z}} = 0, \\
& M_{u_z u_x}^{\tau_{u_z} s_{u_x}} = 0, \qquad M_{u_z u_y}^{\tau_{u_z} s_{u_y}} = 0,
\end{aligned}
\tag{3.55}
$$

the nine components of the primary damping nucleus:

$$
\begin{aligned}
& D_{\Omega u_y u_z}^{\tau_{u_y} s_{u_z}} = \rho \ \tilde{\Omega} \int_l \psi_{y_i} \ \psi_{z_j} \ [\int_\Omega F_{\tau_{u_y}} F_{s_{u_z}} \ d\Omega] dz, \\
& D_{\Omega u_z u_y}^{\tau_{u_z} s_{u_y}} = -\rho \ \tilde{\Omega} \int_l \psi_{z_i} \ \psi_{y_j} \ [\int_\Omega F_{\tau_{u_z}} F_{s_{u_y}} \ d\Omega] dz, \\
& D_{\Omega u_x u_x}^{\tau_{u_x} s_{u_x}} = 0, \qquad D_{\Omega u_x u_y}^{\tau_{u_x} s_{u_y}} = 0, \\
& D_{\Omega u_x u_z}^{\tau_{u_x} s_{u_z}} = 0, \qquad D_{\Omega u_y u_x}^{\tau_{u_y} s_{u_x}} = 0, \\
& D_{\Omega u_y u_y}^{\tau_{u_y} s_{u_y}} = 0, \qquad D_{\Omega u_z u_x}^{\tau_{u_z} s_{u_x}} = 0, \\
& D_{\Omega u_z u_z}^{\tau_{u_z} s_{u_z}} = 0,
\end{aligned}
\tag{3.56}
$$

the nine components of the primary softening nucleus:

$$
\begin{aligned}
& K_{\Omega u_y u_y}^{\tau_{u_y} s_{u_y}} = \frac{1}{2} \rho \ \tilde{\Omega}^2 \int_l \psi_{y_i} \ \psi_{y_j} \ [\int_\Omega F_{\tau_{u_y}} F_{s_{u_y}} \ d\Omega] dz, \\
& K_{\Omega u_z u_z}^{\tau_{u_z} s_{u_z}} = \frac{1}{2} \rho \ \tilde{\Omega}^2 \int_l \psi_{z_i} \ \psi_{z_j} \ [\int_\Omega F_{\tau_{u_z}} F_{s_{u_z}} \ d\Omega] dz, \\
& K_{\Omega u_x u_x}^{\tau_{u_y} s_{u_y}} = 0, \qquad K_{\Omega u_x u_y}^{\tau_{u_x} s_{u_y}} = 0, \\
& K_{\Omega u_x u_z}^{\tau_{u_x} s_{u_z}} = 0, \qquad K_{\Omega u_y u_x}^{\tau_{u_y} s_{u_x}} = 0, \\
& K_{\Omega u_y u_z}^{\tau_{u_y} s_{u_z}} = 0, \qquad K_{\Omega u_z u_x}^{\tau_{u_z} s_{u_x}} = 0, \\
& K_{\Omega u_z u_y}^{\tau_{u_z} s_{u_y}} = 0,
\end{aligned}
\tag{3.57}
$$

and the three components of the vector of the body forces:

$$\begin{aligned} F_{\Omega u_x}^{\tau_{u_x}} &= 0, \\ F_{\Omega u_y}^{\tau_{u_y}} &= \rho\, \tilde{\Omega}^2 \int_l \psi_{y_i}\ [\int_\Omega F_{\tau_{u_y}}\ d\Omega] dz, \\ F_{\Omega u_z}^{\tau_{u_z}} &= \rho\, \tilde{\Omega}^2 \int_l \psi_{z_i}\ [\int_\Omega F_{\tau_{u_z}}\ d\Omega] dz. \end{aligned} \tag{3.58}$$

Hence the Ritz fundamental primary mass, damping, stiffness, stiffening, softening nucleus and the vector of the body forces, respectively:

$$\boldsymbol{M}^{ij} = \begin{bmatrix} M_{u_x u_x}^{\tau_{u_x} s_{u_x}} & 0 & 0 \\ 0 & M_{u_y u_y}^{\tau_{u_y} s_{u_y}} & 0 \\ 0 & 0 & M_{u_z u_z}^{\tau_{u_z} s_{u_z}} \end{bmatrix} \tag{3.59}$$

$$\boldsymbol{D}_{\boldsymbol{\Omega}}^{ij} = \begin{bmatrix} 0 & 0 & 0 \\ 0 & 0 & D_{\Omega u_y u_z}^{\tau_{u_y} s_{u_z}} \\ 0 & D_{\Omega u_z u_y}^{\tau_{u_z} s_{u_y}} & 0 \end{bmatrix} \tag{3.60}$$

$$\boldsymbol{K}^{ij} = \begin{bmatrix} K_{u_x u_x}^{\tau_{u_x} s_{u_x}} & K_{u_x u_y}^{\tau_{u_x} s_{u_y}} & K_{u_x u_z}^{\tau_{u_x} s_{u_z}} \\ K_{u_y u_x}^{\tau_{u_y} s_{u_x}} & K_{u_y u_y}^{\tau_{u_y} s_{u_y}} & K_{u_y u_z}^{\tau_{u_y} s_{u_z}} \\ K_{u_z u_x}^{\tau_{u_z} s_{u_x}} & K_{u_z u_y}^{\tau_{u_z} s_{u_y}} & K_{u_z u_z}^{\tau_{u_z} s_{u_z}} \end{bmatrix} \tag{3.61}$$

$$\boldsymbol{K}^{ij}_{\boldsymbol{\sigma_0}} = \begin{bmatrix} 0 & 0 & 0 \\ 0 & K^{\tau_{u_y} s_{u_y}}_{\sigma_0 u_y u_y} & 0 \\ 0 & 0 & K^{\tau_{u_z} s_{u_z}}_{\sigma_0 u_z u_z} \end{bmatrix} \tag{3.62}$$

$$\boldsymbol{K}^{ij}_{\boldsymbol{\Omega}} = \begin{bmatrix} 0 & 0 & 0 \\ 0 & K^{\tau_{u_y} s_{u_y}}_{\Omega u_y u_y} & 0 \\ 0 & 0 & K^{\tau_{u_z} s_{u_z}}_{\Omega u_z u_z} \end{bmatrix} \tag{3.63}$$

$$\boldsymbol{F_\Omega} = \begin{Bmatrix} 0 \\ F^{\tau_{u_y}}_{\Omega u_y} \\ F^{\tau_{u_z}}_{\Omega u_z} \end{Bmatrix} \tag{3.64}$$

Using the above matrices, the problem can be written as:

$$[\boldsymbol{M}]\{\ddot{\boldsymbol{U}}\} + [\boldsymbol{D_\Omega}]\{\dot{\boldsymbol{U}}\} + ([\boldsymbol{K}] + [\boldsymbol{K_{\sigma_0}}] - [\boldsymbol{K_\Omega}])\{\boldsymbol{U}\} + \{\boldsymbol{F_\Omega}\} = 0 \tag{3.65}$$

Grouping the stiffness terms:

$$[\boldsymbol{M}]\{\ddot{\boldsymbol{U}}\} + [\boldsymbol{D_\Omega}]\{\dot{\boldsymbol{U}}\} + [\boldsymbol{K_{tot}}]\{\boldsymbol{U}\} + \{\boldsymbol{F_\Omega}\} = 0 \tag{3.66}$$

where $[\boldsymbol{U}]$ is the vector of the nodal unknowns.

In order to analyze the free vibration behavior of the beam the vector $\{\boldsymbol{F_\Omega}\}$ has to be neglected. The structure of the problem vary considering different effects due to the rotation.

In absence of rotation the equation leads to the classic free vibration problem:

$$[\boldsymbol{M}]\{\ddot{\boldsymbol{U}}\} + [\boldsymbol{K}]\{\boldsymbol{U}\} = 0 \tag{3.67}$$

Assuming a periodic solution $\boldsymbol{U} = \tilde{\boldsymbol{U}}e^{i\omega t}$ the frequencies can be obtained by solving the eigenvalues problem:

$$\tilde{\boldsymbol{U}}e^{i\omega t}\left\{-\omega^2[\boldsymbol{M}] + [\boldsymbol{K}]\right\} = 0 \tag{3.68}$$

In order to consider the effect of the centrifugal force, the stiffening matrix, must be added. Each of the three problems in which the Coriolis effect is disregarded can be solved as the previous by substituting to the matrix $\boldsymbol{K}$ the sum of the stiffness matrix with one or either the contributes of stiffening and softening. Therefore including only $\boldsymbol{K_{\sigma_0}}$ and both $\boldsymbol{K_{\sigma_0}}$, $\boldsymbol{K_{\Omega}}$, the classic eigenvalues problem became, respectively:

$$\tilde{\boldsymbol{U}}e^{i\omega t}\left\{-\omega^2[\boldsymbol{M}] + [\boldsymbol{K}] + [\boldsymbol{K_{\sigma_0}}]\right\} = 0 \tag{3.69}$$

and

$$\tilde{\boldsymbol{U}}e^{i\omega t}\left\{-\omega^2[\boldsymbol{M}] + [\boldsymbol{K_{tot}}]\right\} = 0 \tag{3.70}$$

Accounting for the Coriolis effect, assuming a periodic solution $\boldsymbol{U} = \tilde{\boldsymbol{U}}e^{i\omega t}$ and substituting in Eq.3.65, the problem became a quadratic eigenvalues problem (QEP):

$$\tilde{\boldsymbol{U}}e^{i\omega t}\left\{-\omega^2[\boldsymbol{M}] + i\omega[\boldsymbol{D_{\Omega}}] + [\boldsymbol{K}] + [\boldsymbol{K_{\sigma_0}}] - [\boldsymbol{K_{\Omega}}]\right\} = 0 \tag{3.71}$$

The Eq.3.71 can be transformed in a classical linear system:

$$\begin{cases} [\boldsymbol{M}]\{\ddot{\boldsymbol{U}}\} + [\boldsymbol{D_\Omega}]\{\dot{\boldsymbol{U}}\} + \left([\boldsymbol{K}] + [\boldsymbol{K_{\sigma_0}}] - [\boldsymbol{K_\Omega}]\right)\{\boldsymbol{U}\} + \{\boldsymbol{F_\Omega}\} = 0 \\ \\ -\dot{\boldsymbol{U}} + \dot{\boldsymbol{U}} = 0 \end{cases} \tag{3.72}$$

Therefore, by introducing:

$$\boldsymbol{q} = \begin{Bmatrix} \boldsymbol{U} \\ \\ \dot{\boldsymbol{U}} \end{Bmatrix} \qquad \dot{\boldsymbol{q}} = \begin{Bmatrix} \dot{\boldsymbol{U}} \\ \\ \ddot{\boldsymbol{U}} \end{Bmatrix} \tag{3.73}$$

The equation of motion assume the following form:

$$\boldsymbol{Q}^{-1}\boldsymbol{S} - \frac{1}{i\omega}\boldsymbol{I} = 0 \tag{3.74}$$

where

$$\boldsymbol{Q}^{-1}\boldsymbol{S} = \begin{bmatrix} ([\boldsymbol{K}] + [\boldsymbol{K_{\sigma_0}}] - [\boldsymbol{K_\Omega}])^{-1}[\boldsymbol{D_\Omega}] & ([\boldsymbol{K}] + [\boldsymbol{K_{\sigma_0}}] - [\boldsymbol{K_\Omega}])^{-1}[\boldsymbol{M}] \\ \\ -\boldsymbol{I} & \boldsymbol{0} \end{bmatrix} \tag{3.75}$$

The problem of Eq.3.74 is in the classical form and can be solved by using standard eigen-solvers.

Chapter 4

Results for Pre-twisted, Tapered Metallic and FG Beams

In the present section the results obtained by using the refined and advanced quasi-3D beam models are validated and assessed by comparing those with the results available in literature.

The results are given using the acronym $TE_{N_{u_x},N_{u_y},N_{u_z}}$, where TE states that Taylor's series expansion is used to describe the displacement field over the beam cross-section and N_{u_x}, N_{u_y}, and N_{u_z} are the independent expansion orders used in the beam model.

In the proposed analysis, the difference between the results obtained by using the developed beam models (f_p) and those selected from the literature (f_0), *Relative Difference,* ε, is evaluated as follows:

$$\varepsilon = \frac{||\omega_p - \omega_0||}{\omega_0} \tag{4.1}$$

Validation of the results for Tapered Beams

In order to validate the proposed method, the first case of study is focused on the computation of eigenfrequencies of a metallic clamped-clamped beam. The material properties considered are: Elastic Modulus, $E = 71.7\ GPa$, Poisson ratio, $\nu = 0.3$ and density $\rho = 2700 kg/m^3$. The geometrical characteristics of the beam are: root transverse dimension $h = 1\ m$, root longitudinal dimension $b = 1\ m$ and length $L = 10\ m$.

The first ten free vibration frequencies of the square cross-section beam are evaluated considering two different values of the $TaperRatio$, $TR = c_t/c_r$ 0.50 and 0.25 (where $c_r = h(0)$ is the transverse dimension of the beam at the root and $c_t = h(L)$ is the transverse dimension of the beam at $z = L$).

The results obtained are listed and compared with the ones taken from the literature [85] in the Table 4.1. From the left the results obtained using the Eulero Bernoulli Beam Theory, EBBT, and the Timoshenko Beam Theory, TBT. The results obtained by the refined theory follows the previous two. The last two column of the Table shows the results obtained by using a FEM[85] analysis with elements characterized by a displacement field developed by using Maclaurin polynomial function (considering expansion $N = 3$), and results obtained by using ANSYS[85]. ANSYS results are obtained representing the cross-section of beams by 44 $SOLID45$ elements whereas 40 $SOLID45$ elements are used in the longitudinal direction − thus making a total of 640 elements.

Table 4.1. Comparison of the first ten natural frequencies (Hz) of a CC square metallic beam with $h = 0.1\ m,\ b = 1\ m\ and\ l = 10\ m$. *results from [85]

c_t/c_r	$Mode$	Theory						
		$EBBT$	TBT	TE$_{222}$	TE$_{333}$	TE$_{444}$	FEM^*	$ANSYS^*$
0.50	1	38.66	37.60	37.76	37.60	37.56	37.86	37.71
	2	52.28	49.72	49.96	49.56	49.52	49.79	49.96
	3	105.64	99.67	99.99	99.13	99.03	99.84	100.42
	4	142.78	129.04	129.35	127.57	127.47	128.23	129.27
	5	204.60	186.49	151.04^t	150.87^t	139.58^t	152.21^t	144.25^t
	6	256.19^a	235.55	186.92	184.48	184.29	185.82	187.93
	7	274.84	256.19^a	236.11	231.33	231.11	232.47	235.50
	8	332.93	292.54	256.58^a	256.55^a	256.45^a	257.54^a	257.79^a
	9	443.16	360.53	292.93^t	287.88^t	277.83^t	290.05^t	287.35^t
	10	514.63	413.42	300.50	300.16	287.55	302.88	295.15
ε_{Av}	[%]	-	-	1.04	1.43	1.75	1.37	-
ε_{Max}	[%]	-	-	4.71	4.59	3.31	5.52	-
0.25	1	30.32	29.79	29.70	29.63	29.60	30.06	29.87
	2	51.21	48.66	48.76	48.35	48.32	48.66	48.77
	3	82.77	79.72	79.51	79.08	79.00	80.14	80.10
	4	141.33	127.58	127.57	125.79	125.70	126.61	127.50
	5	160.59	151.03	138.69^t	138.32^t	128.60^t	139.73^t	132.87^t
	6	252.32^a	234.02	150.81	149.48	149.30	151.27	152.29
	7	262.20	240.18	234.04	229.30	229.09	230.66	233.48
	8	273.38	252.31^a	240.13	237.21	236.93	239.63	243.36
	9	385.82	343.96	252.35^a	252.34^a	249.66^a	253.34^a	253.62^a
	10	441.83	359.06	268.79^t	267.85^t	252.25^t	270.57^t	258.07^t
ε_{Av}	[%]	-	-	1.30	1.88	1.81	1.51	-
ε_{Max}	[%]	-	-	4.38	4.10	3.21	5.16	-

The first ten natural frequencies represent free vibration bending, torsional as well as axial modes which are marked in Table 4.1 (a − axial mode; t − torsional mode). EBBT overestimate the bending vibration frequencies. Torsional modes are completely missed by the classical theories whereas these are predicted using refined theory with expansion order as low as $N = 1$ albeit with slightly erroneous mode shapes.

Further refined theory enables to predict torsional as well as bending and axial modes adequately which are in good agreement with ANSYS 3D results.

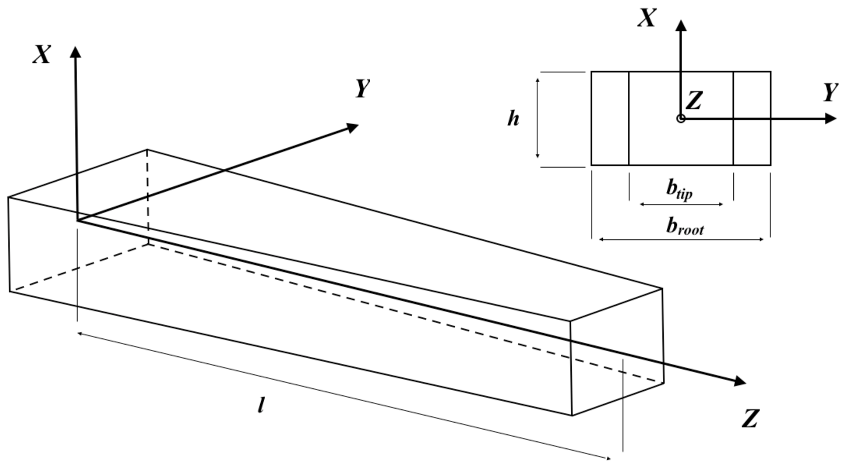

Figure 4.1. Schematic representation of a rectangular section tapered beam with taper ratio $c_b = 0.5$ along the width.

The less refined model involved in the present analysis is the TE_{222} and associated with $i = j = 18$ in the Ritz expansion, involves a total of 324 DOFs, a tenth of the DOFs involved using ANSYS (1025 nodes with 3 DOFs each one − 3075 DOFs). In addition this model produce better results if compared with the ones evaluated by the FEM analysis associated with the use of elements with the displacement field built on a Maclaurin expansion of order $N = 3$. The averaged as well as the maximum relative difference is lower in both cases, $c_t/c_r = 0.50$ and $c_t/c_r = 0.25$.

In fact, comparing the Averaged Relative Difference for $c_t/c_r = 0.50$ considering the FEM analysis and the refined model TE_{222}, it decrease of 24.0 % changing from 1.37 % to 1.04 %. Additionally comparing the Maximum Relative Difference for $c_t/c_r = 0.50$ considering the FEM analysis and the refined model TE_{222}, it decrease of 14.7 % changing from 5.52 % to 4.71 %. As well considering $c_t/c_r = 0.25$ the Averaged Relative Difference and the Maximum Relative difference decreases of 13.9 % and 15.1 %, respectively.

Furthermore the Maximum Relative Difference decrease by using higher order beam theories. In particular comparing the Maximum Relative Difference obtained by using a TE_{222} beam model with the one obtained by using a TE_{444} beam model, it decrease of 29.7 % changing from 4.71 % to 3.31 % and of 26.7 % changing from 4.38 % to 3.21 % for $c_t/c_r = 0.50$ and $c_t/c_r = 0.25$ respectively.

Convergence Analysis for Tapered Beams

A comprensive analysis of the algebraic Ritz functions used in the analysis has been carried out for a cantilever rectangular beam (CF). The beam is metallic, made up of an aluminium alloy, with Young's Modulus $E = 69\ GPa$, Poisson's ratio $\nu = 0.33$ and density $\rho = 2700\ kg/m^3$. The geometric characteristics are $h = 0.1\ m$, $b = 1\ m$ and $L = 10\ m$.

The expansion indexes i and j in the Ritz functions are progressively increased from 4 to 18, namely till convergence is reached, and the results of the analysis have been proposed in Tables 4.2 and 4.3. Three different beam theories accounting for distinct expansion orders have been tested for both lower (ω_1) and higher (ω_7) modes for three different values of Taper Rateo, 1.00, 0.50 and 0.25.

The rate of convergence is higher for higher modes and is also sightly affected by the selected beam theory. Higher-order beam models are mandatory to accurately describe mode shapes which involves torsion, distortion and warping of the beam cross-section.

An example is the torsional mode ω_7, indeed, in this case the addition of degrees of freedom (DOFs) over the beam cross-section leads to a remarkable enhancement in the results accuracy while any refinement in the Ritz approximation does not affect significantly the result accuracy.

In sharp contrast, bending modes are instead accurately described by lower-order beam models and further significant improvements can only be achieved by increasing the number of DOFs in the Ritz expansion.

These conclusions can be drawn by comparing the convergence ratio in the tables 4.2 and 4.3 that show the results in terms of first natural frequency ω_1 and seventh natural frequency ω_7 (torsional mode), respectively.

More specifically, in the computation of the fundamental frequency, related to a bending mode in the $xz - plane$, the convergence ratio is of an higher order than the one observed in the table 4.3.

Effect of the taper ratio on beam's natural frequencies

The beam under investigation has the same geometrical characteristics and is made up of the same material of that studied in the convergence analysis. In this case the first ten natural frequencies have been computed using different beam models for various boundary conditions for two different values of the taper rateo, 1.00 and

Table 4.2. Convergence of the first natural frequency (Hz) of a cantilever (CF) rectangular metallic beam with $h = 0.1\ m,\ b = 1\ m\ and\ l = 10\ m$.

c_t/c_r	Theory	(i,j) 4	6	8	10	12	14	16	18
1.0									
	TE_{222}	0.8840	0.8579	0.8468	0.8412	0.8379	0.8358	0.8344	0.8334
	TE_{333}	0.8815	0.8539	0.8415	0.8352	0.8317	0.8297	0.8284	0.8275
	TE_{444}	0.8792	0.8526	0.8407	0.8345	0.8311	0.8290	0.8277	0.8267
0.5									
	TE_{222}	1.0740	1.0465	1.0349	1.0289	1.0254	1.0231	1.0216	1.0205
	TE_{333}	1.0723	1.0425	1.0291	1.0223	1.0186	1.0164	1.0150	1.0140
	TE_{444}	1.0637	1.0400	1.0276	1.0213	1.0177	1.0155	1.0141	1.0131
0.25									
	TE_{222}	1.2753	1.2452	1.2323	1.2256	1.2217	1.2191	1.2174	1.2161
	TE_{333}	1.2737	1.2405	1.2255	1.2179	1.2137	1.2112	1.2096	1.2084
	TE_{444}	1.2636	1.2357	1.2228	1.2161	1.2123	1.2100	1.2084	1.2073

Table 4.3. Convergence of the seventh natural frequency (Hz) of a cantilever (CF) rectangular metallic beam with $h = 0.1\ m,\ b = 1\ m\ and\ l = 10\ m$.

TR	Theory	(i,j) 4	6	8	10	12	14	16	18
1.0									
	TE_{222}	51.352	48.171	47.883	47.750	47.733	47.729	47.726	47.725
	TE_{333}	51.061	48.030	47.698	47.403	47.287	47.196	47.133	47.087
	TE_{444}	51.060	47.515	47.186	47.097	47.067	47.045	47.026	47.010
0.5									
	TE_{222}	60.909	42.069	41.820	41.698	41.628	41.585	41.558	41.538
	TE_{333}	60.762	41.953	41.703	41.581	41.512	41.470	41.442	41.423
	TE_{444}	60.750	41.902	41.674	41.562	41.498	41.458	41.431	41.411
0.25									
	TE_{222}	56.286	37.385	37.200	37.112	37.063	37.032	37.013	36.999
	TE_{333}	56.217	37.320	37.136	37.047	36.997	36.967	36.947	36.933
	TE_{444}	56.186	37.246	37.096	37.023	36.981	36.954	36.936	36.922

0.50. In tables 4.4 – 4.9 the beam is supposed to be under CC, CS, SS, SF, and FF boundary conditions, respectively. Besides the results obtained by the refined theories, for $c_t/c_r = 1.00$, results evaluated by using ABAQUS are included in the tables in order to enhance the confidence on the results obtained. More specifically, the brick element C3DR20 with 20 nodes has been used and a mesh of 5 x 5 x 50 has been applied, with a total number of 37593 DOFs. The most refined beam model involved in the present analysis is the TE_{444} and associated with $i = j = 18$

in the Ritz expansion, involves a total of 810 DOFs.

Table 4.4. Comparison of the first ten natural frequencies (Hz) of a square metallic beam with $h = 0.1\ m,\ b = 1\ m\ ,\ l = 10\ m$ for *Clamped – Clamped* Boundary Conditions.

c_t/c_r	Theory	*Mode* 1	2	3	4	5	6	7	8	9	10
1.0											
	ABAQUS	5.267	14.50	28.42	31.47	46.97	48.91	63.48	70.16	96.55	97.97
	TE_{222}	5.351	14.64	28.73	32.76	47.54	49.87	66.26	71.51	99.51	101.3
	TE_{333}	5.319	14.64	28.70	32.42	47.42	49.16	65.37	70.91	99.00	99.40
	TE_{444}	5.309	14.61	28.65	32.08	47.32	49.14	64.69	70.73	98.42	98.70
0.5											
	TE_{222}	5.276	14.49	28.69	37.06	41.74	47.52	71.12	85.30	98.14	99.44
	TE_{333}	5.250	14.51	28.49	36.92	41.56	47.09	70.39	84.76	97.32	98.23
	TE_{444}	5.242	14.49	28.45	36.90	40.82	47.03	70.27	83.26	97.29	98.06

Table 4.5. Comparison of the first ten natural frequencies (Hz) of a square metallic beam with $h = 0.1\ m,\ b = 1\ m\ ,\ l = 10\ m$ for *Clamped – Supported* Boundary Conditions.

c_t/c_r	Theory	*Mode* 1	2	3	4	5	6	7	8	9	10
1.0											
	ABAQUS	3.607	8.118	11.69	24.40	30.58	41.75	48.66	61.69	63.76	90.40
	TE_{222}	3.647	8.149	11.76	24.79	31.57	42.62	49.46	64.03	64.51	92.83
	TE_{333}	3.625	8.141	11.75	24.54	31.49	42.01	48.80	63.50	64.18	91.06
	TE_{444}	3.622	8.139	11.74	24.51	41.15	41.95	48.79	62.83	64.07	90.84
0.5											
	TE_{222}	3.787	11.93	24.77	28.10	41.34	42.34	64.66	83.01	84.53	91.71
	TE_{333}	3.769	11.87	24.61	28.05	41.18	41.98	63.98	82.55	84.04	90.62
	TE_{444}	3.765	11.86	24.59	28.04	40.44	41.94	63.91	82.52	82.53	90.50

The aim of this section is to analyze the effect of the taper ratio on the natural frequencies of the beam. The *Relative Averaged and Maximum Difference* is evaluated as follows:

$$\varepsilon = \frac{||\omega_{0.50} - \omega_{1.00}||}{\omega_{1.00}} \tag{4.2}$$

The value of the Relative Averaged Difference and the Relative Maximum Difference vary depending of the different boundary conditions. This two differences are listed for each one of the three theory and for all different boundary condition considered, in Table 4.10. The data submitted in the Tables are analyzed below.

Table 4.6. Comparison of the first ten natural frequencies (Hz) of a square metallic beam with $h = 0.1\ m,\ b = 1\ m\ ,\ l = 10\ m$ for $Clamped - Free$ Boundary Conditions.

c_t/c_r	Theory	*Mode* 1	2	3	4	5	6	7	8	9	10
1.0											
	ABAQUS	0.823	5.153	8.118	14.43	15.31	28.29	46.18	46.79	48.67	69.93
	TE_{222}	0.833	5.182	8.151	14.66	15.80	28.87	47.73	47.92	49.06	71.79
	TE_{333}	0.828	5.182	8.143	14.51	15.76	28.46	47.09	47.52	48.81	70.42
	TE_{444}	0.827	5.177	8.141	14.50	15.59	28.42	47.01	47.02	48.79	70.29
0.5											
	TE_{222}	1.020	5.555	8.865	14.93	26.75	28.96	41.54	47.73	66.41	71.24
	TE_{333}	1.014	5.524	8.863	14.84	26.67	28.74	41.42	47.27	66.12	70.44
	TE_{444}	1.013	5.520	8.862	14.83	26.28	28.71	41.41	47.23	64.97	70.35

Table 4.7. Comparison of the first ten natural frequencies (Hz) of a square metallic beam with $h = 0.1\ m,\ b = 1\ m\ ,\ l = 10\ m$ for *Simply Supported* Boundary Conditions.

c_t/c_r	Theory	*Mode* 1	2	3	4	5	6	7	8	9	10
1.0											
	ABAQUS	2.293	9.182	20.69	29.74	36.84	50.20	57.66	59.99	83.13	91.27
	TE_{222}	2.307	9.240	20.73	30.93	36.99	50.92	58.57	62.24	83.81	95.68
	TE_{333}	2.293	9.185	20.71	30.61	36.90	50.20	57.78	61.72	83.38	93.85
	TE_{444}	2.293	9.185	20.70	30.27	36.88	50.20	57.72	61.06	83.24	92.91
0.5											
	TE_{222}	2.285	9.218	16.40	20.82	37.14	39.81	58.22	65.19	81.52	84.04
	TE_{333}	2.282	9.184	16.39	20.67	36.78	39.78	57.52	64.97	81.27	82.88
	TE_{444}	2.282	9.184	16.39	20.67	36.77	39.06	57.49	64.97	79.81	82.82

Table 4.8. Comparison of the first ten natural frequencies (Hz) of a square metallic beam with $h = 0.1\ m,\ b = 1\ m\ ,\ l = 10\ m$ for $Supported - Free$ Boundary Conditions.

c_t/c_r	Theory	*Mode* 1	2	3	4	5	6	7	8	9	10
1.0											
	ABAQUS	3.582	11.62	14.89	24.28	41.58	44.90	50.20	63.54	75.64	90.14
	TE_{222}	3.605	11.75	15.33	24.55	41.75	46.85	50.88	64.22	78.16	92.17
	TE_{333}	3.583	11.63	15.31	24.30	41.64	46.18	50.20	63.68	77.76	90.41
	TE_{444}	3.583	11.62	15.14	24.29	41.62	45.68	50.20	63.61	76.94	90.25
0.5											
	TE_{222}	3.788	11.88	24.66	25.87	28.65	42.17	64.12	64.42	84.42	91.41
	TE_{333}	3.782	11.83	24.48	25.87	28.62	41.74	63.63	64.00	84.10	90.15
	TE_{444}	3.782	11.83	24.48	25.49	28.62	41.73	62.89	63.60	84.10	90.07

Table 4.9. Comparison of the first ten natural frequencies (Hz) of a square metallic beam with $h = 0.1\ m,\ b = 1\ m\ ,\ l = 10\ m$ for $Free - Free$ Boundary Conditions.

c_t/c_r	Theory	$Mode$									
		1	2	3	4	5	6	7	8	9	10
1.0											
	$ABAQUS$	5.198	14.34	28.15	29.93	46.60	50.20	60.31	69.70	91.57	97.42
	TE_{222}	5.230	14.36	28.21	31.08	46.79	50.92	62.82	70.44	94.56	99.62
	TE_{333}	5.199	14.35	28.18	30.76	46.67	50.20	61.98	69.85	94.08	97.72
	TE_{444}	5.198	14.35	28.17	30.42	46.64	50.20	61.31	69.77	93.09	97.54
0.5											
	TE_{222}	5.279	14.48	28.40	38.13	43.18	47.03	70.41	83.47	98.51	100.6
	TE_{333}	5.272	14.43	28.23	38.08	43.15	46.63	69.64	83.25	97.28	100.3
	TE_{444}	5.272	14.43	28.22	38.08	42.41	46.61	69.61	81.76	97.19	100.2

Table 4.4 represent the variation of the first ten frequencies in case of *Clamped – Clamped* boundary conditions. In this case, introducing a taper ratio lower than 1.00 causes a reduction of the bending frequencies along the axe on which there is no tapering and a growth of the bending frequencies related to the other direction. While the first torsional frequency, ω_5, decrease the second torsional frequency, ω_7 increase. Table 4.5 represent the variation of the first ten frequencies in case of *Clamped – Supported* boundary conditions. In this case, introducing a taper ratio lower than 1.00 causes a growth of all frequencies except the sixth and tenth, ω_6 and ω_{10}(bending frequencies). Data submitted in Table 4.6 represents the variation of the first ten frequencies in case of *Clamped – Free* boundary conditions. In this case, introducing a taper ratio lower than 1.00 causes a growth of the bending frequencies and of the first torsional frequency. On the contrary the second torsional frequency ω_7 decrease. Table 4.7 represent the variation of the first ten frequencies in case of *Simply Supported* boundary conditions. In this case, introducing a taper ratio lower than 1.00 causes a global reduction of all frequencies except the eighth, ω_8, that increase.

Data submitted in Table 4.8 represents the variation of the first ten frequencies in case of *Supported – Free* boundary conditions. In this case, introducing a taper ratio lower than 1.00 causes a growth of the bending frequencies except the sixth, ω_6. On the contrary both the first and second torsional frequencies, ω_5 and ω_7 decrease. In Table 4.9 data representative of *Free–Free* boundary conditions are reported. In this case, the introduction of a taper ratio lower than 1.00 causes a growth of all frequencies except the fifth and sixth, ω_5 and ω_6, torsional and bending frequencies, respectively.

Finally in Table 4.10 are listed, for each theory, TE_{222}, TE_{333} and TE_{444} and all the boundary conditions, $Clamped - Clamped$, $Clamped - Supported$, $Clamped - Free$, $Supported - Supported$, $Supported - Free$ and $Free - Free$, the value of the Relative Averaged Difference and the Relative Maximum Difference.

Table 4.10. Comparison of the Averaged difference and the Maximum difference of the first ten natural frequencies of a square metallic beam with taper rateo $c_t = 1.0$ and $c_t = 0.5$ for different Boundary Conditions.

Theory	*Boundary Conditions*						
		CC	CS	CF	SS	SF	FF
TE_{222}	$\varepsilon_{Av.}$	6.25	29.84	15.94	9.72	14.90	7.62
	ε_{Max}	19.29	110.6	69.30	32.68	60.91	22.69
TE_{333}	$\varepsilon_{Av.}$	6.36	29.69	15.84	9.48	15.02	7.82
	ε_{Max}	19.61	109.5	69.30	32.47	59.90	23.80
TE_{444}	$\varepsilon_{Av.}$	6.40	26.68	15.54	9.73	14.87	8.14
	ε_{Max}	17.82	109.5	68.57	31.71	61.69	25.18

Validation and analysis of the results for Pre-Twisted Beams

Firstly, in order to validate the proposed method for the vibrational analysis of pre−twisted beams, various numerical results are obtained and compared with available literature. The case of study concerne a cantilever pre−twisted beam. The geometrical characteristics of the beam are: height, $h = 0.17272$ cm, depth $b = 2.54$ cm, length $l = 15.24$ cm and a pre−twisting angle, $\theta = 45$. The beam is made up of a material with the following characteristics: Young's Modulus, $h = 206.85$ GPa, Shear Modulus, $G = 82.74$ GPa and density $\rho = 7857.6$ kg/m^3. The beam have been treated experimentally by Carngie Carnegie and by theoretical means by Lin et al. [58], Subrahmanyam et al. Subrahmanyam and Yardimoglu et al. [103]. The results obtained by the refined method are compared with the ones taken from the literature in Table 4.11.

In theory, using the refined method with order $N = 1$, should provide more accurate results. The displacement field obtained by using a theory model TE_{111} is analogue to the Timoshenko's one. The difference between the results obtained by the TE_{111} and the ones given by the literature is due to the so called *Poisson Locking*. The costitutive equations used are $3D$ and not reduced. In order to avoid this effect the reduced form of the costitutive equation should be used.

An alternative is the use of a higher order theory. By the use of a TE_{222} or a TE_{333} it is possible to overcome the limit linked to the *Poisson Locking* and to highlight the power of the $3D$ costitutive equations.

Although the higher order model used the results are not as good as the ones proposed by the other authors, that is because those have been obtained by the use of Timoshenko Beam Theory and ad−hoc shear coefficients.Therefore their solution are strictly problem dependent. The shear coefficients depends on the geometry of the cross section.

In Addition, in order to enhance the results obtained by the Refined Method, for the same reason explained in the section of the *Convergence Analysis* the Ritz

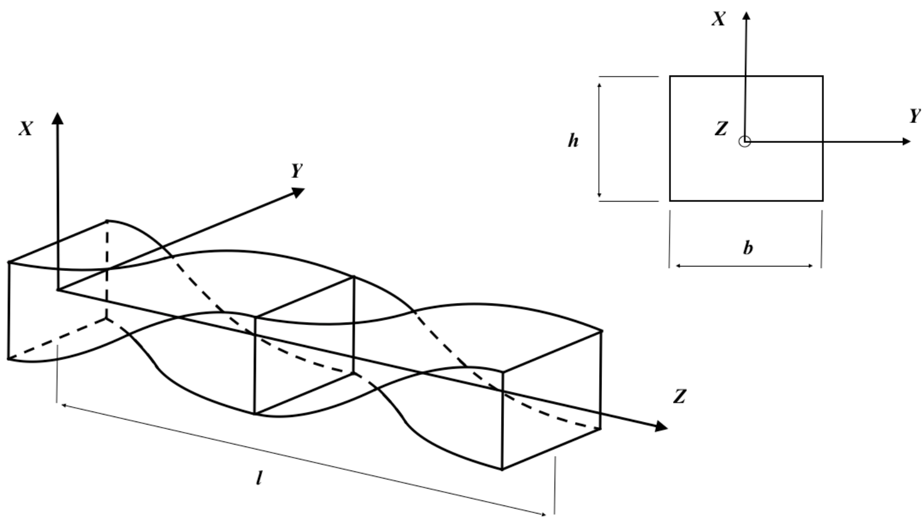

Figure 4.2. Schematic representation of a rectangular section pre-twisted beam.

Table 4.11. Comparison of the first four natural frequencies (Hz) of a cantilever (CF) rectangular metallic beam ($E = 206.85\ GPa$, $G = 82.74\ GPa$, $\rho = 7857.6\ kg/m^3$) with $h = 0.17272\ cm,\ b = 2.54\ cm\ and\ l = 15.24\ cm$ and a pre−twist angle $\theta = 45$.

Theory	$Mode$							
	1	ε_1	2	ε_2	3	ε_3	4	ε_4
TE_{111}	68.1	15.4	364.8	34.7	1025.2	11.4	1190.2	7.23
TE_{222}	63.7	7.97	390.6	25.8	944.0	2.61	1111.8	0.16
TE_{333}	62.9	6.61	360.8	24.4	939.9	2.16	1110.4	0.04
Yardimoglu et al. [103]	61.8	4.75	304.8	5.10	944.5	2.66	1193.0	7.48
Lin et al. [58]	61.7	4.58	300.9	3.76	917.0	0.33	1175.1	5.86
Subrahmanyam et al. [88]	62.0	5.08	305.1	5.21	955.1	3.82	1214.7	9.43
Subrahmanyam et al. [88]	61.9	4.92	304.7	5.07	937.0	1.85	1205.1	8.57
Carneige [15]	59.0	-	290.0	-	920.0	-	1110.0	-

expansion order should be increased. This shrewdness should lead to enhance the performance of the proposed method.

Secondly the variation of the natural frequencies of a beam parameterized with respect to the angle of pre−twist have been analyzed. The beam under investigation is metallic, made up of an aluminium alloy, with Young's Modulus $E = 69\ GPa$, Poisson's ratio $\nu = 0.33$ and density $\rho = 2700\ kg/m^3$.

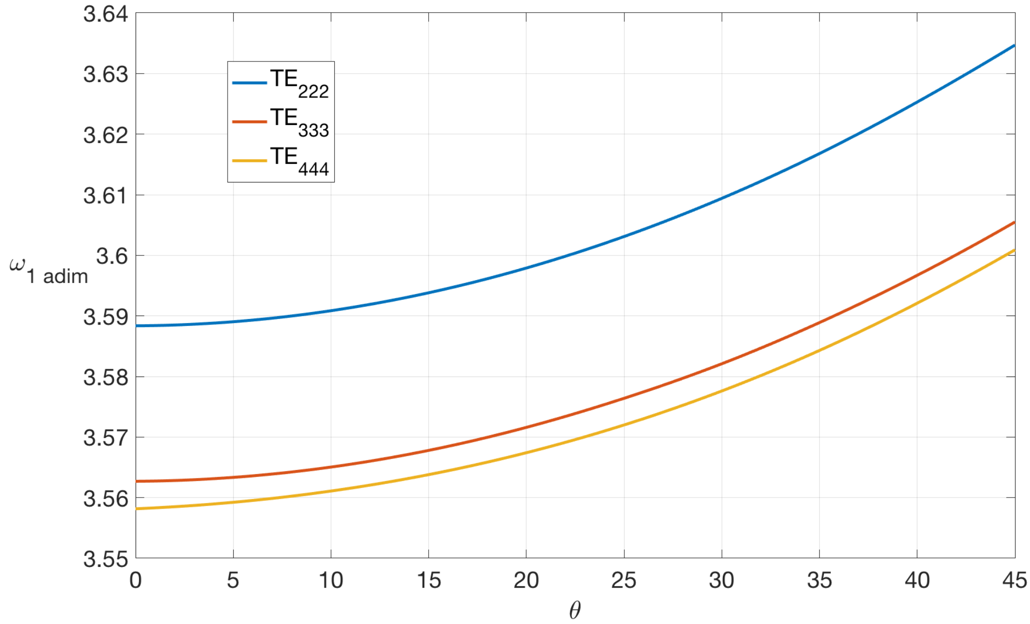

Figure 4.3. Variation of the *first* non-dimensional frequency of a cantilever, rectangular section, metallic beam with respect to the *pre-twist* angle θ for different theories.

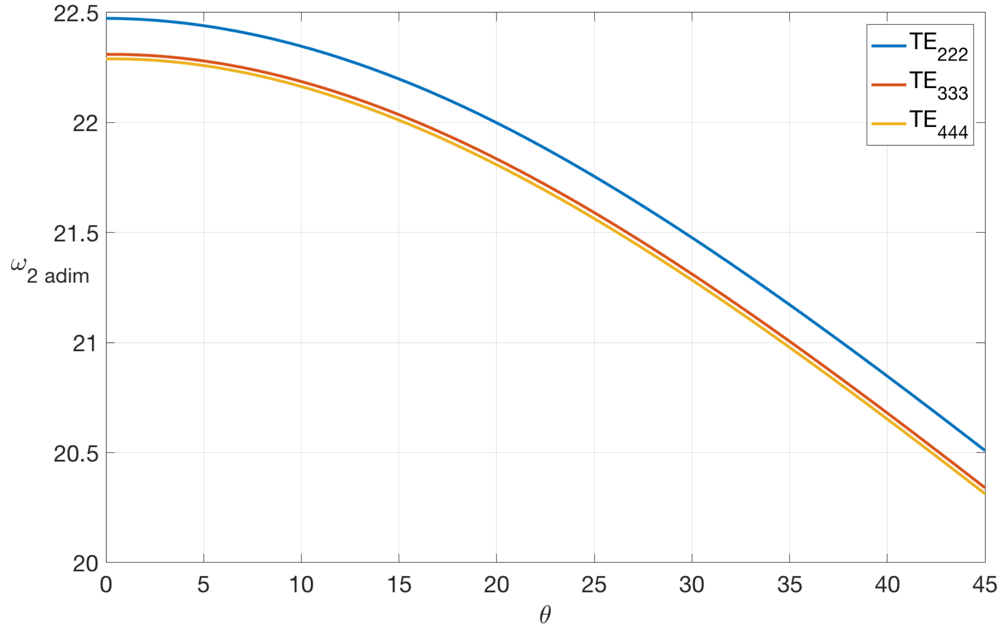

Figure 4.4. Variation of the *second* non-dimensional frequency of a cantilever, rectangular section, metallic beam with respect to the *pre-twist* angle θ for different theories.

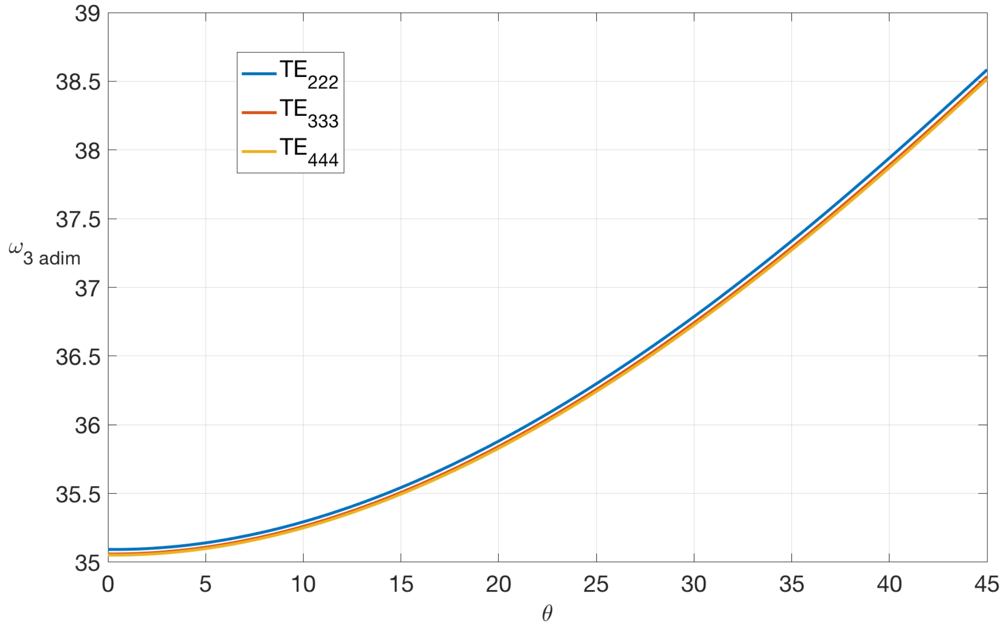

Figure 4.5. Variation of the *third* non-dimensional frequency of a cantilever, rectangular section, metallic beam with respect to the *pre-twist* angle θ for different theories.

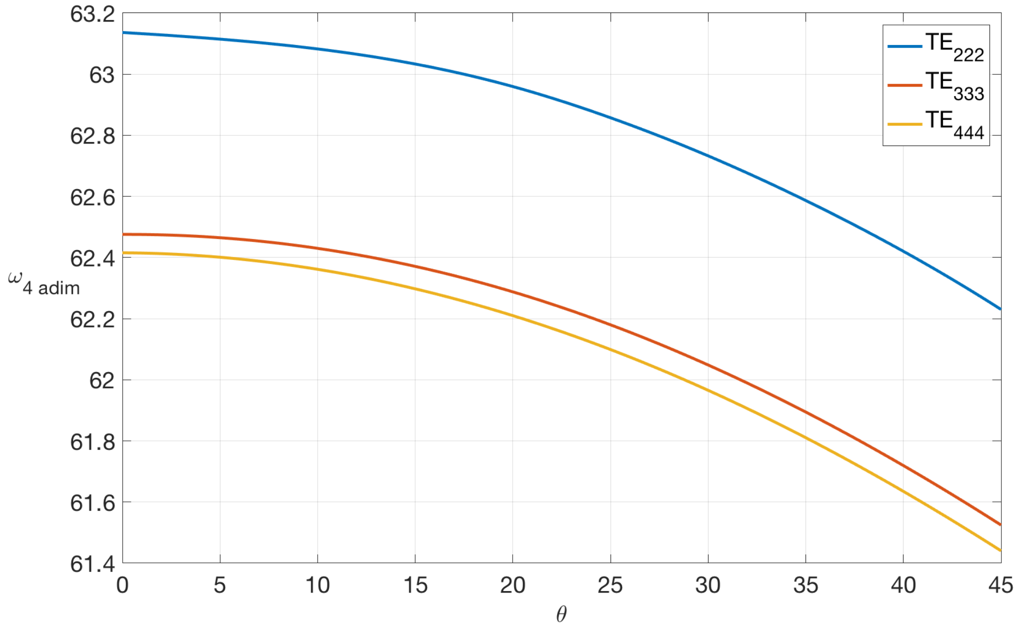

Figure 4.6. Variation of the *fourth* non-dimensional frequency of a cantilever, rectangular section, metallic beam with respect to the *pre-twist* angle θ for different theories.

The geometric characteristics are $h = 0.1\ m$, $b = 1\ m$ and $L = 10\ m$. The three different curves represent three different beam models, characterized by an expansion order 2, 3 and 4 despite the order of the polynomial expansion vary, i and j − Ritz expansion indexes − are fixed, $i = j = 18$. Figure 4.1 − 4.4 represents the variation of the first, the second, the third and the fourth non dimensional natural frequency of the metallic pre−twisted cantilevered beam with respect to the variation of the pre−twist angle.

It is clear the advantage obtained by the use of a refined beam model of higher order. The improvement obtained using a higher order beam theory decrease with the growth of the order of expansion of the displacement field, thereby the highest order beam model used is TE_{444}.

Figure 4.5 represents the variation of the first four natural frequencies adimensionalized with their value without pre−twisting the beam as functions of the pre−twist angle θ. The trends of the four frequencies are due only to the variation of the momentum of inertia along the axes. The momentum of inertia varies with the inverse of a trigonometric function of the rotation angle of the cross section. In particular the growing trend of the first and third frequencies suggest that those are the bending modes in the xz plane. On the other hand the declining trend of the second and fourth frequencies suggest that those are the bending modes in the yz plane.

Hollow tapered beams

This case study is relative to a hollow rectangular cantilever beam. The beam is made up of an aluminium alloy characterized by a Young Modulus, $E = 69\ GPa$, Poisson's ratio, $\nu = 0.33$ and density $\rho = 2700\ kg/m^3$. The geometric characteristics of the cross section are $h = 0.1\ m$, $b = 1\ m$. The analysis have been carried out using three different values of slenderness ratio $\lambda = 10$, $\lambda = 25$ and $\lambda = 100$.

Data submitted in Table 4.12 represents the first four natural frequencies of the beam studied for the three different values of the slenderness ratio and for three different beam refined models, TE_{222}, TE_{333} and TE_{444}. For high values of slenderness ratio the difference between the three theories is not appreciable because the case study falls within the hypothesis of EBBT. Discrepancies between the results of different theories are appreciable for dumpy beams. In addition, for hollow beams, higher order beam models allows to obtain better results for lower values of taper ratio.

In contrast with the decrescent trend of the fourth frequency, the first three frequencies increase with the reduction of the taper ratio. For the first three frequencies the reduction of the inertia is predominant on the reduction of the rigidity of the beam due to the variation of the momentum of inertia. On the contrary for the forth frequency the reduction of the momentum of inertia is predominant.

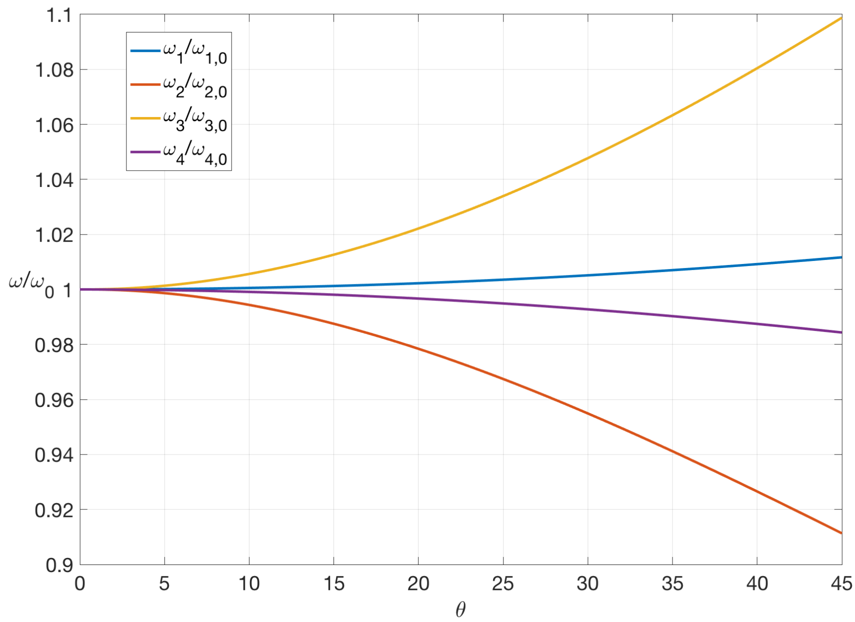

Figure 4.7. Variation of the first four natural frequencies of a cantilever, rectangular section, metallic beam with respect to the *pre-twist* angle θ.

Table 4.12. Comparison of the first four natural frequencies (Hz) of a cantilever, squared cross section, metallic, hollow beam with $h = 1\ m,\ b = 0.1\ m$ for different values of aspect rateo: $\lambda = 10,\ \lambda = 25,\ \lambda = 100$.

Theory	$\lambda = 10$				$\lambda = 25$				$\lambda = 100$			
	1	2	3	4	1	2	3	4	1	2	3	4
c_t/c_r	1.0											
TE_{222}	5.70	9.92	35.0	58.6	0.912	1.60	5.69	9.91	0.057	0.100	0.357	0.626
TE_{333}	5.67	9.88	34.0	57.5	0.911	1.60	5.66	9.88	0.057	0.100	0.357	0.626
TE_{444}	5.66	9.88	34.0	57.5	0.910	1.60	5.66	9.88	0.057	0.100	0.357	0.626
c_t/c_r	0.75											
TE_{222}	5.98	10.1	35.3	55.1	0.957	1.61	5.73	9.22	0.060	0.101	0.359	0.581
TE_{333}	5.95	10.0	34.3	54.2	0.956	1.61	5.71	9.20	0.060	0.101	0.359	0.581
TE_{444}	5.95	9.99	34.3	54.1	0.956	1.61	5.70	9.19	0.060	0.101	0.359	0.581
c_t/c_r	0.50											
TE_{222}	6.34	10.2	35.5	50.9	1.01	1.63	5.78	8.45	0.063	0.102	0.362	0.531
TE_{333}	6.31	10.1	34.7	50.2	1.01	1.63	5.75	8.42	0.063	0.102	0.362	0.531
TE_{444}	6.30	10.1	34.6	50.2	1.01	1.63	5.75	8.42	0.063	0.102	0.362	0.531
c_t/c_r	0.25											
TE_{222}	6.80	10.3	35.9	45.7	1.09	1.65	5.83	7.51	0.068	0.103	0.365	0.472
TE_{333}	6.78	10.3	35.1	45.2	1.09	1.65	5.80	7.50	0.068	0.103	0.365	0.472
TE_{444}	6.77	10.3	35.0	45.2	1.09	1.65	5.80	7.49	0.068	0.103	0.365	0.471

Hollow FGM beams

In this section the advantages of the presented method are show by analyzing a hollow functionally graded beam. The beam is characterized by a rectangular cross section, with $b = 1.0\ m$ and $h = 0.5\ m$. The length is $l = 10\ m$ and the thickness rateo is 0.1. The material properties are $E_c = 380\ GPa$, $\nu_c = 0.3$, $\rho_c = 3690\ kg/m^3$ for the ceramic phase and $E_m = 70\ GPa$, $\nu_m = 0.3$, $\rho_m = 2702\ kg/m^3$ for the metal phase.

In Table 4.13 are listed the values of the fist six frequencies of the presented beam. The results obtained with the method have been compared with others obtained by a commercial solver, ABAQUS. Using a TE_{999} beam theory and an order of expansion of the Ritz function 18, the amount of DOFs involved in the analysis, using the presented method, is 2970. On the other side, for the FEA there have been used 73899 brick elements $C3DR20$ with 20 nodes, that means 1477980 DOFs. The averaged and maximum relative differences, $\varepsilon_{Av.}$ and $\varepsilon_{Max.}$, respectively, have been evaluated as in Eq. 4.1.

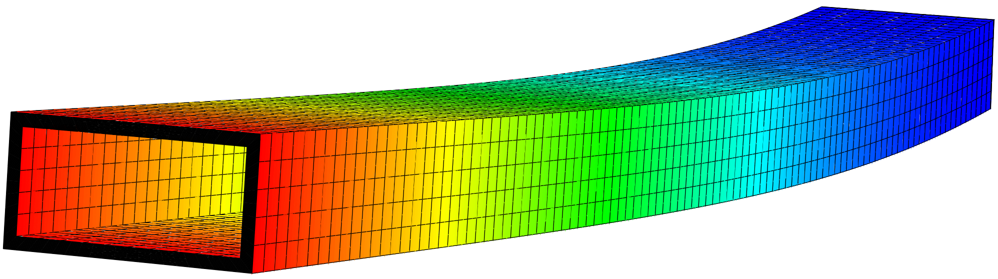

Figure 4.8. Representation of the *first* mode of the FGM beam.

In Figures 4.8 to 4.13 the first six modes reported in Table 4.13 have been represented. The first four and the last one are bending frequencies, the fifth is a torsional frequency. As it can be seen by the shape modes reported the the presented method allows to observe and evaluate the distortion of the beam's cross section.

Table 4.13. Comparison of the first six natural frequencies (Hz) of a cantilever square FGM hollow beam with $h = 1\ m$, $b = 0.5\ m$ and length $l = 10\ m$.

Theory	Mode						$\varepsilon_{Av.}$ [%]	$\varepsilon_{Max.}$[%]
	1	2	3	4	5	6		
ABAQUS	2.3435	4.0638	13.761	23.531	24.075	34.525	-	-
TE_{999}	2.3285	4.0334	13.761	23.386	24.610	35.331	1.09	2.33

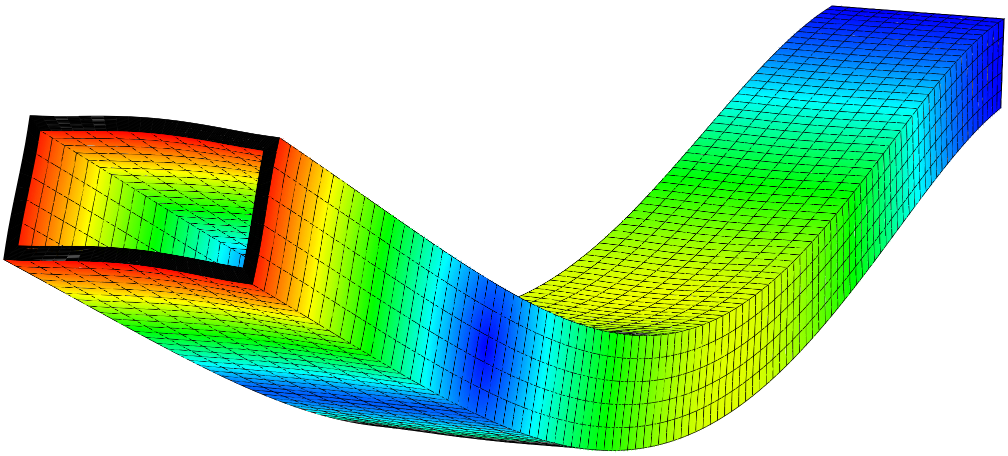

Figure 4.9. Representation of the *second* mode of the FGM beam.

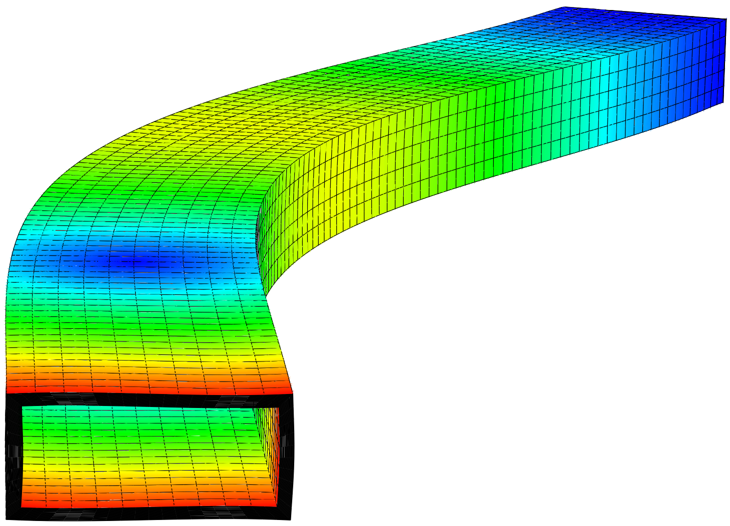

Figure 4.10. Representation of the *third* mode of the FGM beam.

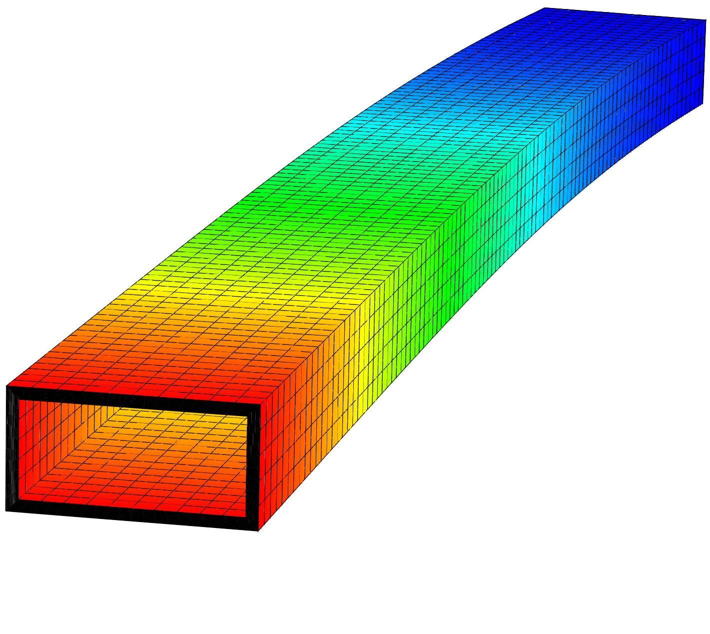

Figure 4.11. Representation of the *fourth* mode of the FGM beam.

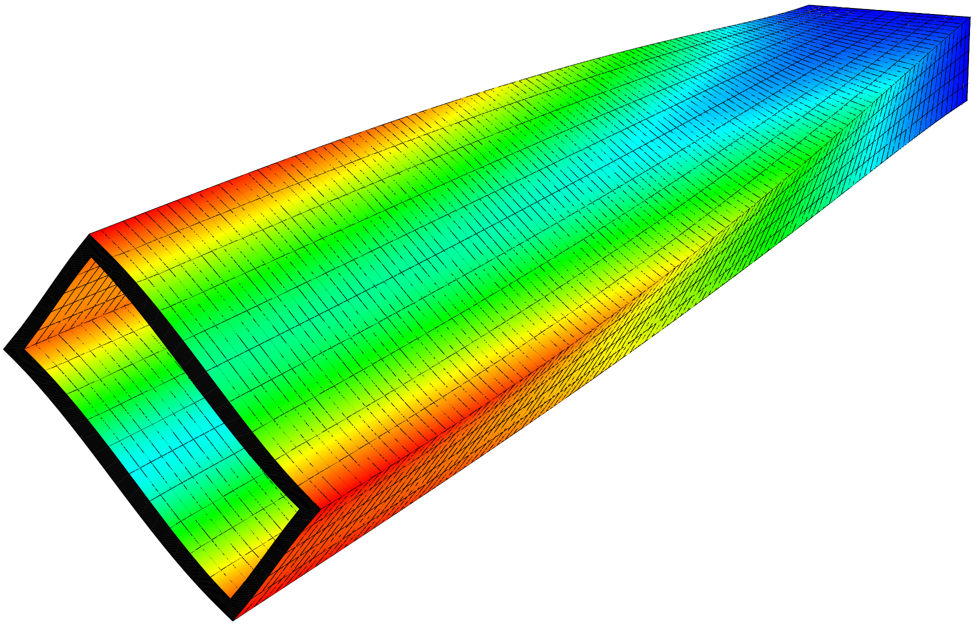

Figure 4.12. Representation of the *fifth* mode of the FGM beam.

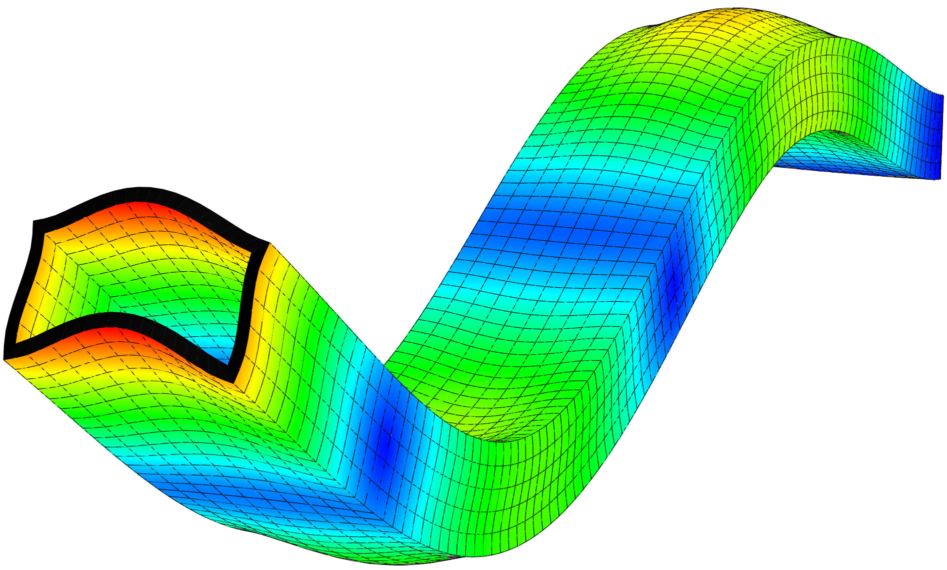

Figure 4.13. Representation of the *sixth* mode of the FGM beam.

Chapter 5

Results for Rotating Structures

Understand how the behavior of a structure, such as a rotor balde, changes spinning the structure around a axe of rotation is important when analyzing systems of different type (Compressors, turbines, rotors etc.). In this section are listed and discussed the results obtained by analyzing rotating structures of different type. A first paragraph is dedicated to the validation of the present theory. The aim of the second paragraph is the analysis of the results obtained for a FGM rotating Beam.

Validation of the proposed method for a rotating structure

In order to validate the proposed method, several illustrative examples are presented below. The Boundary conditions and the geometrical as well as the physical characteristic of the beam are assumed to be problem parameters.

To enable a general application of results they are presented in non−dimensional form adopting the following expressions:

$$\omega_0 = \sqrt{\frac{\rho A l^4}{E J_{yy}}}, \qquad \delta_r = \frac{r_{hub}}{l}, \qquad \Omega^* = \tilde{\Omega}\,\omega_0, \qquad \omega^* = \frac{\omega}{\omega_0}, \qquad S = \sqrt{\frac{A l^2}{J_{yy}}} \tag{5.1}$$

where J_{yy} is the moment of inertia about the y axe, E is the Young Modulus, ρ is the density of the material, r_{hub} represent the hub radius, l the length of the beam and A the area of the cross−section.

First case is the analysis of a thin beam characterized by a slenderness ratio $S = 1000$ and a squared cross section. The results obtained for different values of the non−dimensional speed parameter, the non−dimensional hub radius and different boundary conditions are listed in Table 5.1 and compared with those presented in references [14, 17].

Datas reported from references have been obtained by using the Dynamic Stiffness Method and the CUF, respectively considering reference [14] and [17]. In order to obtain values of frequencies that can be compared with those from literature, both Coriolis and Softening effects are disregarded.

The results obtained by the Refined method are in strong agreement with the references for all the different Boundary Conditions (B.C.) and different values of the two non−dimensional parameters. The B.C. considered are *Clamped − Free*, *Clamped − Supported* and *Supported − Supported*. In Figure 5 all the different B.C. are schematically represented.

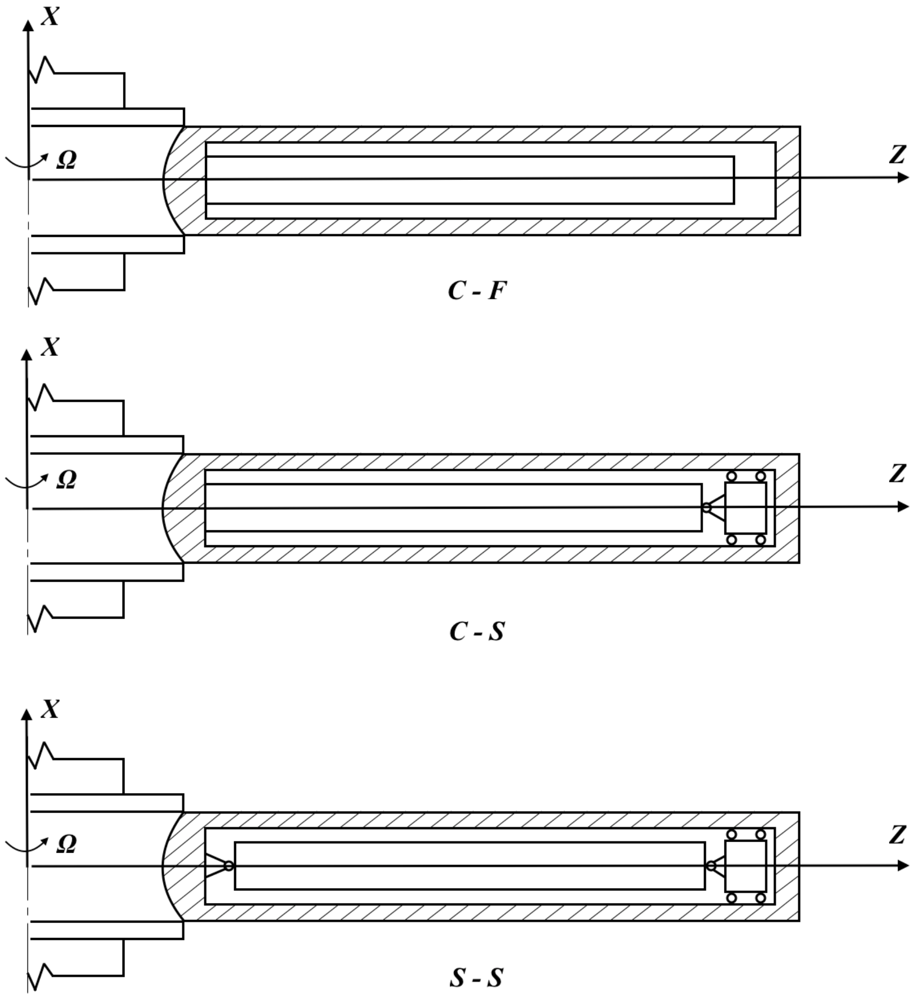

Figure 5.1. Schematic representation of various Boundary Conditions.

Table 5.1. Dependency of the first three dimensionless natural frequencies on the variations of the dimensionless angular speed and dimensionless hub dimension of a $Eulero - Bernoulli$ beam.

B.C.	ω^*	$Theory$	$\Omega^* = 1$		$\Omega^* = 5$	
			$\delta_r = 0$	$\delta_r = 1$	$\delta_r = 2$	$\delta_r = 5$
$C - F$	1	[14]	3.6816	3.8888	10.862	12.483
		[17]	3.6816	3.8895	10.866	12.488
		Present	3.6914	3.8980	10.872	12.494
	2	[14]	22.181	22.375	32.764	35.827
		[17]	22.178	22.375	32.773	35.840
		Present	22.241	22.435	32.818	35.880
	3	[14]	61.842	62.043	73.984	77.935
		[17]	61.836	62.032	73.986	77.939
		Present	62.003	62.204	74.135	78.083
$C - S$	1	[14]	15.513	15.650	22.663	24.729
		[17]	15.512	15.649	22.670	24.738
		Present	15.551	15.689	22.698	24.764
	2	[14]	50.093	50.277	60.906	64.382
		[17]	50.092	50.275	60.919	64.399
		Present	50.213	50.396	61.018	64.492
	3	[14]	104.39	104.59	116.99	121.30
		[17]	104.42	104.62	117.04	121.36
		Present	104.62	104.82	117.21	121.52
$S - S$	1	[14]	10.022	10.264	19.684	22.078
		[17]	10.021	10.264	19.690	22.086
		Present	10.022	10.264	19.684	22.078
	2	[14]	39.642	39.889	53.132	57.235
		[17]	39.638	39.886	53.141	57.248
		Present	39.638	39.886	53.129	57.233
	3	[14]	88.991	89.241	103.92	108.93
		[17]	88.003	89.253	103.94	108.96
		Present	88.976	89.225	103.91	108.92

The second case of analysis regards a beam that is not thin as the previous, in fact the slenderness rateo is $S = 30$ and the cross−section is a square.

As a consequence, the Eulero−Bernoulli model is no longer valid and, for this reason a FSDT (First Order Deformation Theory) is needed. The behavior of such beam, in terms of first natural frequency is shown in Table 5.2. The difference between the present method and reference [54] is calculated as:

$$\varepsilon = \frac{||\omega^* - \omega^*_{ref}||}{\omega^*_{ref}} \tag{5.2}$$

The first dimensionless natural frequency of this cantilever Timoshenko beam are listed and compared with [17] and [54] in Table 5.2. As in the previous case the results are in agreement with the references with a difference lower than the 1%. By using the refined method no shear factor is used.

In the third case, a uniform and a tapered cantilever beams are considered. For those the dimensionless hub parameter is settled as $\delta_r = 1.0$ and $\delta_r = 0.0$, respectively. The variation of the chord is linear in the width for the tapered beam. The taper rateo is assumed to be $c_t/c_r = 0.5$. In order to provide a comparison the results presented in [47] have been reported. The results obtained by using the refined method are listed with those of reference [47] in Table 5.3. As can be seen by a close look at this table, for all the different values of the non−dimensional angular speed, the values of the first three dimensionless frequencies are in strong agreement with those of the reference. For both, uniform and tapered beams, the difference, evaluated by using Eq. 5.2, is lower than 1%. In [47] the beam is approximated by adopting a variable−order Finite Element Method conceived for tapered structures.

The refined method allows to observe the complete behavior of a body. In the following example the *chorwise* motion is analyzed for a rotating uniform beam. The results obtained are compared in Table 5.4 with those of references [17] and [27]. With respect to [27], the difference on the fundamental *chordwise* frequency is evaluated by using the Eq. 5.2. Figure 5 shows the *chordwise* motion behavior, here the dimensionless frequencies are reported as functions of the angular speed parameter. The frequency related to the stretching mode (marked with the letter S in the graph) vary with the parameter *, in particular it increase with the angular velocity. This effect can not be appreciate in the results presented in reference [27] because there the term $u_{z,z}$ of the displacement field is neglected.

Table 5.2. First dimensionless natural frequency of a cantilever Timoshenko beam as a function of the rotating speed.

Ω^*	0	1	2	3	5	7	9
[54]	3.4798	3.6452	4.0994	4.7558	6.3934	8.2184	10.109
[17]	3.4831	3.6494	4.1064	4.7567	6.4144	8.2538	10.164
Present	3.5036	3.6694	4.1250	4.7839	6.4295	8.2673	10.177
ε (%)	0.68	0.66	0.62	0.59	0.56	0.59	0.67

Figure 5 represents the behavior of the dimensionless frequency parameter of a beam characterized by a slenderness rateo $S = 100$ and a rectangular cross section with $\tau = h/b = 0.5$, with the variation of the dimensionless angular speed parameter. Moreover the beam is tapered and pre−twisted, the twist rateo is $\dot{\theta} = 15.6\ deg/m$ (the cross section at the tip of the beam is twisted of 45 with respect to the root cross section), the taper rateo

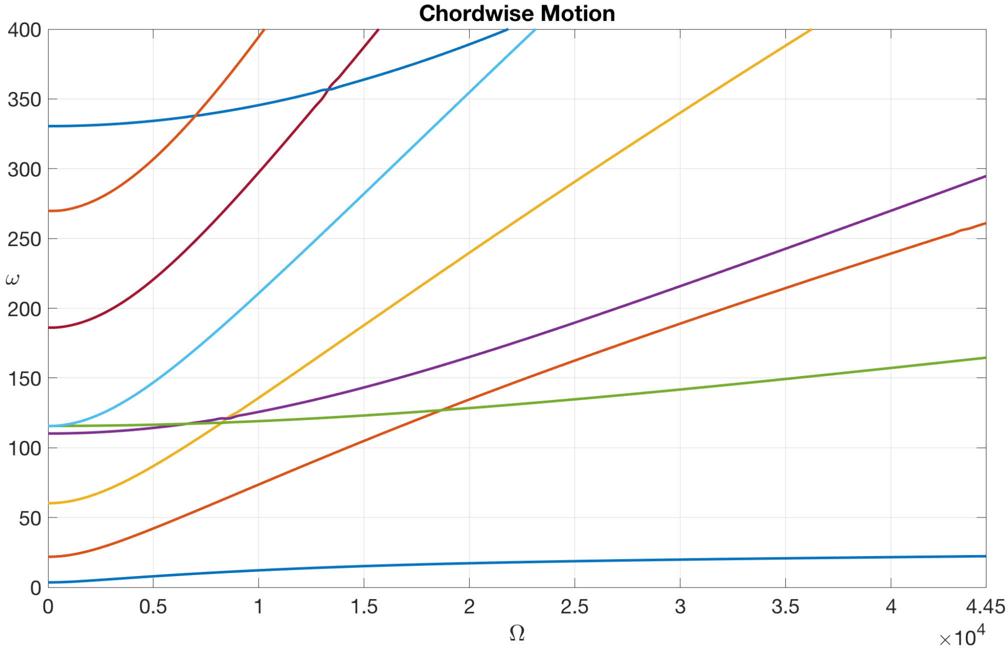

Figure 5.2. Variation of the non−dimensional *chordwise* natural frequencies for the speed parameter whith $\delta_r = 0.1$ and $S = 70$.

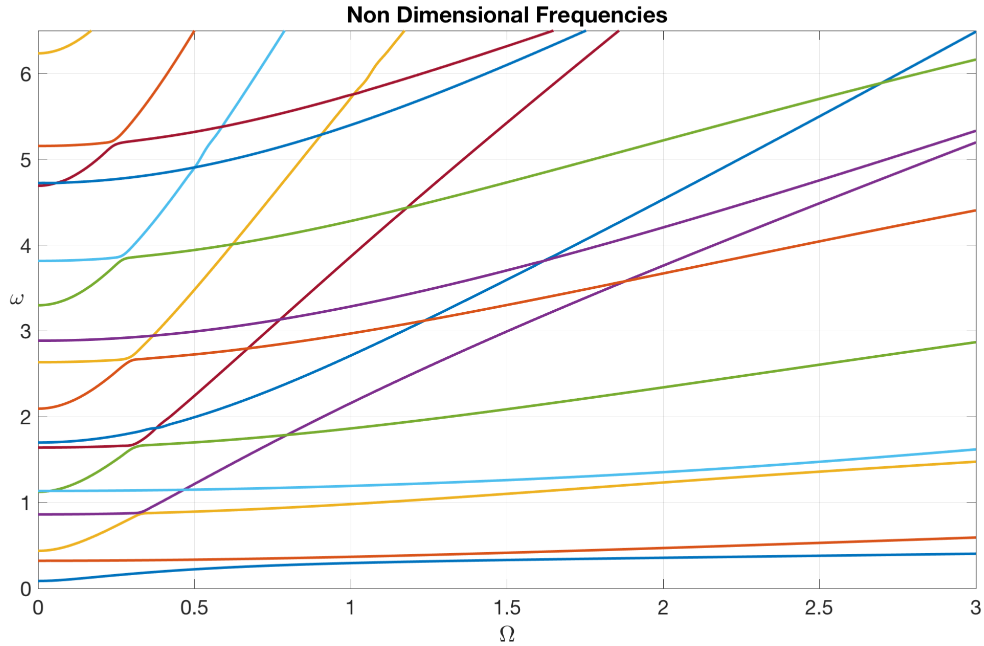

Figure 5.3. Frequencies envelope with the speed parameter.

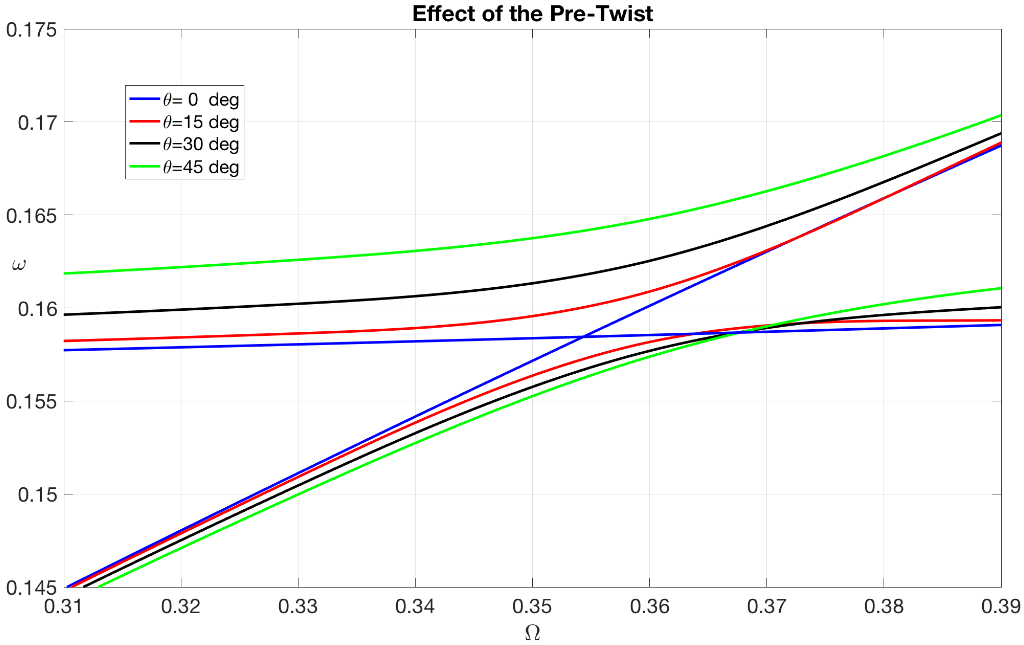

Figure 5.4. Effect of the pre−twist on the behavior of the third and fourth frequencies.

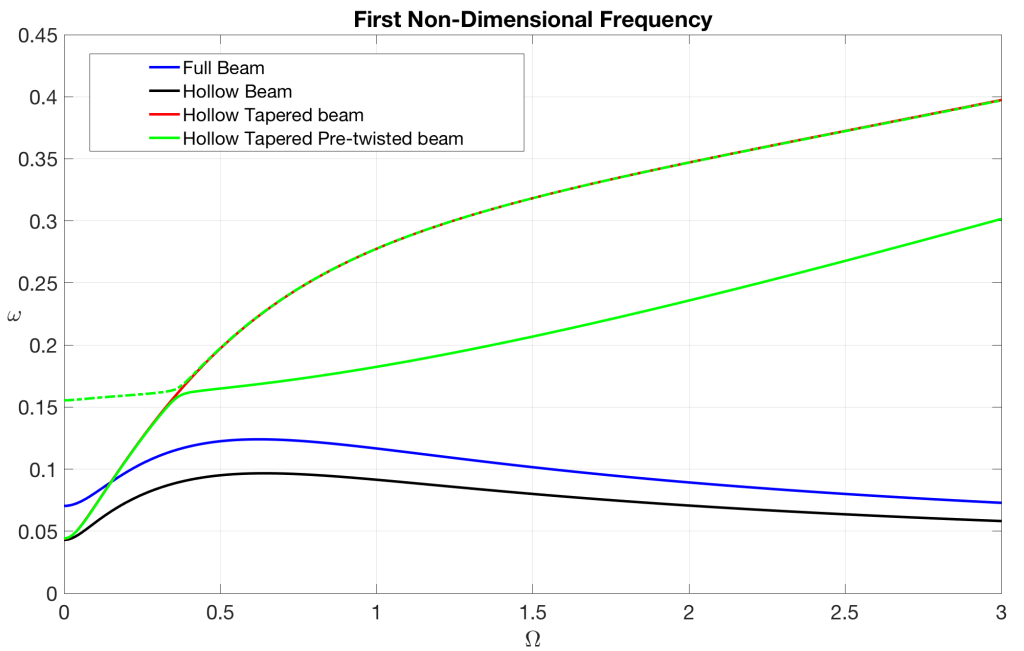

Figure 5.5. Effect of different parameters on the first frequency.

Table 5.3. Dependency of the first three dimensionless natural frequencies on the variations of the dimensionless angular speed for uniform ($\delta_r = 1$) and tapered ($\delta_r = 0$, $c_t/c_r = 0.5$) beams.

Ω^*	ω^*	Uniform			Tapered		
		[47]	Present	ε (%)	[47]	Present	ε (%)
0	1	3.5160	3.5277	0.33	3.8237	3.8028	0.55
	2	22.034	22.106	0.32	18.317	18.255	0.34
	3	61.697	61.888	0.31	47.264	47.043	0.47
1	1	3.8888	3.8791	0.25	3.9866	3.9605	0.66
	2	22.375	22.328	0.21	18.474	18.437	0.20
	3	62.043	61.907	0.22	47.417	47.351	0.14
5	1	8.9403	8.8843	0.63	6.7344	6.6960	0.57
	2	29.352	29.290	0.21	21.905	21.866	0.18
	3	69.760	69.524	0.34	50.933	50.765	0.33
10	1	16.606	16.495	0.67	11.501	11.493	0.27
	2	44.368	44.231	0.31	30.182	30.098	0.28
	3	89.156	88.978	0.20	60.564	60.485	0.13

Table 5.4. Dependency of the first three dimensionless natural frequencies on the variations of the dimensionless angular speed and hub dimension.

δ_r	Ω^*	[17]	[27]	Present	ε (%)
0	2	3.6196	3.6173	3.6282	0.30
	10	4.9700	4.9619	4.9779	0.32
	50	7.3337	7.4553	7.3260	1.73
1	2	4.3978	4.3960	4.4058	0.22
	10	13.048	13.047	13.049	0.02
	50	41.227	41.346	41.657	0.75
5	2	6.6430	6.6421	6.6499	0.12
	10	27.266	27.276	27.270	0.02
	50	74.003	74.178	74.685	0.68

(along the width) is $c_{tip}/c_{root} = 0.5$. By a closer look at the graph it is possible to see how the interaction between the third and fourth frequencies gives birth to a *veering*. Without the pre-twist angle, θ, there is a crossing between those two frequencies. Comparing the behavior of this beam parameterized with the total pre−twist angle θ, it is possible to observe how, by pre−twisting the beam, the mixing of the frequencies (that are no longer of pure bending or torsional motion) originates the veering (see Figure 5). By increasing θ the gap between the two curves increase.

In Figure 5 it is possible to appreciate the variation of the first dimensionless frequency of the beam with the introduction of different geometric parameters. The blue curve represent a uniform rotating beam with a rectangular cross section; the black curve represents a beam with the same geometrical characteristics but hollow, the thickness rateo of this thin walled structure is 0.1 ; with the red curve it has been identified the behavior of the previous thin walled structure with a taper rateo $TR = 1$; at least, the green curve represents the variation of the first natural frequency of the thin walled, tapered and pre−twisted uniform beam (the geometrical characteristics are the same of the previous cases, in adjunction the total pre−twisting angle is 45 degrees).

By looking at this graph it is possible to understand how the combination of all the different parameters that have been considered modify the behavior of the structure. In particular, the thin walled beam is less rigid than the full beam. Adding a taper rateo , $TR < 1$, the effect due to the Coriolis therm decrease, the trend of the frequency increase till reaching a stationary grow rate. By introducing the pre−twist angle there are no appreciable differences between the green and red curves for low non dimensional rotating speed values. Increasing this parameter it is possible to observe how the gap between the two curves start increasing. This effect is linked to the geometrical characteristics of the beam, in particular to the fact that the first frequency is no longer of pure bending.

Functionally Graded Rotating Beam

In this last section the analysis is focused on a rotating FGM beam. The analyzed beam (see Figure 5.6) is characterized by a slenderness rateo $S = 20$ and a rectangular cross section with $\tau = h/b = 0.5$. Moreover the beam is tapered and pre−twisted, the twist rateo is $\dot{\theta} = 15.6\ deg/m$ (the cross section at the tip of the beam is twisted of 45 with respect to the root cross section), the taper rateo (along the width) is $c_{tip}/c_{root} = 0.5$. The thickness rateo is $t/b = 0.1$. The beam is made of Functionally Graded Material, with the ceramic phase characterized by $E_c = 380\ GPa$, $\nu_c = 0.30$, $\rho_c = 3960\ kg/m^3$ and a metal phase characterized by $E_m = 70\ GPa$, $\nu_c = 0.30$, $\rho_c = 2702\ kg/m^3$.

The behavior of the presented beam as function of the non dimensional angular speed is shown in Figure 5.7. It is interesting to note how the behavior of the first two frequencies is affected by their interaction. The second frequency appear to decrease because of the Coriolis Effect. In sharp contrast with this, the first frequency increase. The interaction between this two modes leads to a drop of the growth rate of the first frequency and an increment of the growth rate of the second frequency that starts growing. Increasing the non dimensional angular speed, the second frequency appears at first to grow and than becomes steady. Again the interaction between the first two modes provoke a drop of the growth rate of the first frequency and an increment of the growth rate of the second frequency.

In Table 5.5 are listed the first ten frequencies for the presented beam. The results have been obtained by approximating with a different number of layers the FG beam. Increasing first from 15 to 20 and then from 20 to 25 the number of layers in which the

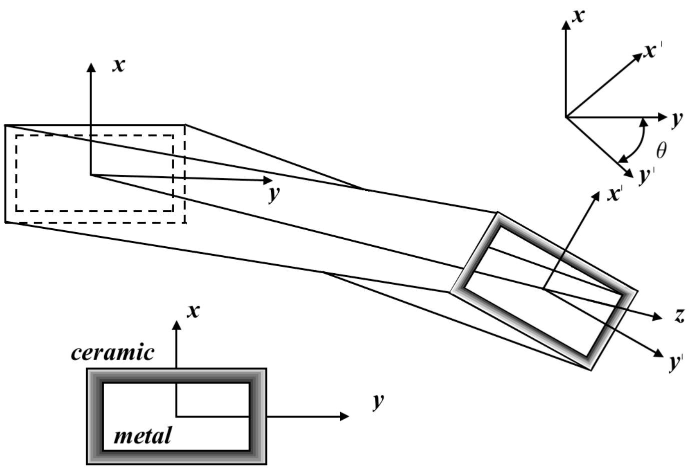

Figure 5.6. Schematic representation of the analyzed FG Beam.

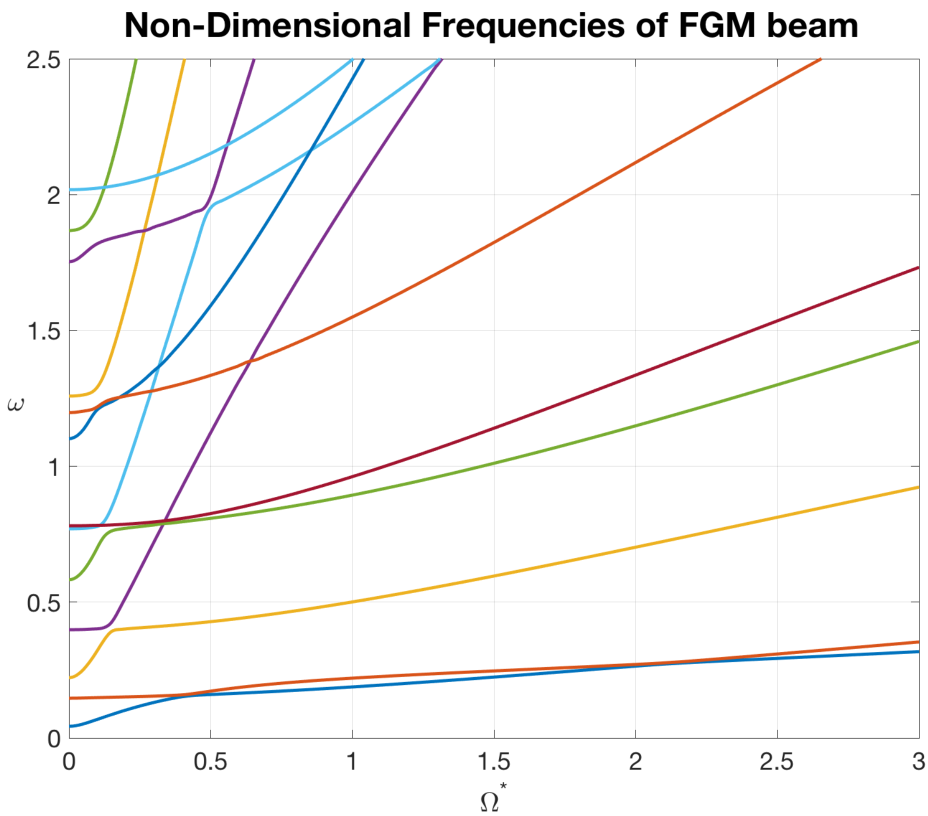

Figure 5.7. Non Dimensional Frequencies of a FG, cantilever, tapered, pre−twisted and rotating beam.

thickness have been divided, it is possible to observe, raising fro 15 to 20, an averaged growth of 1.17% for all ten frequencies, while the second boost leads to an averaged increment of 1.94%.

Table 5.5. Variation of the first ten dimensionless natural frequencies with the dimensionless angular speed and number of layers. *respect the case $nl = 15$.

Mode	Angular speed parameter							ε^*_{Av}	ε^*_{Max}
	0.0	0.1	0.3	1.0	1.5	2.4	3.0	[%]	[%]
$nl = 15$									
1	0.0259	0.0282	0.0298	0.0345	0.0393	0.0494	0.0568	-	-
2	0.0431	0.0650	0.1308	0.1872	0.2241	0.2881	0.3177	-	-
3	0.1465	0.1483	0.1541	0.2195	0.2467	0.3004	0.3534	-	-
4	0.2222	0.3056	0.4093	0.4990	0.5961	0.7902	0.9233	-	-
5	0.3984	0.4013	0.7216	1.993	2.777	3.940	4.633	-	-
6	0.5827	0.6806	0.7840	0.8918	1.011	1.269	1.460	-	-
7	0.7699	0.7763	1.309	2.257	2.648	3.364	3.806	-	-
8	0.7809	0.7823	0.7952	0.9586	1.140	1.495	1.732	-	-
9	1.102	1.197	1.352	2.407	3.364	5.137	6.347	-	-
10	1.198	1.213	1.278	1.544	1.824	2.353	2.692	-	-
$nl = 20$									
1	0.0263	0.0286	0.0303	0.0349	0.0397	0.0498	0.0572	1.26	1.72
2	0.0439	0.0655	0.1318	0.1894	0.2262	0.2911	0.3206	1.08	1.78
3	0.1490	0.1508	0.1566	0.2224	0.2499	0.3024	0.3554	1.24	1.72
4	0.2262	0.3085	0.4160	0.5049	0.6017	0.7957	0.9291	1.12	1.77
5	0.4052	0.4081	0.7235	2.000	2.788	4.072	4.911	1.47	5.99
6	0.5930	0.6895	0.7967	0.9026	1.021	1.277	1.467	1.14	1.77
7	0.7831	0.7893	1.316	2.285	2.675	3.394	3.841	1.16	1.72
8	0.7932	0.7946	0.8074	0.9701	1.151	1.507	1.745	1.17	1.57
9	1.121	1.215	1.371	2.419	3.373	5.143	6.407	0.80	1.76
10	1.220	1.235	1.298	1.563	1.842	2.373	2.714	1.26	1.87
								1.17	5.99
$nl = 25$									
1	0.0266	0.0289	0.0307	0.0353	0.0400	0.0501	0.0575	2.15	2.94
2	0.0445	0.0659	0.1325	0.1910	0.2276	0.2932	0.3227	1.85	3.04
3	0.1508	0.1526	0.1583	0.2243	0.2521	0.3038	0.3568	2.12	2.94
4	0.2290	0.3106	0.4207	0.5092	0.6057	0.7996	0.9332	1.91	3.03
5	0.4101	0.4129	0.7248	2.005	2.795	4.081	4.920	1.90	6.18
6	0.6003	0.6959	0.8056	0.9102	1.028	1.283	1.472	1.94	3.02
7	0.7925	0.7985	1.320	2.305	2.695	3.416	3.865	1.98	2.94
8	0.8019	0.8033	0.8162	0.9783	1.159	1.514	1.753	2.00	2.69
9	1.135	1.228	1.385	2.427	3.379	5.147	6.449	1.36	3.02
10	1.236	1.251	1.313	1.577	1.855	2.387	2.730	2.16	3.20
								1.94	6.18

Chapter 6

Conclusions

The free vibration behavior of metallic and FG short and slender, tapered and pre−twisted, rotating and non−rotating beams with arbitrary boundary conditions have been investigated. The results have been obtained by using advanced and refined quasi−$3D$ beam models developed by using the method of power of series expansion of the displacement field components. The governing equations have been derived in their weak form by the Principle of the Virtual Displacement. The Coriolis effect have been taken into account. The Ritz method has been used as solution technique. In the approximation the algebraic Ritz functions, orthogonalized by using the Gram−Schmidt process, have been employed. The effect of different parameters such as the length, taper ratio, pre−twisting angle, length−to−thickness ratio, material and boundary conditions, have been evaluated and commented.

The results show that the rate of convergence is higher for higher modes and that is slightly affected by the theory adopted. Higher−order models are necessary in order to describe accurately the mode shapes that involves torsion, distortion and warping of the cross section. In addition, in the latter case refinement in the Ritz approximation does not affect significantly the results accuracy while the addiction of DOFs leads to a remarkable enhancement in the results accuracy. In contrast, further improvements in the description of bending modes can only be achieved by increasing the order of the Ritz expansion. When dealing with both three−dimensional FG and metallic beams, the proposed models leads to the same level of accuracy of complex and computationally expansive $3D$ FEM models. The proposed results show the behavior of different beams, the interaction of their frequencies as a function of the non dimensional angular speed and of different parameters such as the taper ratio, pre−twisting angle, and material. Depending on the cross section shape of the beam, both bending and torsional frequencies increase or decrease. The effect linked to the presence of a pre−twisting angle on the interaction and behavior of couples of frequencies of rotating beams have been analyzed leading to the conclusion that the presence of such a geometrical characteristics give birth to a divergence from the potential cross point. Tacking into account both the Coriolis effect and an higher order of expansion along the axe of the beam, it is possible to obtain accurate results in the analysis of the behavior of a generic rotating beam also for high values of the rotational speed (in case of high centrifugal load).

Bibliography

[1] A.E. Alshorbagy, M.A. Eltaher, F.F. Mahmoud *Free vibration characteristics of a functionally graded beam by finite element method*, Appl Math Modell, 35 (1) (2011), pp. 412-425.

[2] Andreassen, M. J., Nielsen, L. O., Jnsson, J., *Distortional Mechanics of Thin-Walled Structural*, Elements. Kgs. Lyngby: Technical University of Denmark (DTU). (BYG Rapport).

[3] Attarnejad R, Ghorbani-Tanha AK, *A general fourth order ordinary differential equation with solution in terms of Bessel functions: theory and engineering applications*, Structural Engineering and Mechanics (2007) 27: 773-776.

[4] R Attarnejad, A Shahba and M Eslaminia, *Dynamic basic displacement functions for free vibration analysis of tapered beams*, Journal of Vibration and Control, 2014.

[5] Auciello NM and Ercolano A, *A general solution for dynamic response of axially loaded non-uniform Timoshenko beams*, International Journal of Solids and Structures (2004) 41: 4861-4874.

[6] Ayaz F., *On the two-dimensional differential transform method*, Applied Mathematics and Computation (2003) 143: 361-374.

[7] Ayaz F., *Solutions of the system of differential equations using differential transform method*, Applied Mathematics and Computation (2004) 147: 547-567.

[8] M. Azadi *Free and forced vibration analysis of FG beam considering temperature dependency of material properties*, J Mech Sci Technol, 25 (1) (2011), pp. 69-80.

[9] Balkaya M., Kaya MO and Saglamer A., *Analysis of the vibration of an elastic beam supported on elastic soil using the differential transform method*, Archive of Applied Mechanics (2009) 79: 135-146.

[10] J.R. Banerjee *Development of an exact dynamic stiffness matrix for free vibration analysis of a twisted Timoshenko beam*, J Sound Vib, 270 (1-2) (2004), pp. 379-401.

[11] H. Su, J.R. Banerjee *Development of dynamic stiffness method for the vibration of functionally graded Timoshenko beams*, Comput Struct, 147 (2015), pp. 107-116.

[12] Banerjee JR, *Free vibration of centrifugally stiffened uniform and tapered beams using the dynamic stiffness method*, Journal of Sound and Vibration (2000) 233: 857-875.

[13] Banerjee JR, Su H and Jackson DR, *Free vibration of rotating tapered beams using the dynamic stiffness method*, Journal of Sound and Vibration (2006) 298: 1034-1054.

[14] Banerjee JR, Williams FW, *Exact Bernoulli-Euler dynamic stiffness matrix for a range of tapered beam*, International Journal of Numerical Methods in Engineering (1985) 21: 2289-2302.

[15] W. Carnegie, *Vibration of pre-twisted cantilever blading allowing for rotary inertia*

and shear deflection, Journal of the Institution of Mechanical Engineers 173 (1959) 343-347.

[16] E. Carrera F. A. Fazzolari e M. Cinefra, *Thermal Stress Analysis of composite beams, plates and shells, computational modelling and applications*, Academic Press, 2017.

[17] E. Carrera, M. Filippi, E. Zappino *Free vibration analysis of rotating composite blades via Carrera Unified Formulation*, Composite Structures 106 (2013) 317-325.

[18] Erasmo Carrera, Marco Petrolo, *On the Effectiveness of Higher-Order Terms in Refined Beam Theories*, Journal of Applied Mechanics, March 2011.

[19] E. Carrera *Theories and finite elements for multilayered anisotropic composite plates and shells*, Arch Comput Eng, 9 (2) (2002), pp. 87-140.

[20] Carlson RM, Wong JT, *An exact solution for the static bending of uniform rotating beams*, Journal of American Helicopter Society (1978) 23: 36-38.

[21] Caruntu DI, *Dynamic modal characteristics of transverse vibrations of cantilevers of parabolic thickness*, Mechanics Research Communications (2009) 36: 391-404.

[22] Catal S., *Solution of free vibration equations of beam on elastic soil by using differential transform method*, Applied Mathematical Modelling (2008) 32: 1744-1757.

[23] B. Chanane, *A series solution for nonlinear differential equations using delta operators*, Applied Mathematics Letters, 11 (6) (1998), pp. 75-80

[24] Chandiramani NK, Librescu L, Shete CD. *On the free-vibration of rotating composite beams using a higher-order shear formulation*, Aerospace Sci Technol 2002;6:545-61.

[25] Chandiramani NK, Librescu L, Shete CD. *Vibration of higher-order-shearable pretwisted rotating composite blades*, Int J Mech Sci 2003;45:2017-41.

[26] Chen CL and Liu YC, *Solution of two-point boundaryvalue problems using the differential transformation method*, Journal of Optimization Theory and Applications (1998) 99: 23−35.

[27] Chung J, Yoo HH, *Dynamic analysis of a rotating cantilever beam by using the finite element method*, J Sound Vib 2002;$249_1$47-64.

[28] X. Chunhua, J. Wang *Accurate free vibration analysis of Euler functionally graded beams by the weak form quadrature element method*, Compos Sci Technol, 125 (2015), pp. 41-50.

[29] Downs B, *Reference frequencies for the validation of numerical solutions of transverse vibrations of non-uniform beams*, Journal of Sound and Vibration (1978) 61: 71-78.

[30] Eisenberger M *Exact solution for general variable cross-section members*, Computers Structures (1991) 41: 765-772.

[31] F. Erdogan, *Fracture Mechanics of Functionally Graded Materials*, Composites Engineering (1995), Vol. 5, No. 7.

[32] U. Eroglu *In-plane free vibrations of circular beams made of functionally graded material in thermal environment: Beam theory approach*, Compos Struct, 122 (2015), pp. 217-228.

[33] Fantuzzi N., Tornabene F., Viola E., Ferreira A.J.M., *A strong formulation finite element method (sfem) based on rbf and gdq techniques for the static and dynamic analyses of laminated plates of arbitrary shape*, Meccanica, 49 (1) (2014), pp. 2503-2542.

[34] Fazzolari F.A., Carrera E., *Accurate free vibration analysis of thermo-mechanically pre/post-buckled anisotropic multilayered plates based on a refined hierarchical trigonometric Ritz formulation*, Compos Structures, 2013.

[35] Fazzolari F.A., Carrera E., *Advanced variable kinematics Ritz and Galerkin formulation for accurate buckling and vibration analysis of laminate composite plates*, Composite Structures, 2014.

[36] Fiorenzo A. Fazzolari, *Generalized exponential, polynomial and trigonometric theories for vibration and stability analysis of porous FG sandwich beams resting on elastic foundations*, Composite Part B at ScienceDirect, 2018.

[37] Fiorenzo A. Fazzolari, *Quasi-3D beam models for the computation of eigenfrequencies of functionally graded beams with arbitrary boundary conditions*, Composite Structures at ScienceDirect, 2016.

[38] Fiorenzo A. Fazzolari, *Stability and Vibrations of Thin Walled Composite Structures*, Haim Abramovich, 2017.

[39] A.J.M. Ferreira, G.E. Fasshauer, *Computation of natural frequencies of shear deformable beams and plates by an RBF-pseudospectral method*, Comput Methods Appl Mech, 196 (2006), pp. 134-146.

[40] Gallagher RH and Lee CH, *Matrix dynamic and instability analysis with non-uniform elements*, International Journal of Numerical Methods in Engineering (1970), 2: 265-275.

[41] Amin Ghorbani Shenas, Parviz Malekzadeh, Sima Ziaee, *Thermoelastic buckling of pre-twisted functionally graded beams with temperature-dependent material properties*, Acta Astronautica, Volume 133, April 2017.

[42] G. Giunta, D. Crisafulli, S. Belouettar, E. Carrera *A thermo-mechanical analysis of functionally graded beams via hierarchical modelling*, Compos Struct, 95 (2013), pp. 676-690.

[43] G. Giunta, D. Crisafulli, S. Belouettar, E. Carrera *Hierarchical theories for the free vibration analysis of functionally graded beams*, Compos Struct, 94 (2011), pp. 68-74.

[44] J. P. Gram, *Über die entwickelung reller functionen in reihen mittelst der methode der kleinsten quadrate*, J. Rein Angew Math, 1883.

[45] Yoo Hong Hee, Lee Seung Hyun, Shin Sang Ha. *Flapwise bending vibration analysis of rotating multi-layered composite beams*, J Sound Vib 2005;286: 745-61.

[46] Hodges DH. *Review of composite rotor blade modeling*, AIAA J 1990;28:561-5.

[47] Hodges DH, Rutkowski MJ. *Free-vibration analysis of rotating beams by a variable-order finite-element method*, AIAA J 1981;19:1459-66.

[48] Ho SH and Chen CK, *Analysis of general elastically end restrained non-uniform beams using differential transform*, Applied Mathematical Modelling (1998) 22: 219-234.

[49] Tsai Ming Hsu, Lin Wen Yi, Hsiao Kuo Mo. *Investigation on steady state deformation and free vibration of a rotating inclined euer beam*, Int J Mech Sci 2011;53:1050-68.

[50] Jang MJ, Chen CL and Liu YC, *Two-dimensional differential transform for partial differential equations*, Applied Mathematics and Computation (2001) 121: 261-270.

[51] Karabalis DL and Beskos DE, Static, dynamic and stability analysis of structures composed of tapered beams, Computers Structures (1983) 16: 731-748.

[52] L.L. Ke, Y.S. Wang, J. Yang, S. Kitipornchai, F. Alam *Nonlinear vibration of edged cracked FGM beams using differential quadrature method*, Sci Chin Phys, Mech Astron, 55 (11) (2012), pp. 2114-2121.

[53] Kolousek V, *Dynamics in Engineering Structures*, London: Butterworth, 1973.

[54] Lee SY, Kuo YH. *Bending frequency of a rotating Timoshenko beam with generally elastically restrained root*, J Sound Vib 1993;162:243-50.

[55] S.R. Li, R.C. Batra *Relations between buckling loads of functionally graded Timoshenko and homogeneous euler-bernoulli beams*, Compos Struct, 95 (2013), pp. 5-9.

[56] L. Librescu, S.Y. Oh, O. Song *Thin-walled beams made of functionally graded materials and operating in a high temperature environment: vibration and stability*, J Therm Stress,

28 (2005), pp. 649-712.

[57] S.R. Li, L.L. Fan, *Free vibration of FGM Timoshenko beams with through-width delamination*, Sci Chin Phys, Mech Astron, 57 (5) (2014), pp. 927-934.

[58] S.M. Lin, W. R. Wang, S. Y. Lee, *The dynamic analysis of nonuniformly pre-twisted Timoshenko beams with elastic boundary coditions*, International Journal of Mechanical Science 43 (2001) 2385-2405.

[59] Huang Chih Ling, Lin Wen Yi, Hsiao Kuo Mo. vibration analysis of rotating euler beams at high angular velocity, Comput Struct 2010;88:991-1001.

[60] Li QS, *An exact approach for free flexural vibrations of multistep nonunifom beams*, Journal of Vibration and Control (2000) 6: 963-983.

[61] C.F. Lü, W.Q. Chen, R.Q. Xu, C.W. Lim *Semi-analytical elasticity solutions for bi-directional functionally graded beams*, Int J Solids Struct, 45 (1) (2008), pp. 258-275.

[62] N.V.R. Maganti, M.R. Nullari *Flapwise bending vibration analysis of functionally graded rotating double-tapered beams*, Int J Mech Mater Eng (2015), pp. 10-21.

[63] N.V.R. Maganti, M.R. Nullari *Free vibration analysis of pre-twisted rotating FGM beams*, Int J Mech Mater Des, 9 (4) (2013), pp. 367-383.

[64] Mei C., *Application of differential transformation technique to free vibration analysis of a centrifugally stiffened beam*, Comput Struct 2008;86:1280-4.

[65] Mou Y, Han RSP and Shah AH, *Exact dynamic stiffness matrix for beams of arbitrarily varying cross sections*, International Journal of Numerical Methods in Engineering (1997) 40: 233-250.

[66] Na S, Librescu L, Shim JK. *Modeling and bending vibration control of nonuniform thin-walled rotating beams incorporating adaptive capabilities*, Int J Mech Sci 2003;45:1347-67.

[67] Jung Sung Nam, Nagaraj VT, Chopra Inderjit. *Assessment of composite rotor blade modeling techniques*, J Am Helicopter Soc 1999;44:188-205.

[68] Jung Sung Nam, Nagaraj VT, Chopra Inderjit. *Refined structural dynamics model for composite rotor blades*, AIAA J 2001;39:339-48.

[69] Ozdemir O and Kaya MO, *Flapwise bending vibration analysis of a rotating tapered cantilever Bernoulli- Euler beam by differential transform method*, Journal of Sound and Vibration (2006) 289: 413-420.

[70] Ozdemir O and Kaya MO *Flapwise bending vibration analysis of double tapere rotating Euler-Bernoulli beam by using the differential transform method*, Meccanica (2006) 40: 661-670.

[71] Ozge Ozdemir Ozgumus, Kaya Metin O., *Flapwise bending vibration analysi of doube tapered rotating Euler-Bernoulli beam by using the differential transform method*, Meccanica 2006;41:661-70.

[72] K.K. Pradhan, S. Chackraverty *Effects of different shear deformation theories on the free vibration of functionally graded beams*, Int J Mech Sci, 82 (2014), pp. 149-160

[73] Rao SS, Gupta RS. *Finite element vibration analysis of rotating timoshenko beams*, J Sound Vib 2001;242:103-24.

[74] J. N. Reddy, *Energy principles and variational methods in applied mechanics*, 2nd ed. Hoboken, New Jersey: John and Wiley Sons Inc; 2002.

[75] J. N. Reddy, *Mechanics of Laminated Composite Plates and Shells Theory and Analysis*, second edition, CRC Press, 2004.

[76] Ritz W. , *Über eine neue Methode zur Lösung gewisser Variationsprobleme der matematishen Physik* (About a new method for the solution of certain variational problems of

mathematics and physics), J Rein Angew Math, 1909.

[77] C.M.C. Roque, P.A.L.S. Martins *Differential evolution for optimization of functionally graded beams*, Compos Struct, 133 (2015), pp. 1191-1197.

[78] Ruta P, *Application of Chebyshev series to solution of non-prismatic beam vibration problems*, Journal of Sound and Vibration (1999) 227: 449-467.

[79] N.L. Shegokar, A. Lal *Stochastic finite element nonlinear free vibration analysis of piezoelectric functionally graded materials beam subjected to thermo-piezoelectric loadings with material uncertainties*, Meccanica, 49 (2014), pp. 1039-1068.

[80] A. Shooshtari, M. Rafiee *Nonlinear forced vibration analysis of clamped functionally graded beams*, Acta Mec, 221 (2011), pp. 23-28.

[81] M. Simsek *Bi-directional functionally graded materials (BDFGMs) for free and forced vibration of Timoshenko beams with various boundary conditions*, Compos Struct, 133 (2015), pp. 968-978.

[82] M. Simsek *Fundamental frequency analysis of functionally graded beams by using different higher-order beam theories*, Nucl Eng Des, 240 (4) (2010), pp. 697-705.

[83] Song O, Oh SY, Librescu L. *Dynamic behavior of elastically taiored rotating blades modeled as pretwisted thin-walled beams and incorporating adaptive capabilities*, Int J Rotating Mach 2002;8:13-25.

[84] Song O, Librescu L. *Structural modeling and free vibration analysis of rotating composite thin-walled beams*, J Am Helicopter Soc 1997;42:358-69.

[85] Syed Muhammad Ibrahim, Saleh H Alsayed, Husain Abbas, Erasmo Carrera, Yousef A Al-Salloum and Tarek H Almusallam, *Free vibration of tapered beams and plates based on unified beam theory*, Journal of Vibration and Control, 2014.

[86] Stoykov S, Ribeiro P. *Vibration analysis of rotating 3d beams by p-version finite element method*, Finite Elem Anal Des 2013;65:76-88.

[87] H. Su, J.R. Banerjee, C.W. Cheung *Dynamic stiffness formulation and free vibration analysis of functionally graded beams*, Comput Struct, 106 (2013), pp. 854-862.

[88] K. B. Subrahmanyam, S. V. Kulkarni, J. S. Rao, *Coupled bending-bending vibration of pre-twisted cantilever blading allowing for shear deflection and rotary inertia by the Reissner method*, International Journal of Mechanical Science 23 (1981) 517-530.

[89] Y. Sun, S.R. Li, R.C. Batra *Thermal buckling and post-buckling of FGM Timoshenko beams on nonlinear elastic foundation*, J Therm Stress, 39 (1) (2013), pp. 11-26.

[90] F. Tornabene *2-D GDQ solution for free vibrations of anisotropic doubly-curved shells and panels of revolution*, Compos Struct, 93 (2011), pp. 1854-1876.

[91] F. Tornabene *Free vibration analysis of functionally graded conical, cylindrical shell and annular plate structures with a four-parameter power-law distribution*, Comput Methods Appl Mech Eng, 198 (2009), pp. 2911-2935.

[92] Tornabene F. Meccanica delle strutture a guscio in materiale composito: Il Metodo Generalizzato di Quadratura Differenziale, 1st ed., Esculapio; 2012.

[93] F. Tornabene, E. Viola, N. Fantuzzi *General higher order equivalent single layer theory for free vibrations of doubly-curved laminated composite shells and panels*, Compos Struct, 104 (2013), pp. 94-117.

[94] Trusdell, C., (1960), *The rational mechanics of flexible or elastic bodies 1638-1788*, Venditioni Expount Orell Fussli Turici.

[95] T.P. Vo, H.T. Thai, T.K. Nguyen *Bending and free vibration of functionally graded beams using various higher-order shear deformation beam theories*, Int J Mech Sci, 62 (1) (2012),

pp. 57-66.

[96] T.P. Vo, H.T. Thai, T.K. Nguyen *Static and vibration analysis of functionally graded beams using refined shear deformation theory*, Meccanica, 49 (2014), pp. 155-168.

[97] Z.A. Wang, X.H. Wang, G.D. Xu, S. Cheng, T. Zeng *Free vibration of two-directional functionally graded beams*, Compos Struct, 135 (2016), pp. 191-198.

[98] Wang G. and Wereley N. M., *Free vibration analysis of rotating blades with uniform tapers*, IAA Journal (2004) 42: 2429-2437.

[99] Washizu K. Variational methods in elasticity and plasticity. Oxford: Pergamon Press; 1968.

[100] N. Wattanasakulpong, A. Chaikittiratana *Flexural vibration of imperfect functionally graded beams based on Timoshenko beam theory: Chebyshev collocation method*, Meccanica, 50 (2015), pp. 1331-1342.

[101] N. Wattanasakulpong, J. Charoensuk Vibration characteristics of stepped beams made of FGM using differential transformation method, Meccanica, 50 (2015), pp. 1089-1101.

[102] Y.O. Xu, Y. Quian, J. Cheng, G. Song *Stochastic dynamic characteristics of FGM beams with random material properties*, Compos Struct, 133 (2015), pp. 585-594.

[103] B. Yardimoglu, T. Yildirim, *Finite element model for vibration analysis of pre-twisted Timoshenko beam*, Jpurnal of Sound and Vibration 273 (2004) 741-754.

[104] Yesilce Y, Catal S, *Free vibration of axially loaded Reddy-Bickford beam on elastic soil using the differential transform method*, Structural Engineering and Mechanics (2009) 31: 453-476.

[105] Yesilce Y, *DTM and DQEM for free vibration of axially loaded and semi-rigid-connected Reddy-Bickford beam*, Communications in Numerical Methods in Engineering (2010) DOI: 101002/cnm1313.

[106] A. Yousefi, A. Rastgoo *Free vibration of functionally graded spatial curved beams*, Compos Struct, 93 (11) (2011), pp. 3048-3056.

[107] W. Yu, D.H. Hodges *Elasticity solutions versus asymptotic sectional analysis of homogeneous, isotropic, prismatic beams*, J Appl Mech, 71 (1) (2004), pp. 15-23.

[108] W. Yu, D.H. Hodges *Generalized Timoshenko theory of the variational asymptotic beam sectional analysis*, J Am Helicopter Soc, 50 (1) (2014), pp. 46-55.

[109] W. Yu, V.V. Volvoi, D.H. Hodges, X. Hong, *Validation of the variational asymptotic beam sectional analysis*, AIAA J, 40 (10) (2002), pp. 2105-2112.

[110] N. Zaine, S.A. Meftah, H.A. Belhadj, A. Tounsi, E.A. Bedia Free vibration analysis of thin and thick-walled FGM box beams, Int J Mech Sci, 66 (2013), pp. 273-282.

[111] Zeng H and Bert CW ,*Vibration analysis of a tapered bar by differential transformation*, Journal of Sound and Vibration (2001) 242: 737-739.

[112] Zhou JK, *Differential Transform and its Application for Electrical Circuits*, Huazhong University Press (1986), Wuhan, P.R. China.

[113] H. Zhu, B.V. Sankar *A combined Fourier series - Galerkin method for the analysis of functionally graded beams*, J Appl Mech, 71 (2004), pp. 421-423.